VII. EXTENDED STUDIES WITH SELECTED ULTRASONIC ANGLE BEAM TECHNIQUES

This section will describe the work performed as part of this project on selected ultrasonic flaw detection and characterization techniques. The purpose of this work is to extend the present day evaluations of the reliabilities of such techniques and to indicate possible improvements in new and existing techniques.

The availability of flaw detection techniques is very limited, There appears to be only one interrogation scheme for the detection of a totally embedded flaw content. This scheme is the basis for the ultrasonic method itself. The material or structure being examined is essentially volumetrically scanned with either a single transducer or by multiple transducers utilizing both straight and angle beams. Flaw size characterization by this technique is accomplished by noting the magnitude and shape of the amplitude response envelope. The wide usage of this basic interrogation technique for both detection and characterization necessitates its inclusion for further investigation and evaluation.

Flaw characterization techniques may be divided into amplitude-dependent and amplitude-independent types. In the former, one assumes a direct relationship between the detected amplitude and the flaw area. The basic interrogation scheme described above typifies this and will constitute the amplitude-dependent flaw characterization technique to be studied in this section. The literature search indicates two amplitude-independent flaw characterization techniques worthy of further study. One extracts intelligence about the flaw from the location of the maximum detected amplitude of the response envelope as was briefly described in 2a3 of Section IV. The other technique involves a novel use of spectroscopy by Gilmore and Czerw [48], and was indicated in 2c of Section IV.

1. The Conventional Amplitude-Dependent Flaw Detection Process - In Detail

The basic flaw detection process will be considered in terms of inherent detecting ability, flaw characterization and the attendant reliability involved.

a. Detecting Ability

The flaw detection process was modeled in Section IV for the straight beam and experimentally verified by a number of experiments. Since angle beam interrogation is used almost exclusively in weld evaluation much the same experimentation was performed for the angle beam technique. The angle beam

has additional complications as presented by the plastic shoe used to produce the angled shear wave by mode conversion. As indicated in Figurc 64 the beam produced within the material to be interrogated may not be symmetrical. This can be noted by considering the most extreme rays of the beam. Since the angles of incidence (α_i) at the interface are not equal it is reasonable to assume that the refracted angles (β_i) are not equal as well. The literature indicates the possibility of the beam geometry shown in Figure 65 .[42] Such an unsymmetrical beam can result in different amplitudes for flaws detected by either side of the center of rhe beam. Since all detection models assume a symmetrical beam,it is necessary to evaluate the shape of the transducer radiation field of a mode converted beam. Figure 66 shows the blocks that were used to study the presence and influence of an unsymmetrical angle beam. Four such blocks have been machined,each with a single flat bottom hole size; diameters of 1/4, 3/8, 5/8, and 3/4" were used. The blocks provide for misorientation angles of up to $\pm 20^{o}$ for the 45^{o} entry angle beam and $\pm 30^{o}$ for the 60^{o} beam. Aluminum was used to minimize the influence of attenuation. The flat bottom holes are arranged such that at any given detection point the amplitude response emanuates from only one of the simulated flaws. Early experiments indicated that the larger flat bottom holes yielded multiple responses. The combination of the planar reflector and the sides of the drilled shaft produce additional radiation fields; see Figure 67. The outward effect is that one can note an amplitude response with a number of maxima which at times cannot be interpreted. It is necessary to coordinate the interpretation of such an amplitude response with distance related consideration.

Figure 68 shows the amplitude response for the case of a misorientation angle of zero degrees between the flaw normal and the interrogating beam. It should be noted that both 45^{o} and 60^{o} entry angles are involved. The simulated flaws or reflectors were oriented at 45^{o} and 60^{o} (η) for the 45^{o} and 60^{o} interrogating beams (ρ), respectively; see Figure 66. Also shown is the response predicted by the model as formulated by equation 2. It would appear that the radiation from the angle beam is symmetrical and follows the model very closely. Figures 69 and 70 indicate similar data for these two entry angle beams for the case where the misorientation angle (ϕ) is $+5^{o}$. Since the experiments of the latter displays were designed to

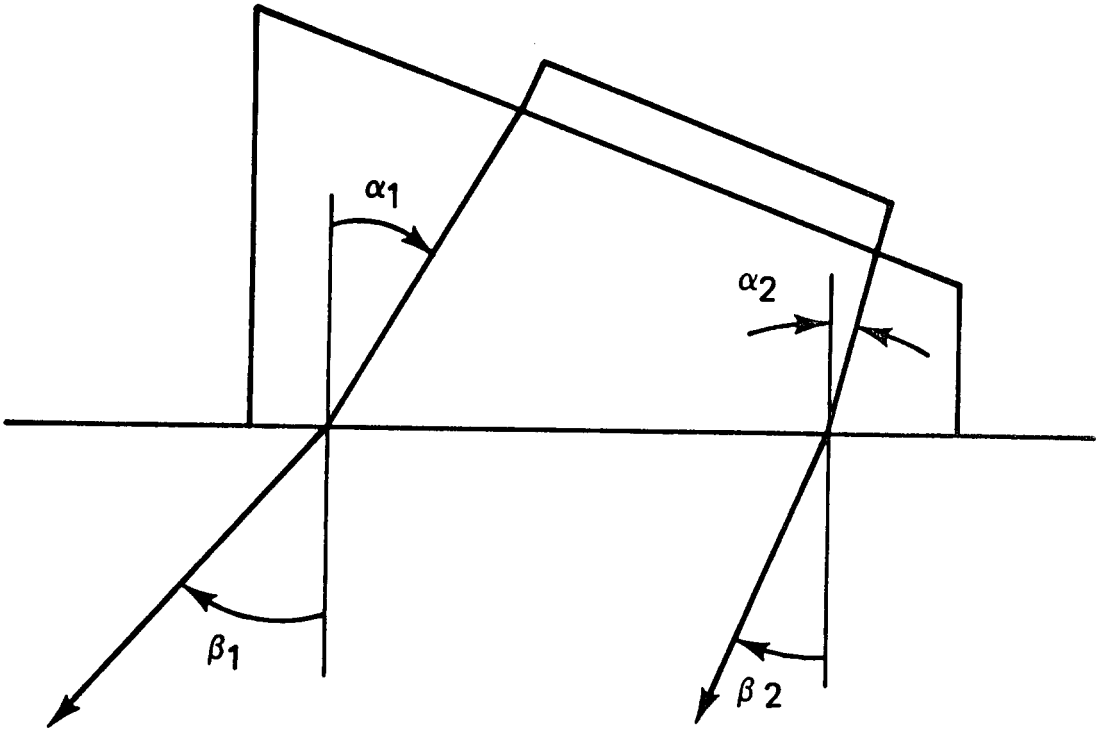

Figure 64 - The material used to incline the transducer for mode conversion can generate an unsymmetrical beam.

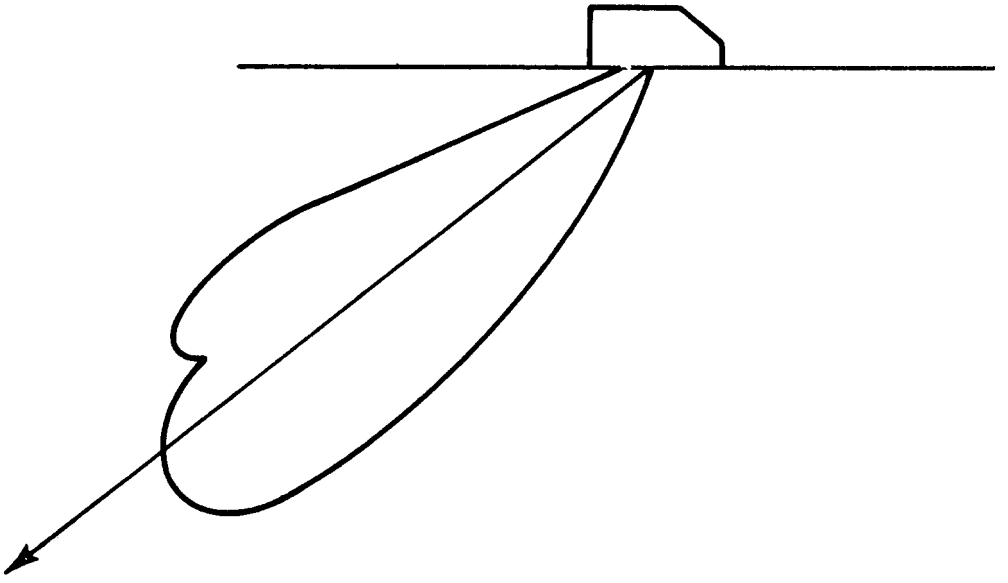

Figurc 65 - A refraction produced unsymmetrical nnglc bcam can lead to an amplitude response from the flaw that is influenced by the flaw misorientation angle involved.

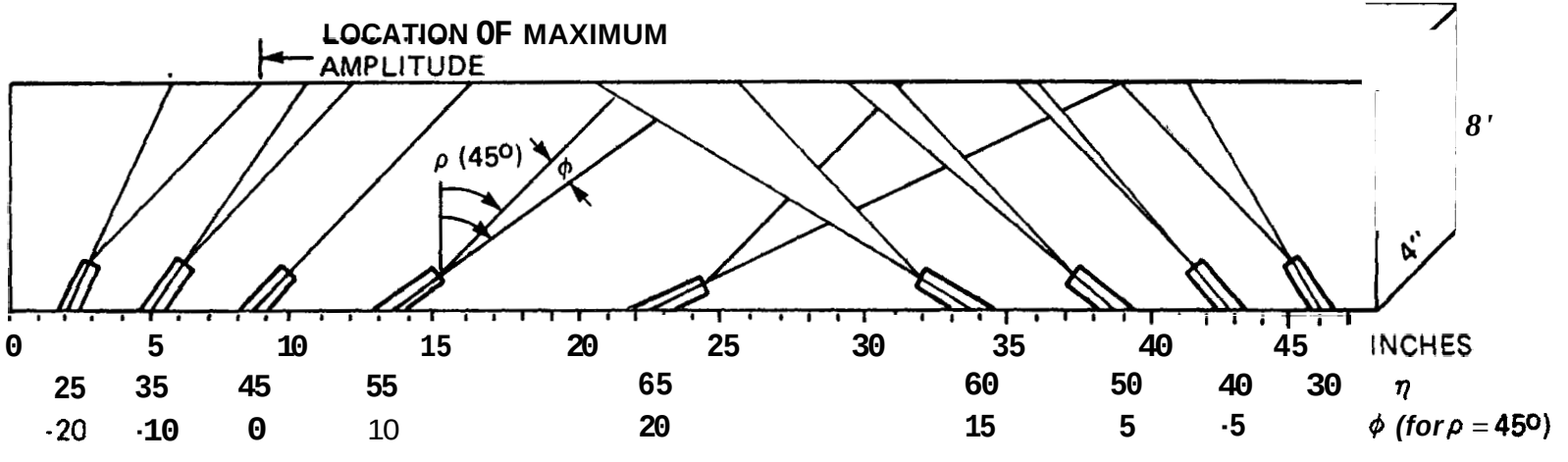

Figure 66 - Specimen used to study amplitude response envelopes for angle beam interrogation.

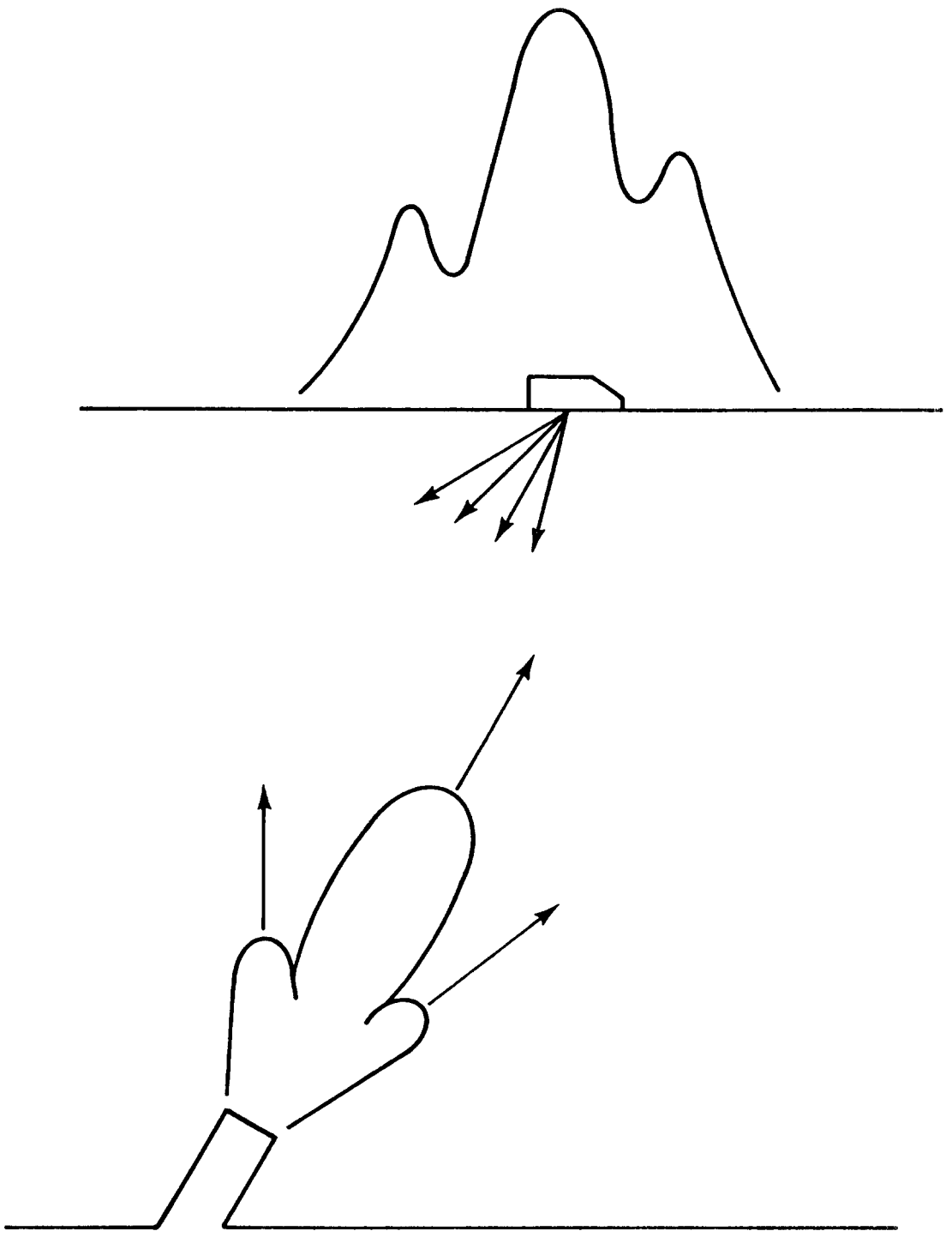

Figure 67 - The edges of the larger flat bottom holes produce amplitude interference effects in the amplitude response.

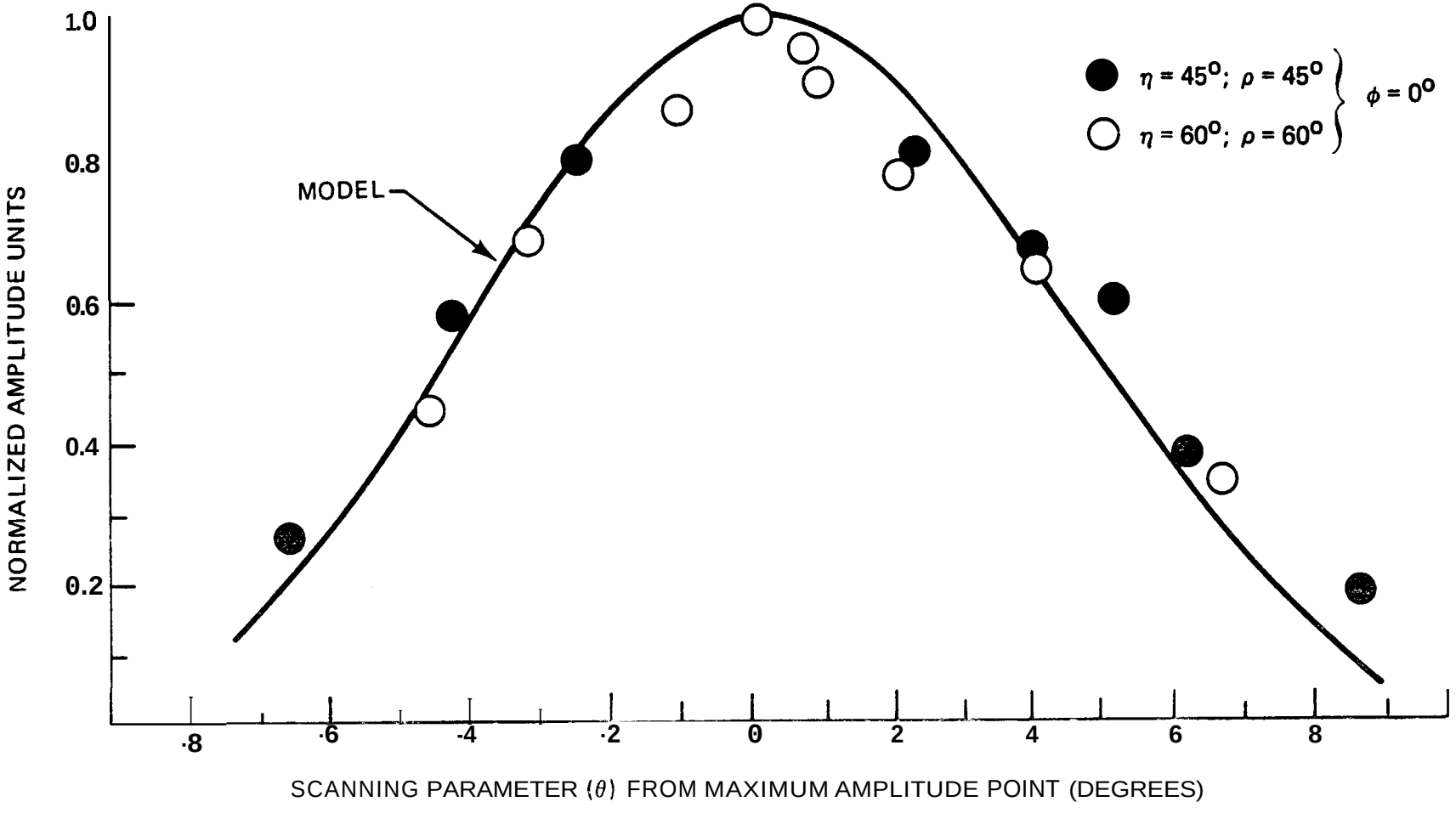

Figure 68 - The amplitude response envelopes from *e* 1/4" diameter flat bottom hole by 45° and 60° entry angle beams. In each case the orientation of the reflectors was such that the misorientation angle was zero; detection was accomplished by a 1/2"-2 1/4 MHz transducer.

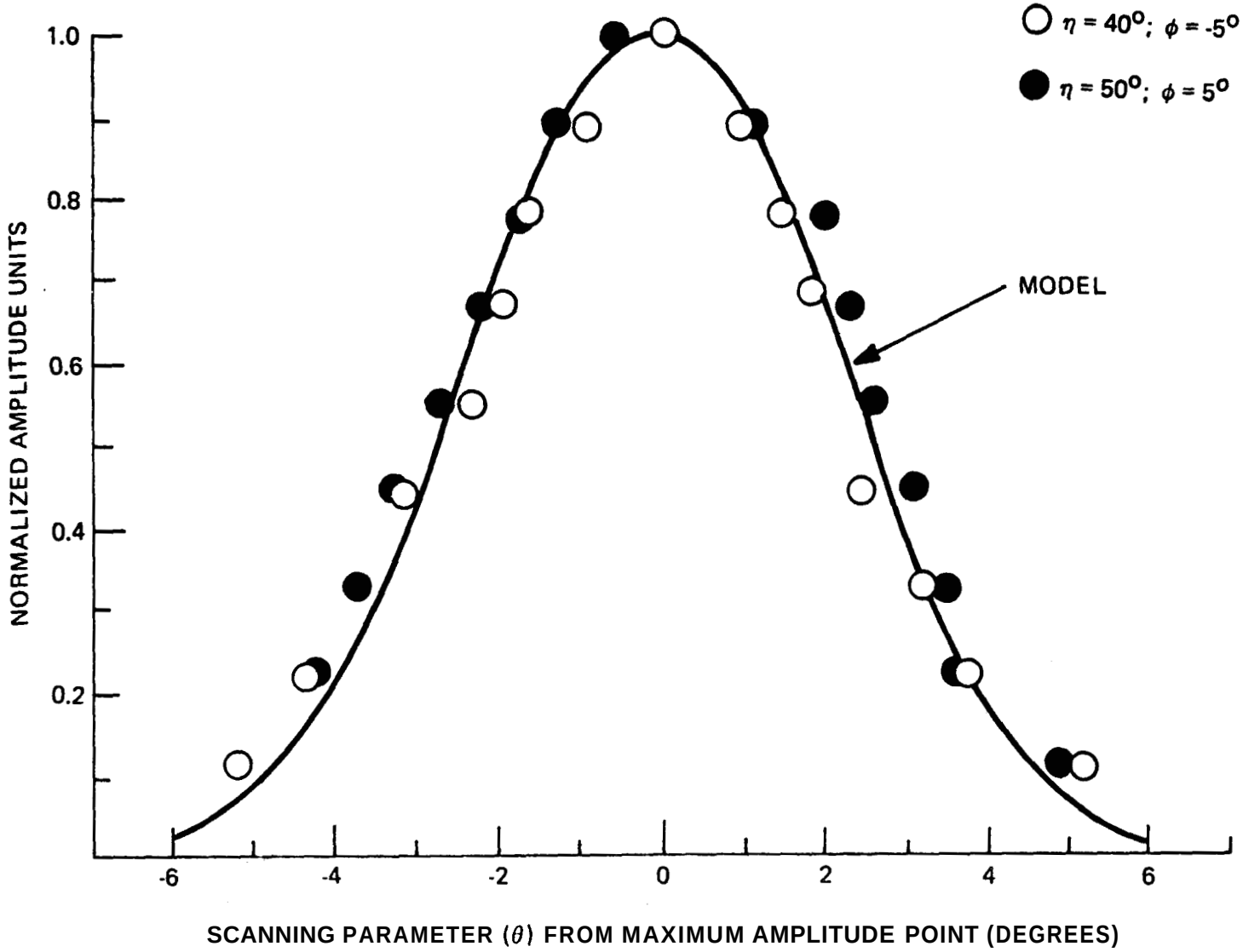

Figure 69 - The amplitude response envelopes for 1/4B reflectors oriented at 50^{o} ($\emptyset=5^{o}$) and 40^{o} ($\emptyset=-5^{o}$). A 1/2" - 2.25 MHz transducer with a **45** entry angle was used for detection.

observe beam symmetry the data were shifted laterally until the maximum amplitude points coincided. The ability of the model to predict location of the amplitude response is shown in Figure 71; the curves represent the model. It should be noted that the amplitude displays have been normalized. The normalization gain necessary is indicated and illustrates the amplitude degradation due to misorientation angle.

Figure 71 shows that the width of the amplitude response envelope for a given reflector decreases with the misorientation angle. It is for this reason that a size determination based upon the width of such envelopes at a given amplitude decay level is substantially influenced by the misorientation angle. All analysis based upon maximum amplitude and envelope width would produce optimistic sizes for flaws misoriented with respect to the interrogating beam. The extent of the undersizing would significantly increase with the flaw misorientation. Moreover, the current fallacious practice of applying a correction based upon transducer beam width does not seem appropriate. It is difficult to comprehend a common size determination for the data displays of Figure 71 by the application of a constant correction.

The influence of transducer and reflector size upon the detecting ability for an angle beam interrogation is shown in Figure 72. The plotted curves are taken from furction F_2 of the model (equation 2) and the experimental data was generated by the use of the blocks of Figure 66. All the data has been corrected for attenuation and diffraction losses because of the fact that all the reflectors are not equidistant from the interrogating transducer at the point where the maximum amplitude is observed. A number of salient observations are in order regarding Figure 72. Perhaps the most obvious observation is that for each transducer size there is an amplitude degradation as a result of the misorientation angle. It is apparent that the amplitude degradation is substantially increased with incrensing transducer size. This is the result of a much more directed beam from the larger transducers, thus making it more difficult to align the radiation fields involved. This notion may be illustrated by Figure 73 which compares the normalized amplitude response envelopes from a 1/4" reflector as noted by a 1/2" and 1/4" diameter transducers. At the 6 db amplitude decay points there is a two to one width ratio for the 1/4" and 1/2" diameter transducers, respectively. For each transducer size of Figure 72 there is a misorientation angle beyond which

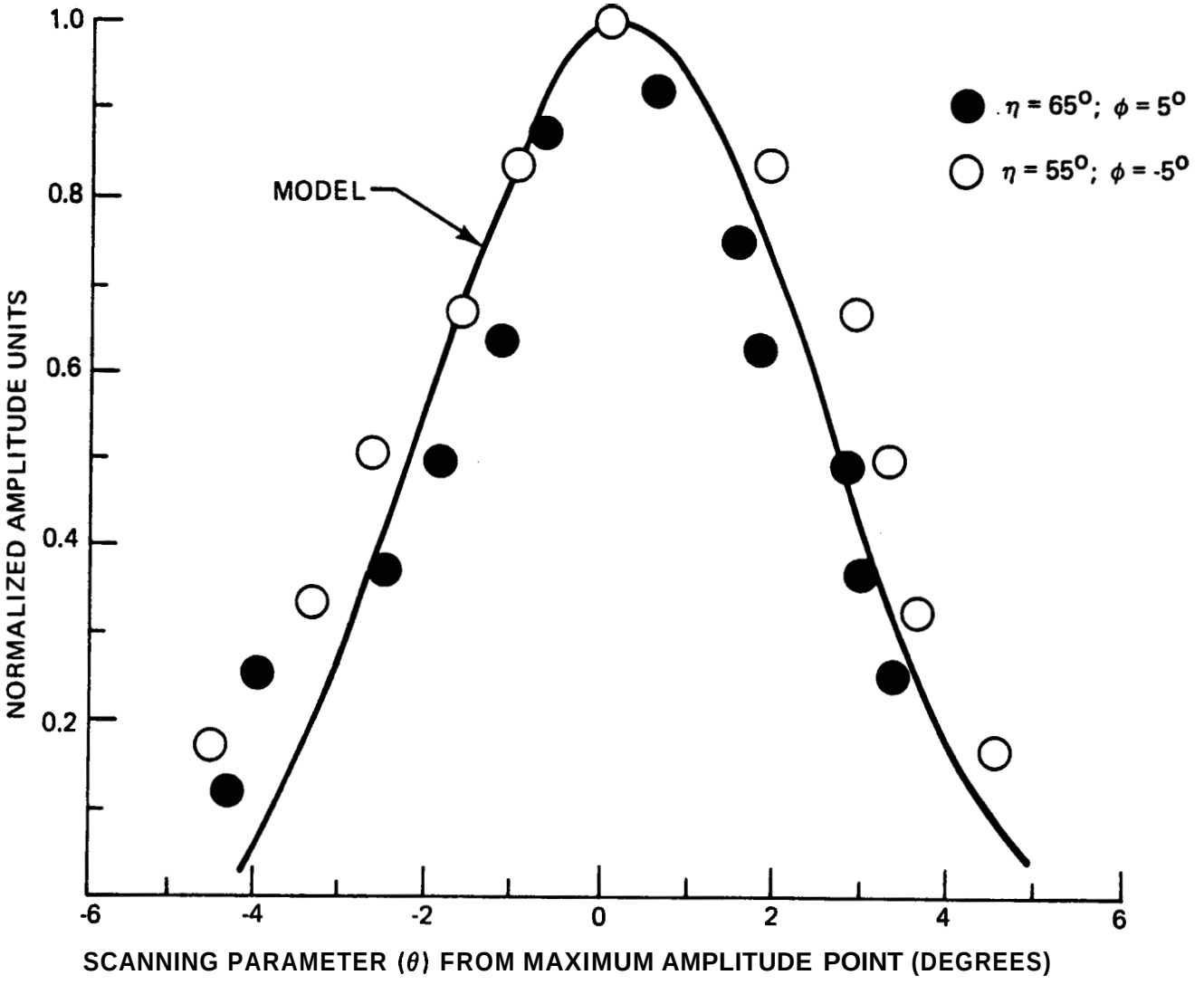

Figure 70 - The amplitude response envelopes for 3/8" reflectors oriented at 65^{o} (Ø=5) and 55^{o} (Ø=-5). A 1/2" - 2.25 MHz transducer with a 60^{o} entry angle was used for detection.

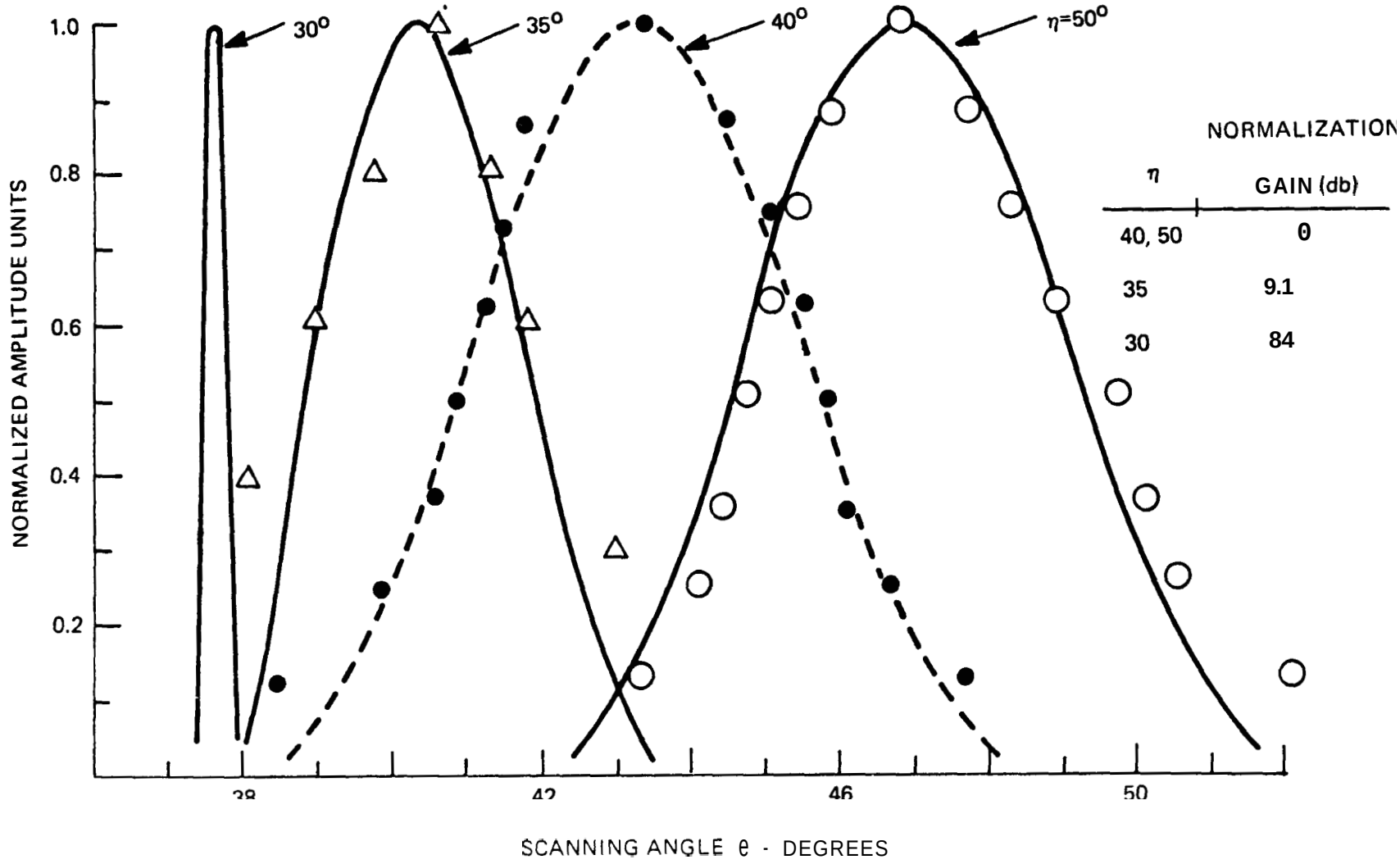

Figure 71 - Amplitude response envelopes for a 1/4" reflector at various misoricntations. A 1/2" - 2.25MHz transducer was used. An entry angle of 45o was used. The curves represent the model.

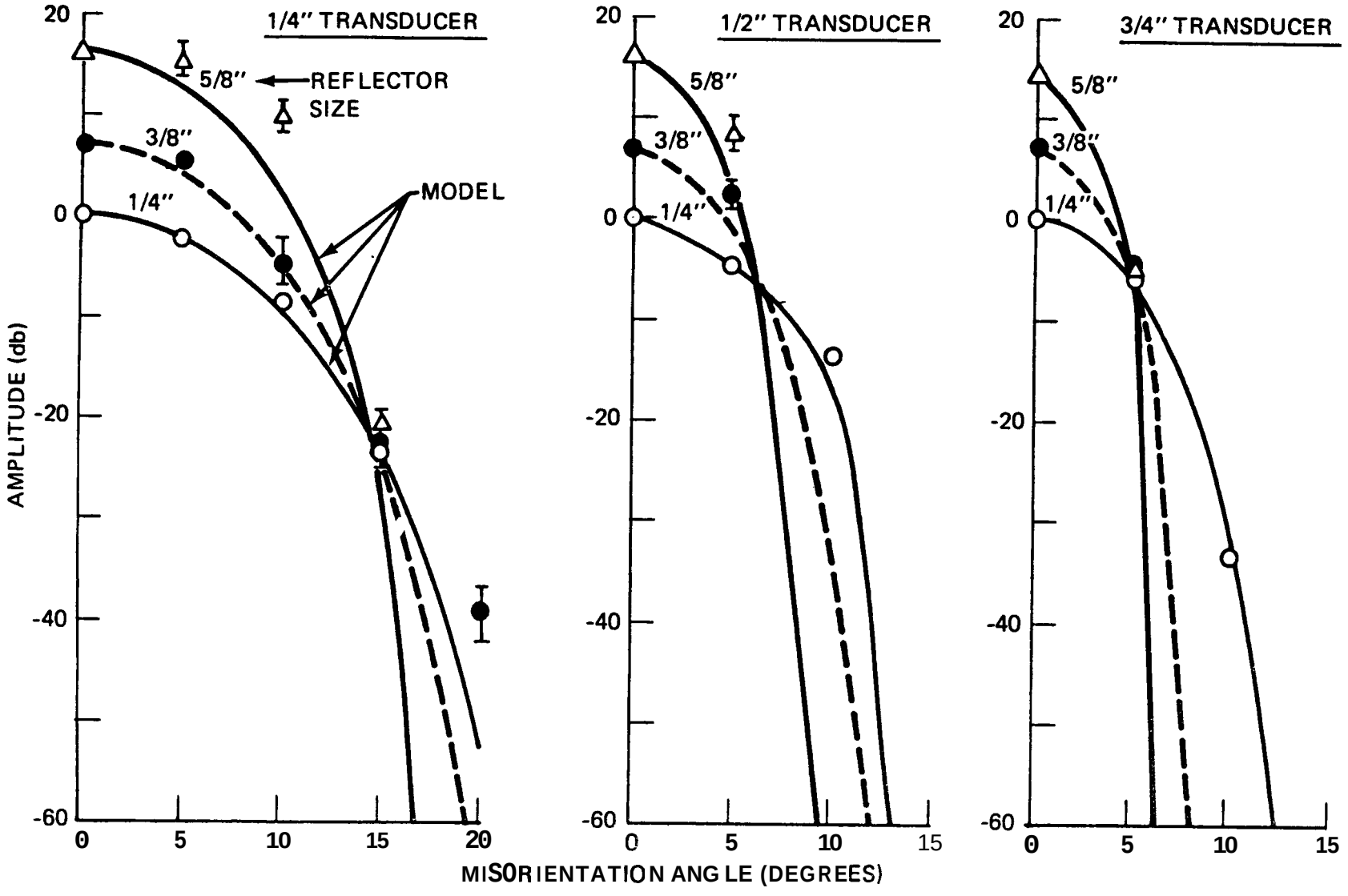

Figure.72 - The effect of reflector misorientation upon the angle shear beam detecting ability of various transducer sizes at 2.25 MHz. The response from a 1/4" diameter reflector was used as an amplitude standard.

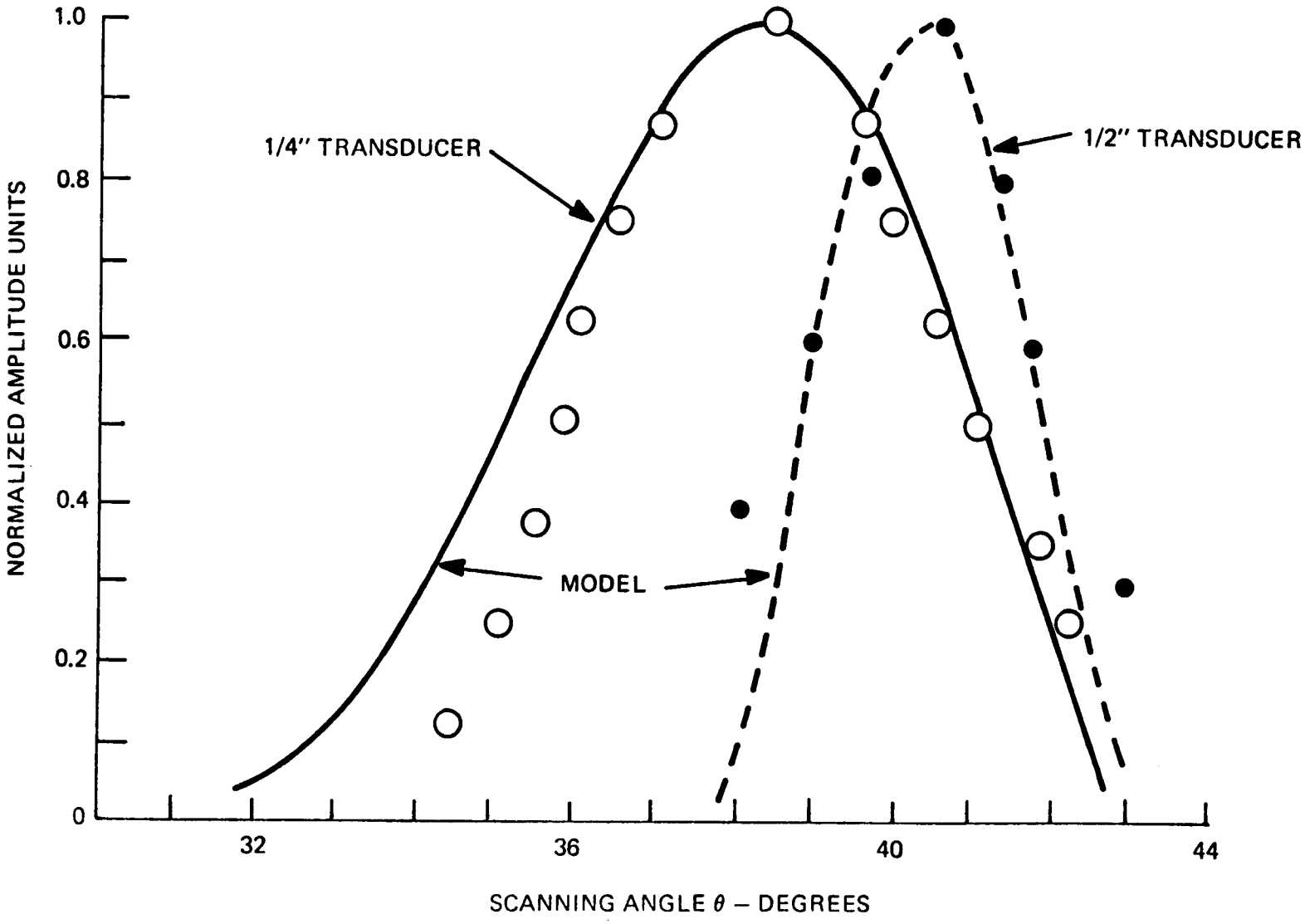

Figure 73 - Amplitude response envelopes from a 1/4" reflector as noted by a 1/4" and 1/2" transducer operating at 2.25 MHz.

the response amplitude advantage due to reflector size is eliminated. From this point on, and in direct opposition to the intuitive interpretation of amplitude data, the smaller flaws would be noted with larger amplitudes. Again, it is a matter of more probable alignment of the transducer radiation field with the wide field from a smaller reflector. It is clear that this amplitude-size cross over point is a function of the transducer size. As it will be indicated later the 1/4" flat bottom hole response is a realistic standard; it is in line with both the German and United States codes governing the construction of nuclear power plants. If we accept a recordable cutoff level of 20 db below the 1/4" amplitude, then the detecting ability of the angle beam is limited to flaws within a misorientation of 15^{o} for the 1/4" diameter transducer and approximately 5^{o}-10^{o} for the 1/2" and 3/4" diameter transducer. Any reflector with greater misorientation would be undetectable no matter how big it is. As indicated in Section IV a, the consideration of flaw roughness does not alter this fact. The use of the tandem technique introduces the ability to detect flaws oriented normal to the interrogating surface. However, the same limitations for detecting flaws misoriented from the normal prevail. One option that one can exercise is to use lower frequencies to be assured of wide interrogating and reflector radiation fields. For example, compare the detecting ability of 1 MHz (Figure 74) with that of 2 1/4 MHz (Figure 72); both transducers are 1/2" in diameter. As to be expected, the amplitude degradation for the lower frequency is much less.

Thus far, the analysis has assumed a homogenious material, or for a welded structure, that the attenuations of the base and weldment materials are equal. The consequences of a weldment attenuation that is greater than the base material were presented in Section VI. Figure 75 indicates the geometric particulars necessary for the addition of the influence of intrinsic material attenuation into the model. The model can produce the amplitude response envelope $A(\theta)$, for a flaw located at the point (X_f, Y_f) within the weldment for zero attenuation. It is a simple matter to transcribe $A(\theta)$ of Equation 2 to $A'(x)$ by using:

$$\begin{aligned} x &= x_f + x_\theta \\ &= x_f + (2T - Y_f) \operatorname{Tan} \theta \end{aligned} \qquad (12)$$

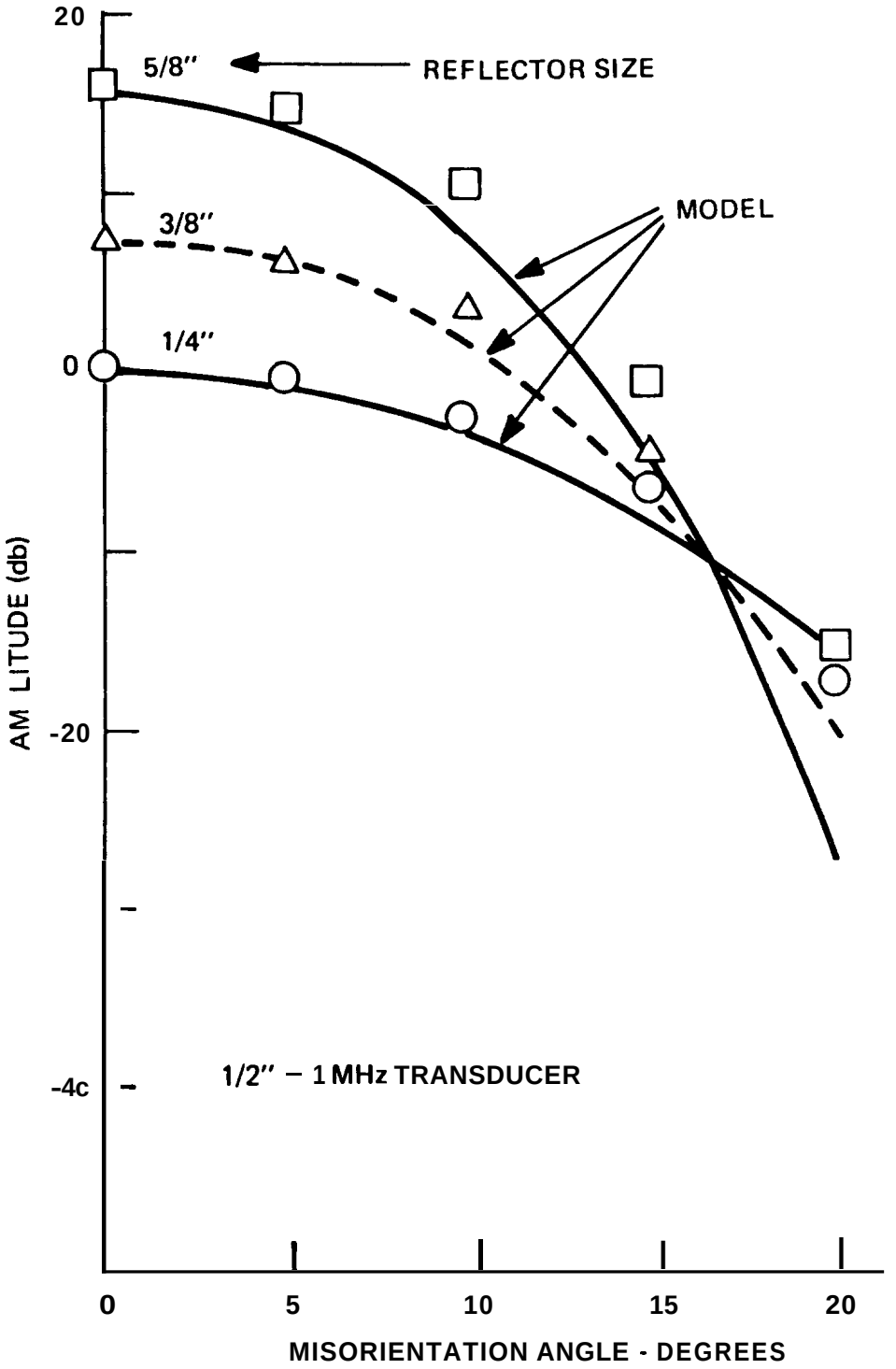

Figure 74 - The effect of reflector orientation upon the angle shear wave detecting ability for a 1/2" - 1 MHz transducer. The response from a 1/4" diameter reflector was used as the amplitude standard.

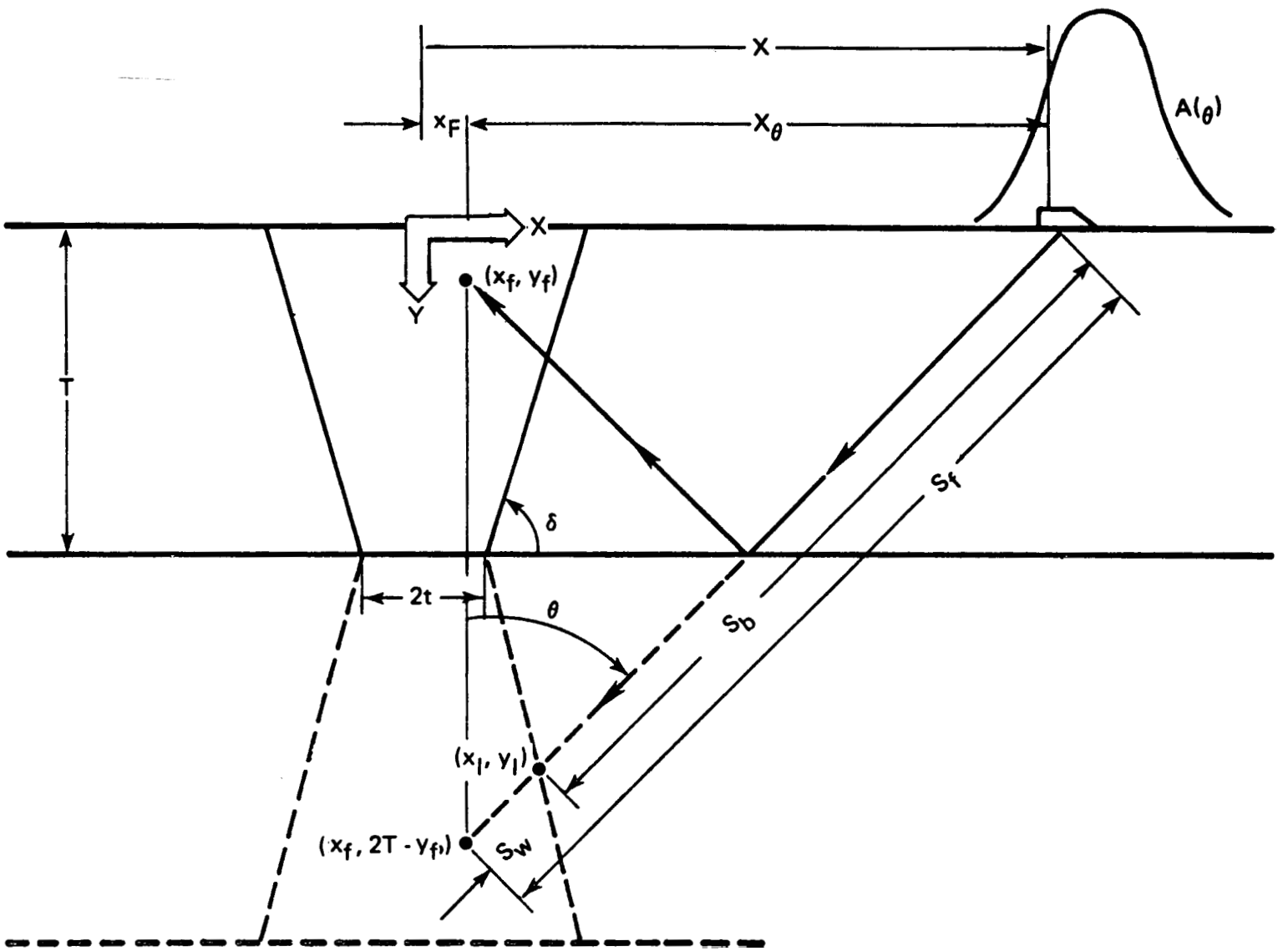

Figure 75 - Geometric particulars for the calculation of weldment attenuation effects.

With the inclusion of attenuation the amplitude response, A(x), at any point (x) on the interrogating surface is given by:

$$A(x) = A'(x) e^{2\alpha_b (s_b + R s_w)} \qquad (13)$$

Where R is the ratio of base material attenuation (α_b) and weldment attenuation (α_w). The distances s_b and s_w are the distances the ultrasound travels within the base and weldment materials, respectively. Their calculation necessitates the determination of the intersection of the beam and the surface of the weldment, i.e., the point (X_I, Y_I). The latter may he written as:

$$X_I = \frac{x - T \tan\theta + t \tan\theta \quad \tan\theta}{1 + \tan\theta \quad \tan\theta}$$

$$Y_I = T + (x - t) \tan\theta \qquad (14)$$

Therefore, the distances traveled by the ultrasound are given by:

$$s_f = [x_\theta^2 + (2T - Y_f)^2]^{1/2}$$

$$s_b = [(x_f + x_\theta + x_I)^2 + Y_I^2]^{1/2} \qquad (15)$$

$$s_w = s_f - s_b$$

Figure 76 indicates a typical weld configuration used to study the influence of attenuation; three specific flaw locations were selected. The attenuation of a mild steel or 0.25 db/in was used for the base material. The attenuation of the weldment was described by the use of the R factor of equation 13. Figure 77 displays the amplitude response envelopes for flaw 2 of Figure 76. Since DAC curves are originally generated for the base material (R=1), the results indicate that the influence of attenuation can be significant. For example, if the R=. response is indicative of a flaw at the DAC amplitude line, and the 50% of DAC level represents the cutoff recordable level, then the flaw would not be recorded when the ratio of the weldment to base attenuations exceeded approximately 7.5. **This** is not a very high weldment attenuation since attenuation ratios of **20-40** are not uncommon. Figure 78 shows the maximum amplitude for the other two flaws of Figure *76*. The cffcct of flaw distance is obvious.

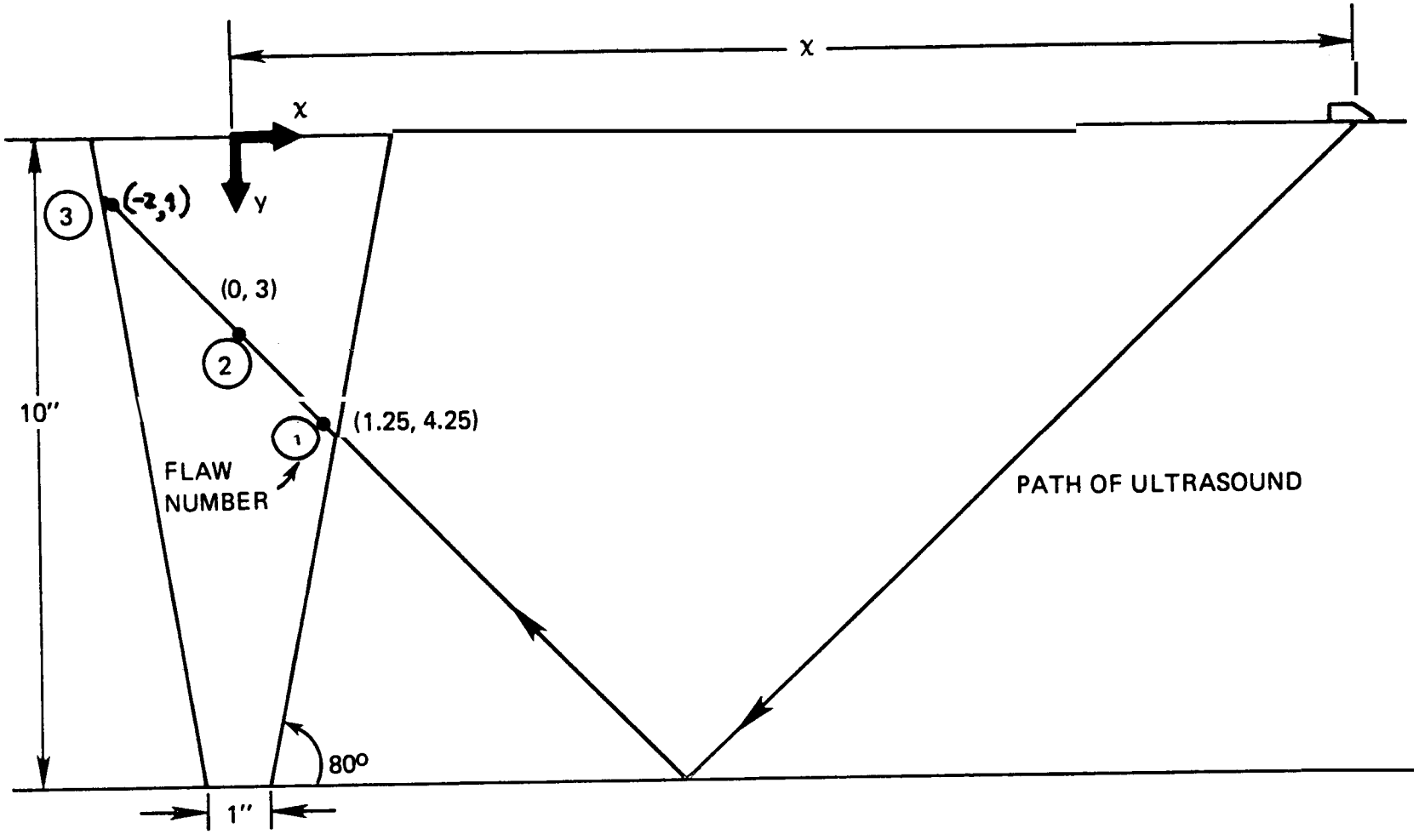

Figure *76* - The weld system used to study the affects of attenuation; three flaw locations are indicated.

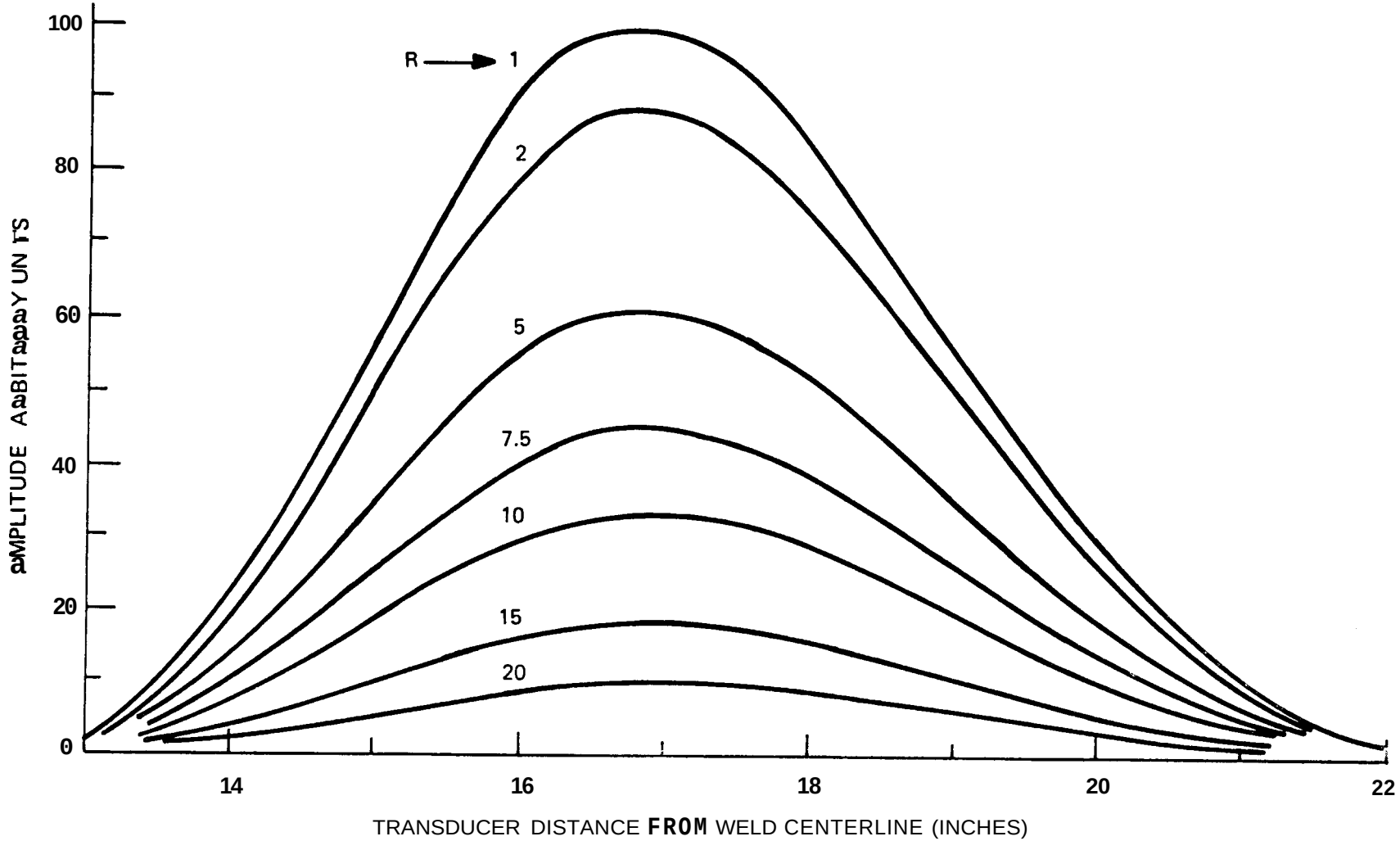

Figure 77 - The amplitude response envelopes for flaw number two of Figure 76 as a function of the ratio (R) of weldment/base material attenuations. A base material attenuation of 0.25 db/in was used.

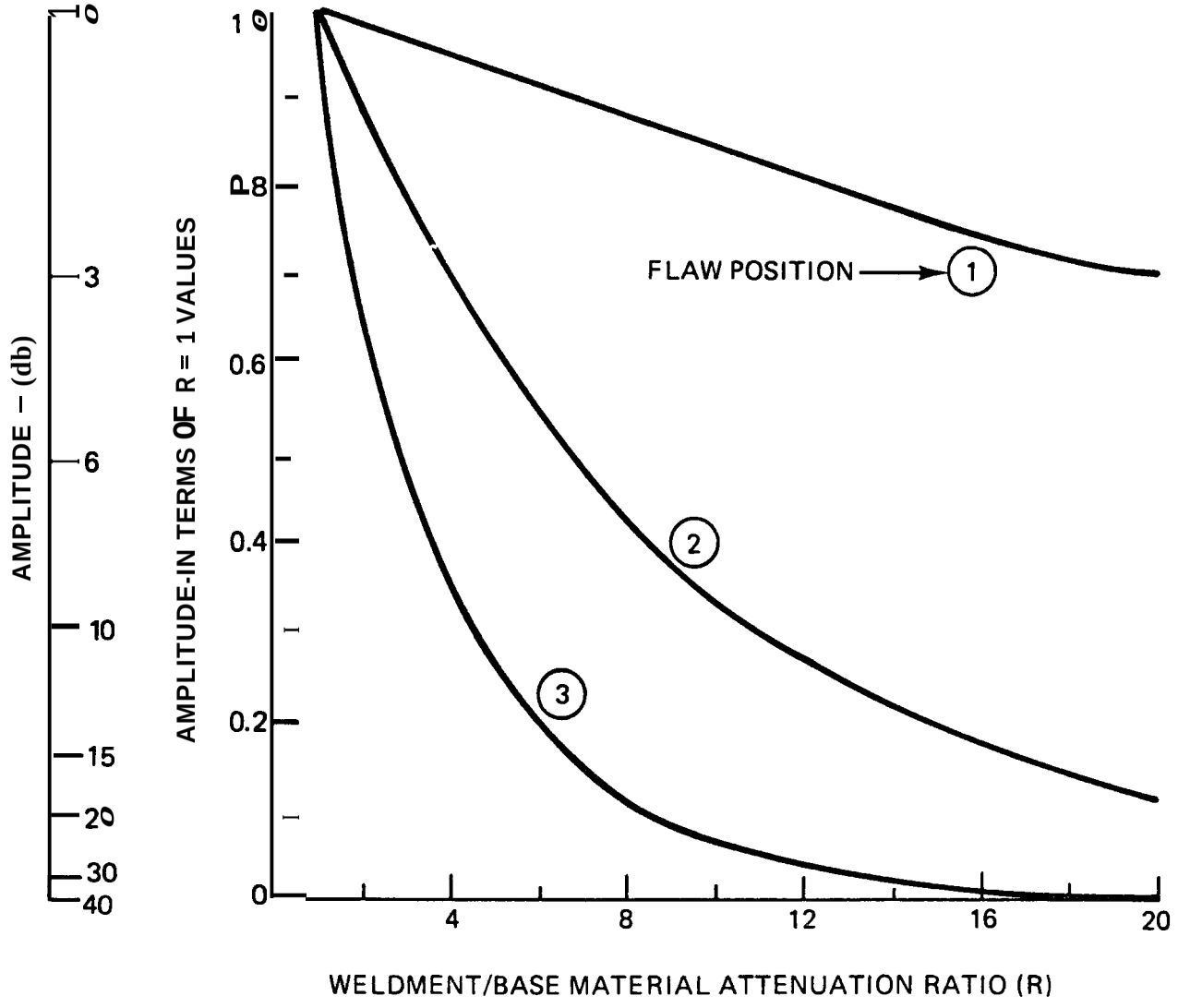

Figure 78 - The maximum amplitude from the three flaws of Figure 76 as a function of the ratio of the weldment/base material attenuations. A base material of 0.25 db/in was used.

From equation 12 and Section VI it can be seen that the correction for attenuation (C_α) is:

$$C_a = e^{2\alpha_b (s_b + Rs_w)} \qquad (11)$$

An on-line computer can be used to continually correct the observed amplitude data for the influence of attenuation. This assumes that the flaw can be accurately located; a reasonable assumption. The parameter x, the distance of the transducer from the weldment centerline, can be continually measured by the linkage assembly diagrammed as Figure 79. Linear potentiometers can produce the θ angles and the linkages ℓ_1 and ℓ_2 can be adjusted to suit the anticipated transducer motion. The measurement of the base material attenuation would offer no problem; however, the measurement of the weldment attenuation would require developmental efforts. This is primarily due to the anisotropic attenuation characteristics of weldments. The measurement problem is a significant one, but its solution is highly feasible -- even on an on-line basis.

b. Flaw Characterization

Flaw characterization for the conventional flaw detection technique is based upon the amplitude from the flaw. Prior to any assessment of this technique, it is necessary to select an amplitude standard. The ASME Boiler and Pressure Vessel Code offers a series of side drilled holes or cylindrical reflector standards which are chosen in accordance with the thickness of the material being evaluated; see Figure 80. These standard side drilled holes are used to generate the appropriate DAC curves used to evaluate indications noted within the weldments. Since it is easier to analytically formulate the amplitude response from planar reflectors, experimentation was performed to relate the amplitudes of these two types of standards. Figure 81 indicates the experimental results of the comparison of the amplitude response from 1/8" diameter side drilled and flat bottom holes. Also, shown are the theoretical results predicted by Ermolov[66]. It would appear that the indicated experimental and theoretical results are of the same form; however, the experimental results have very little sensitivity to frequency.

Using the equations below, the amplitudes from Figure 81 can be transposed into any combination of planar and cylindrical reflectors.

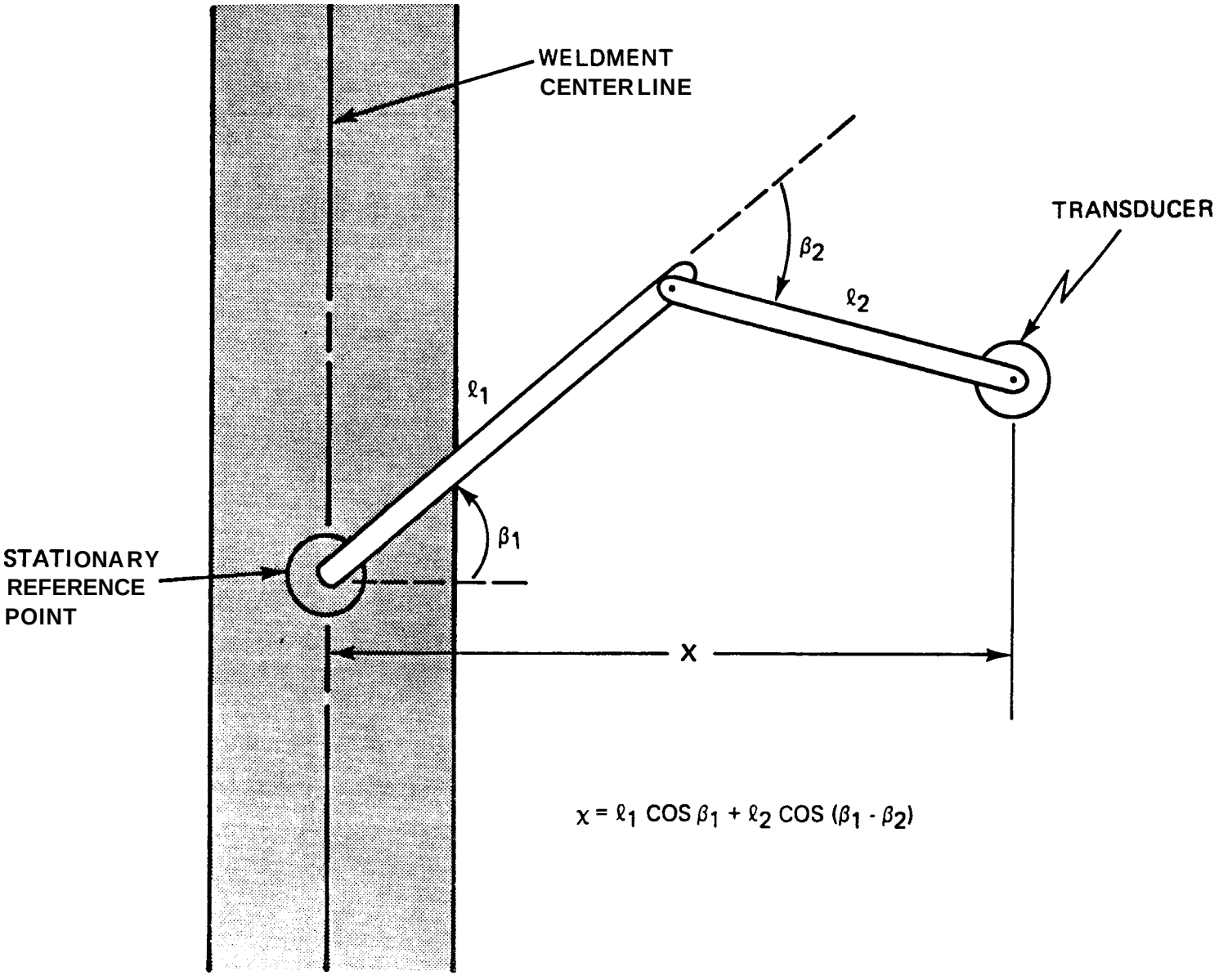

Figure 79 - A possible linkage system for monitoring the distance of the transducer from the centerline of the weldment.

Material Thickness	Reference Side Drilled Hole diameter-inches
1" - 2"	1/8
2" - 4"	3/16
4" - 6"	1/4
6" - 8"	5/16
8" - 10"	3/8

Figure 80 Reference holes for establishing DAC curves for angle beam interrogation of weldment. From ASME Boiler and Pressure Vessel Code (1977 edition).

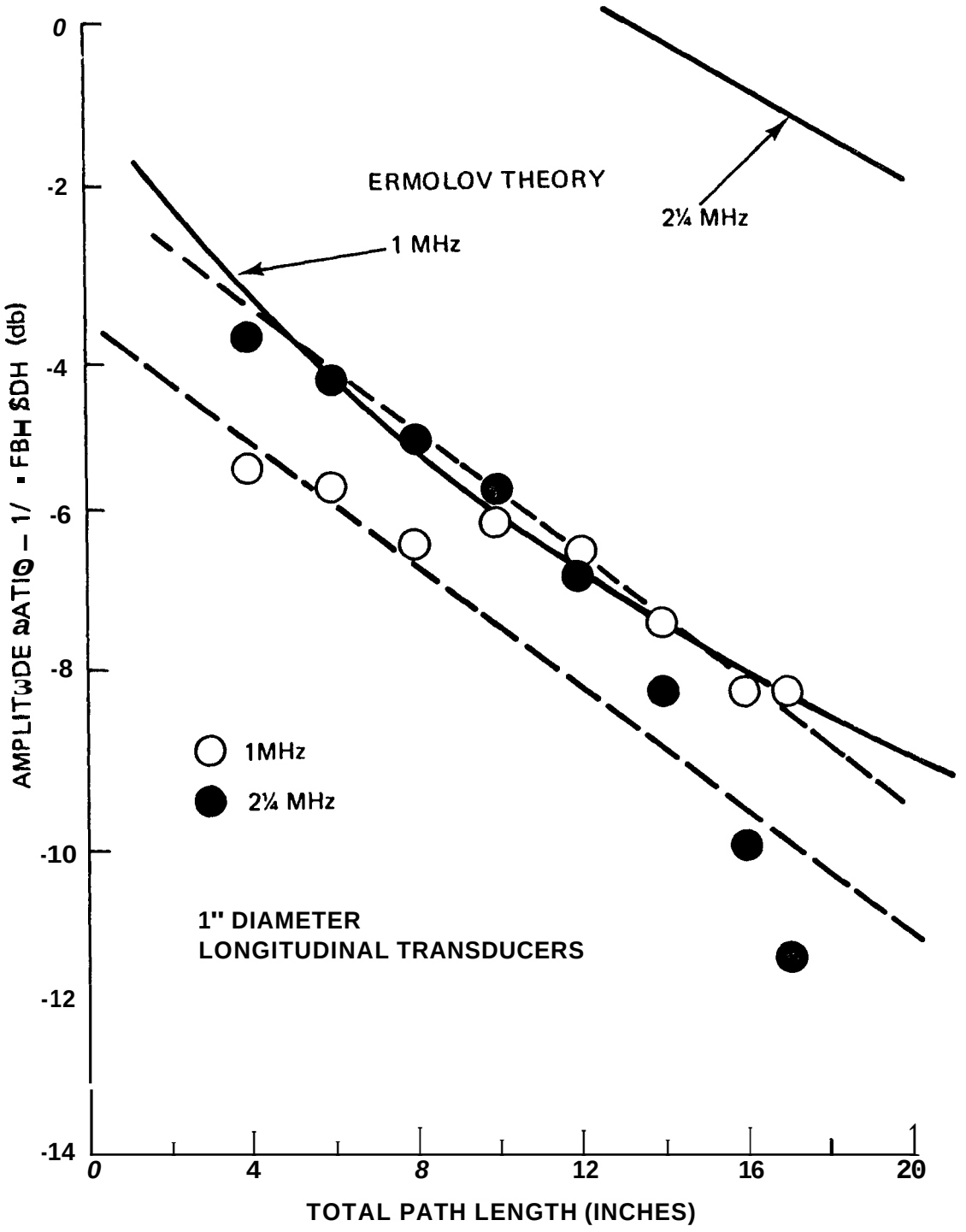

Figure 81 - Distance dependency of the ratio of the amplitudes from 1/8" diameter flat bottom to side drilled holes.

$$A_{SDH} \sim \sqrt{d_c}$$

$$A_{FBH} \sim d_p^2 \qquad (16)$$

where A_{SDH} and A_{FBH} are the amplitudes from cylindrical and planar reflectors of diameters d_c and d_p, respectively. It was found that a 1/4" FBH can adequately approximate the standards used for weldments up to 10" in thickness. As shown below the amplitude from a 1/4" FBH is within ±9 db of the particular DAC curve involved.

Material Thickness	Standard SDH	$\frac{A_{1/4\ FBH}}{A_{std\ SDH}}$	
2"	1/8"	2	(6 db)
5"	1/4"	0.28	(-2 db)
10"	3/8"	0.36	(-9 db)

The above calculations were made by the use of Figure 81 and Equation 16. It is assumed that the flaw is located at a metal distance equal to 1 1/2 nodal distances.

Using a 1/4" diameter reflector as a standard, the amplitude reflector-size displays of Figure 82 to 85 were generated by calculations using the analytical model. Four transducers were used -- i.e., 1/4, 1/2, 3/4 and 1" diameters. These displays assume that the interrogation technique has been properly calibrated for flaw distance and attenuation; all amplitude degradation is due to reflector misorientation. For each transducer display, the zero-degree misorientation line may be used as a reference from which to measure the amplitude degradation due to reflector misorientation. It will be assumed that the limit of the detecting ability is 20 db below the 1/4" FBH sensitivity level. Below this sensitivity level detection is not possible regardless of flaw size or orientation. The latter is well within the dictates of the American (ASME) and German codes for nuclear construction practices.

The ability to characterize the size of an indicated reflector based upon amplitude alone may be obtained by the use of the 1/2" diameter transducer data display of Figure 83. It can be noted that a 1/2" reflector with misorientation angles of 8^o and 4^o would be characterized as approximately 1/8" and 3/8", respectively. Figures 86 through 89 summarize the size characterization ability for the four transducers of this study. It is obvious for even the 1/4" diameter transducer that sizing errors up to two orders of magnitude are

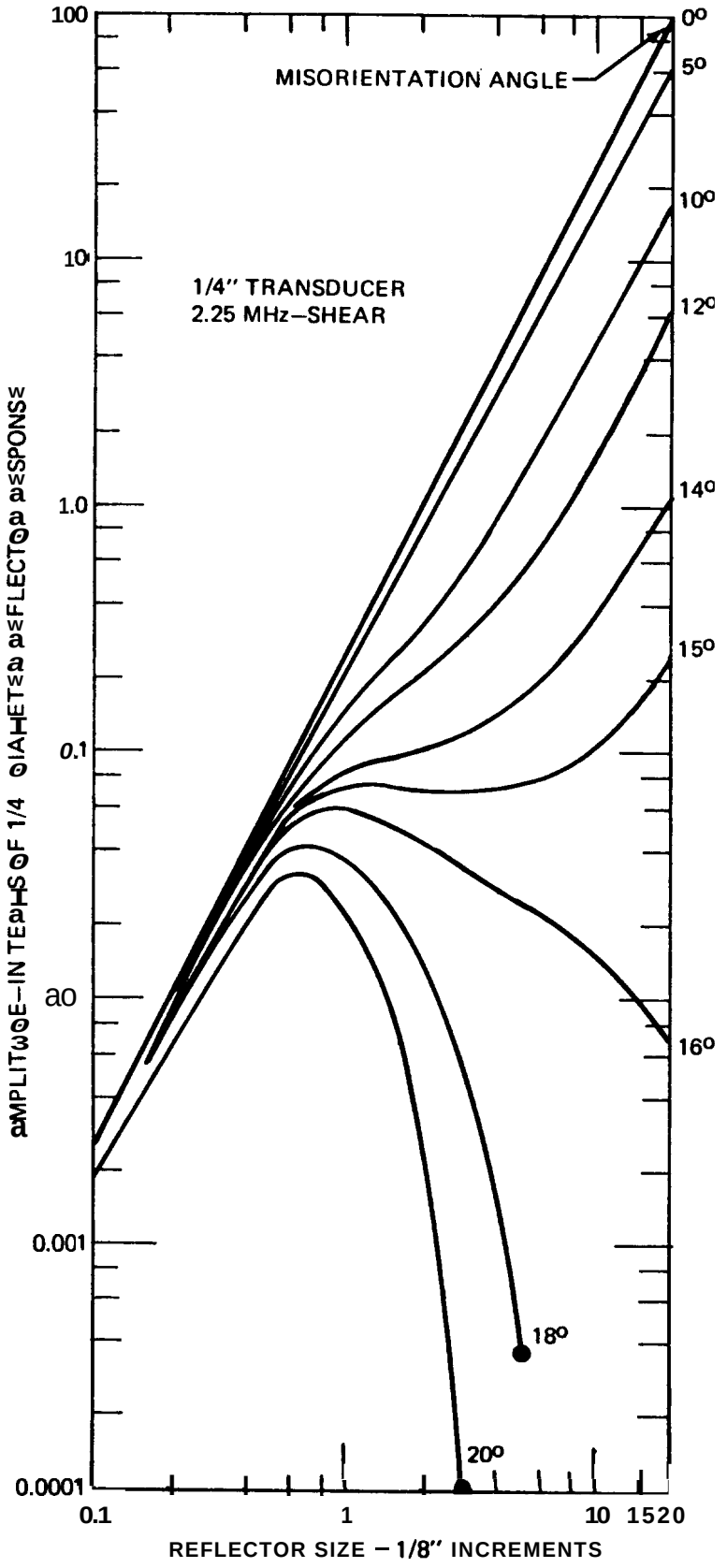

Figure 82 - Influence of flaw misorientation upon the angle shear beam interrogation process for a 1/4" diameter transducer at 2.25 MHz.

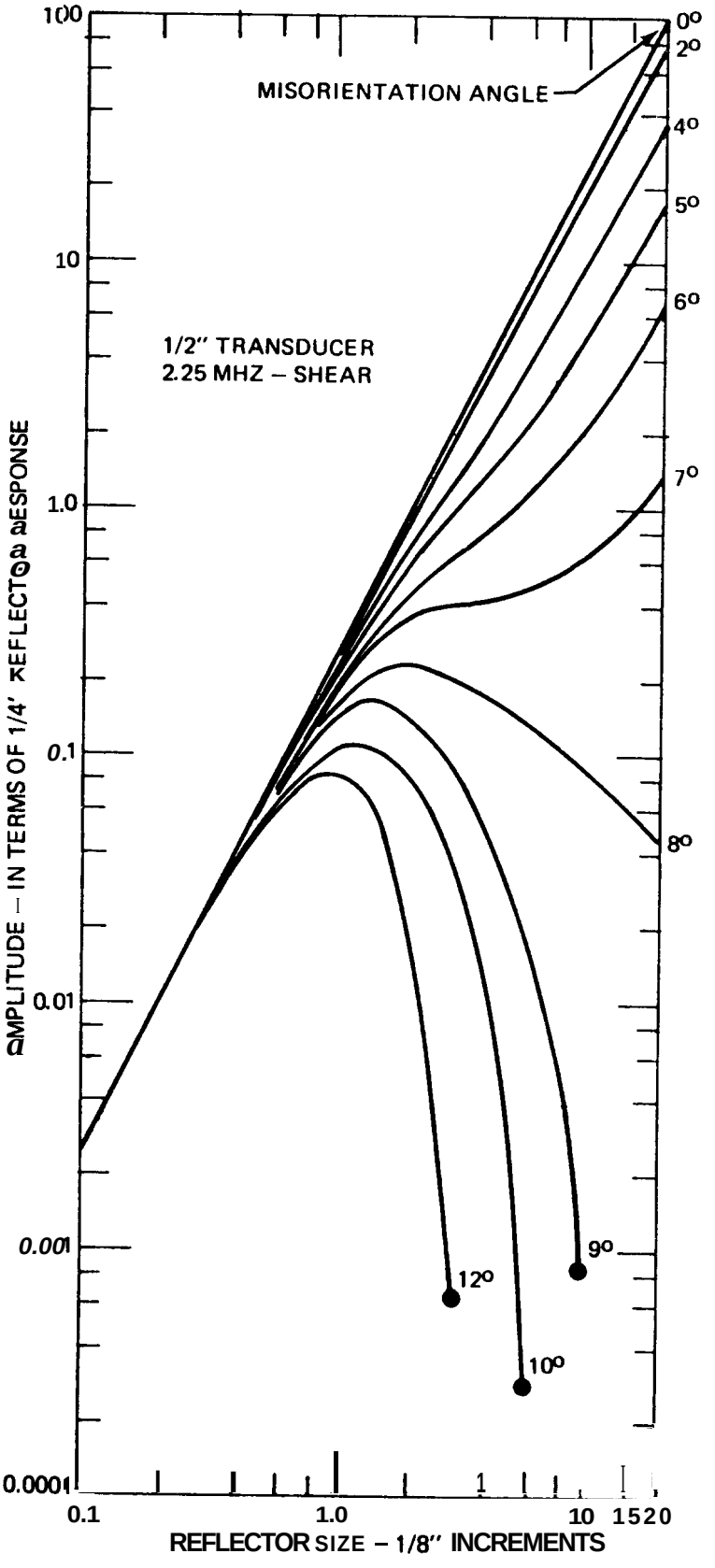

Figure 83 - Influence of flaw misorientation upon the angle shear beam interrogation process for a 1/2" diameter transducer at 2.25 MHz.

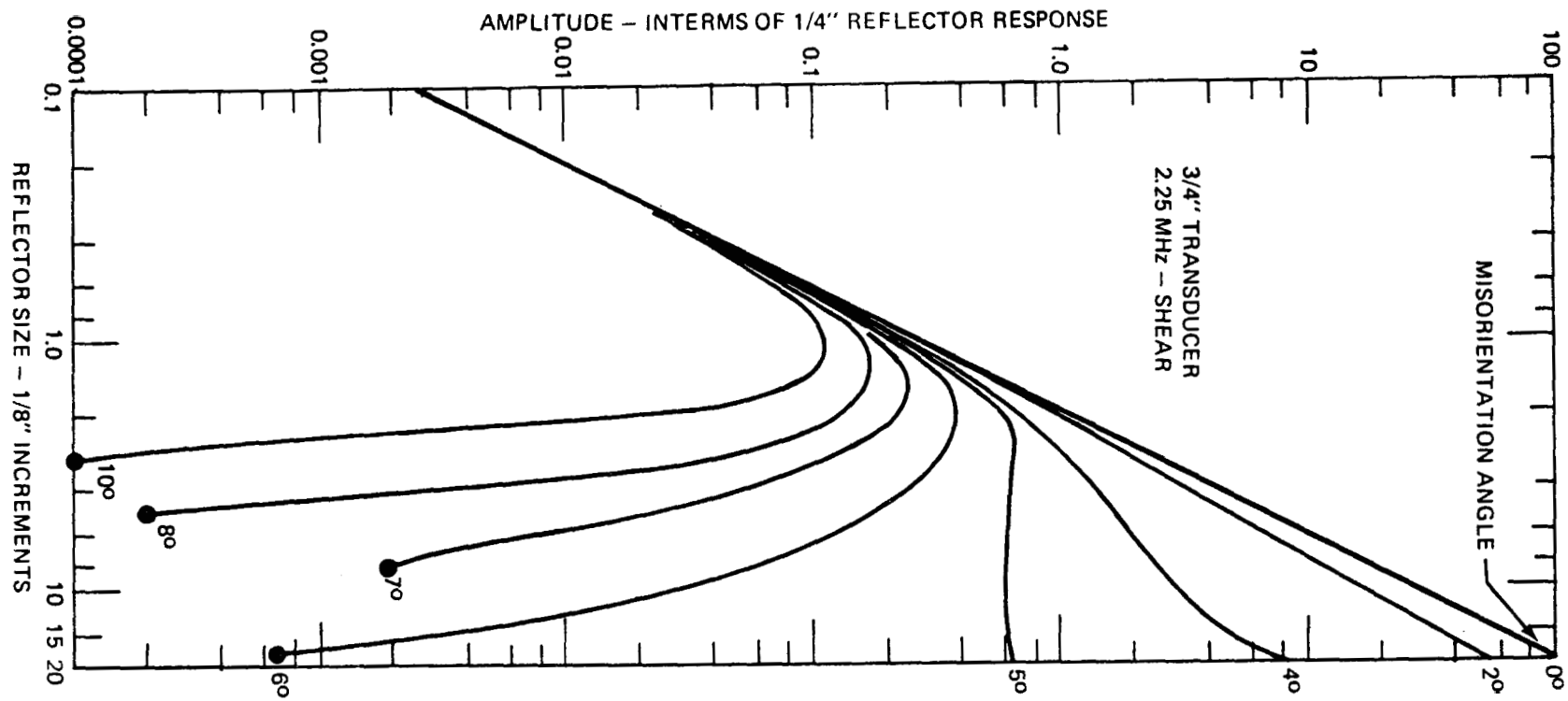

Figure 84 - Influence of flaw misorientation upon the angle shear bean interrogation process for a 3/4" diameter transducer at 2.25 MHz.

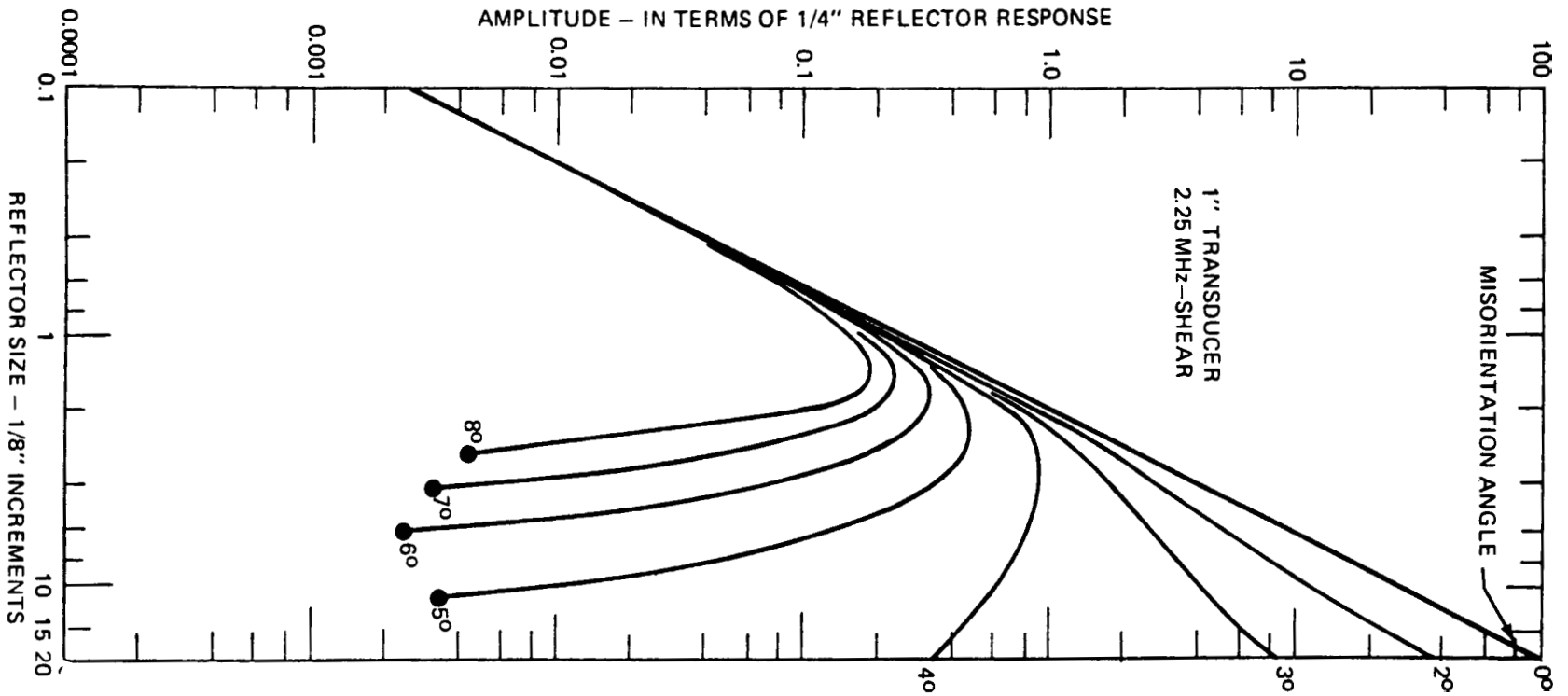

Figure 85 - Influence of flaw misorientation upon the angle shear beam interrogation process for a 1" diameter transducer at 2.25 MHz.

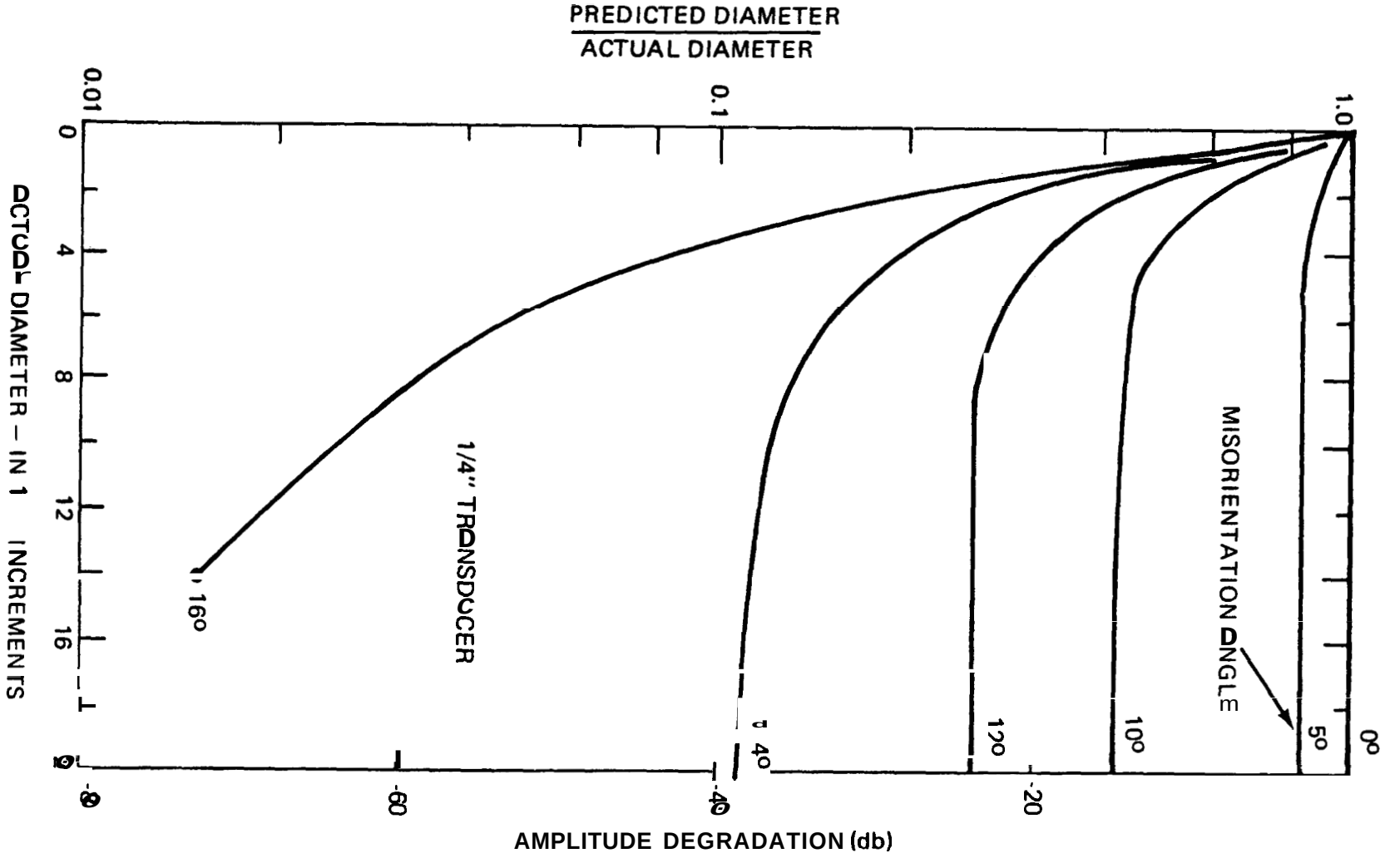

Figure 86 - *Size* characterization *of* misoriented flaws based upon amplitude considerations by a 1/4" shear angle beam transducer.

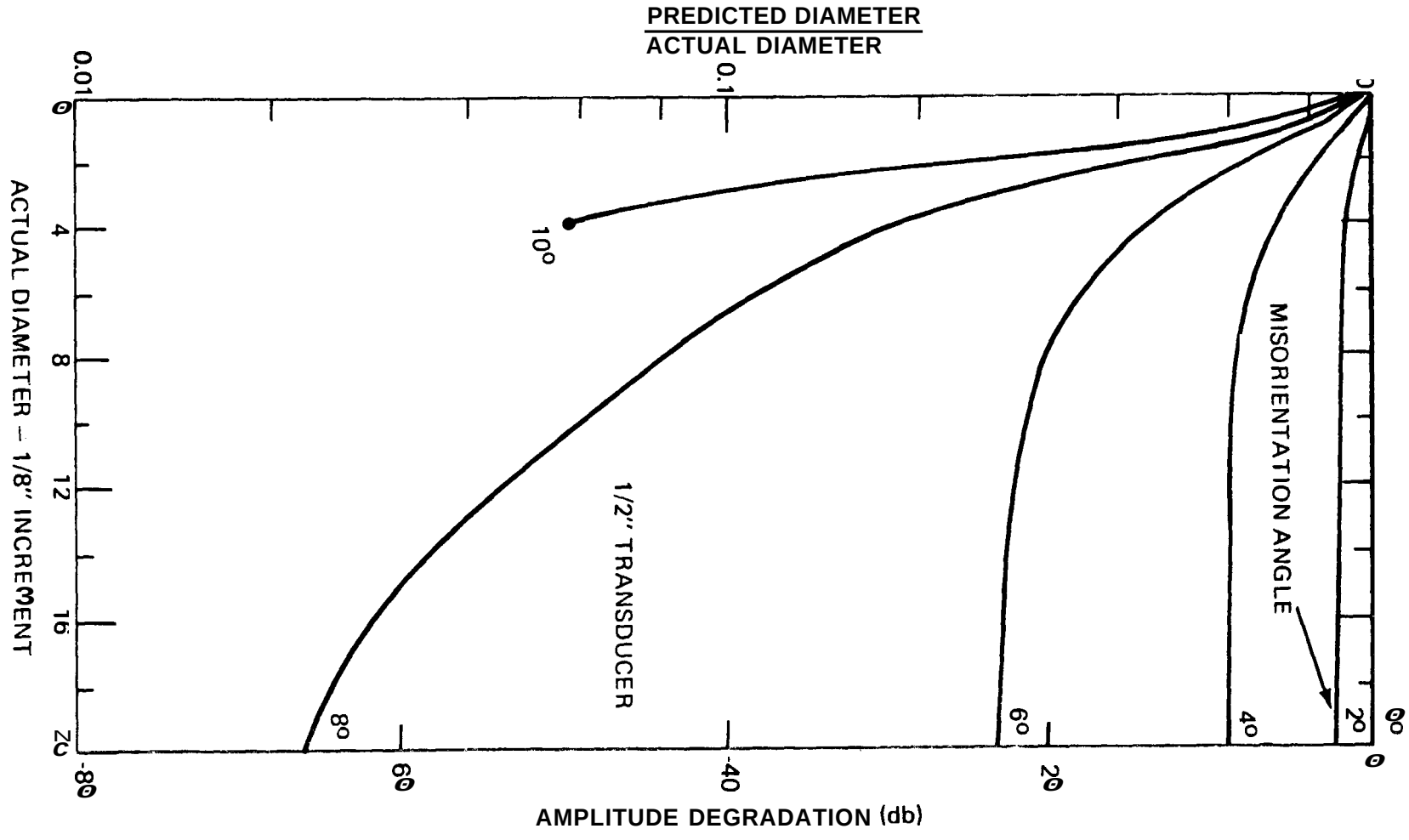

Figure 87 - Size characterization of misoriented flaws based upon amplitude **considerations** by a 1/2" **shear** angle beam transducer.

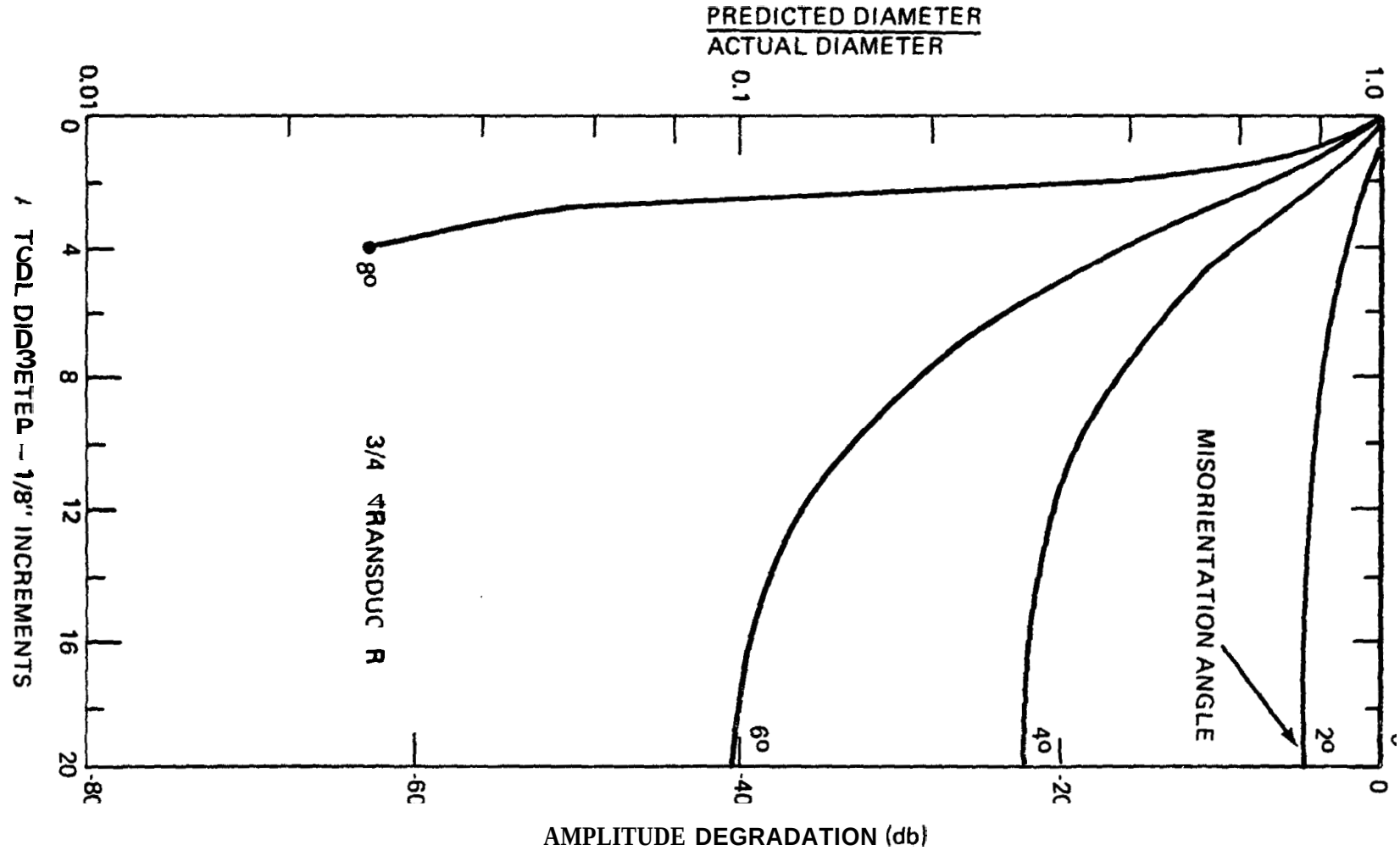

Figure 88 - Size **characterization of misoriented flaws based upon amplitude considerations by a** 3/4" shear **angle** beam **transducer.**

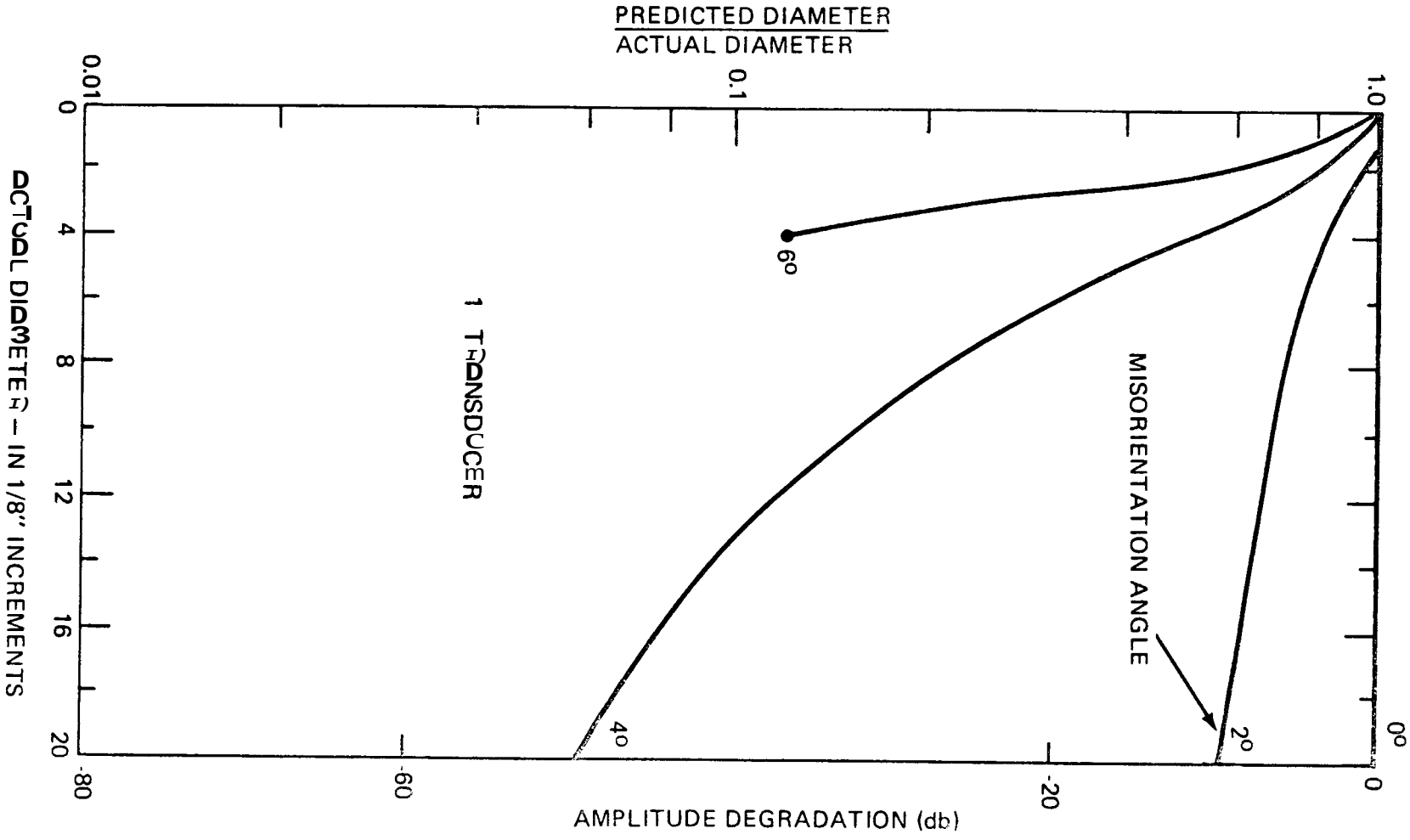

Figure 89 - Size characterization of misoriented flaws based upon amplitude considerations by a 1" shear angle beam transducer.

possible. The extent of the sizing error is governed by the misorientation of the flaw with respect to the interrogating beam. Errors due to attenuation (see Figure 78) and improper calibration (see Figure 54) can also significantly contribute to the indicated error.

c. Reliability of Flaw Characterization

Perhaps the most meaningful reliability studies of the nondestructive methodhave been in the area of surface flaws. Programs dealing with the NDT reliability associated with the detection of subsurface or volumetric flaws are very limited and void of quantitative analysis.

There are unique advantages for studies involving surface crack detection as compared to the detection of subsurface flaws. First, it is possible to generate cracks similar to those found in the natural state: Chin Quan and Scott[76] indicate a compendium of such methods. This is not the case for subsurface flaws. In fact, the simulation of subsurface natural flaws is difficult, if not impossible. Second, in controlled experimentation, the true lengthsfor surface flaws are available to fonn the basis of any analysis.

The work of Packman[1,2,3] and Chang, et al.,[4] form the most complete study to date of the reliability of surface NDT methods. Packman used 7075-TG511 aluminum and high strength D6AC steel plates. Fatique cracks were formed by three point bending with the cracks originating from an initial laser or weld solidification point; crack lengths ranged from 0.008 to 0.25 inches. The plates were finally machined to 4" x 8" x 0 500" and caustic etched to remove 0.0005 inches of the machined surface. Of the total specimen population, approximately SO% did not contain any flaw:;. The specimens were submitted to the operators in groups of 20 to 30 and resubmitted a number of times to obtain sufficient data at each crack length range. Figure 90 shows the penetrant data. To be assured that the small size cracks take on realistic detection probabilities, the total crack spectrum was divided into intervals such that each interval had the same number of cracks. The top line within each interval is the point estimate of the probability as obtained by the ratio of the number of flaws detected to the total number of flaws in the interval. The next three lines down

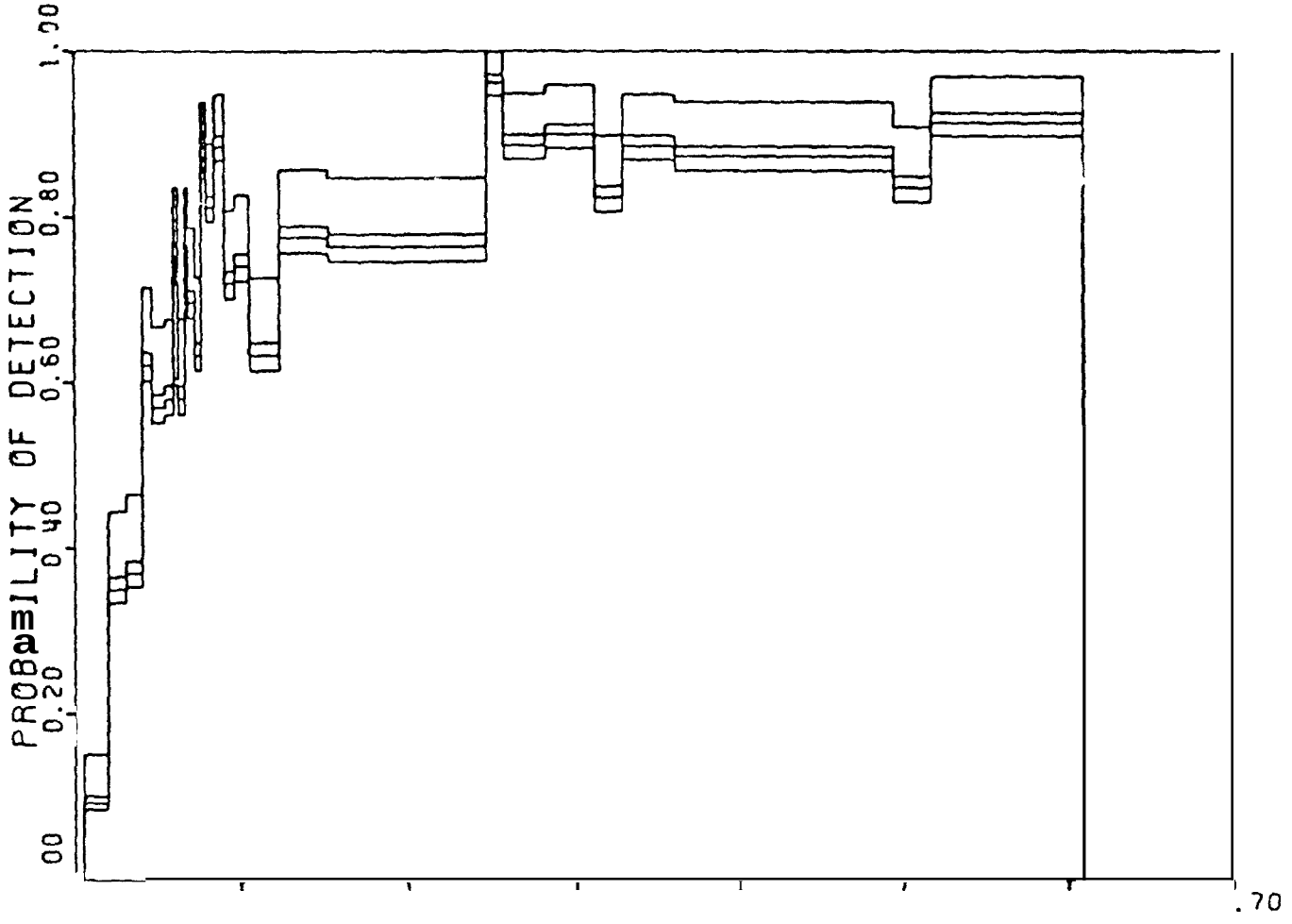

Figure 90 - Plot of probability of detection *as* a function of flaw *size.* The top line is the point estimate; the next three lines are the 90, 95 and 99% confidence interval estimates. Aluminum penetrant inspection *with* equal number of observations in each flaw size **range.** After Packman (1).

are indicative of the 90, 95, 99% confidence limits. Note that at a 95% confidence limit there is a 62% probability that cracks less than 0.050 inches in length will not be detected; the 90% detection probability occurs for cracks larger than 0.25 inches in length. Figure 91, displays Packman's results for the magnetic particle method on the steel specimens; any cracks less than 0.040 inches in length are essentially undetectable. Comparing Figure 90 and 91, it would appear that the magnetic particle inspection on steel is not as reliable as a penetrant inspection on aluminum.

Thus far, the above analysis has really only considered one event, i.e., detection of a flaw when a flaw exists. Unlike most such measurement schemes the unsuccessful inspection passes prior to detection are not recorded. In actuality, there are four possible events that can take place; see Figure 92.

1. Detection of a flaw when a flaw is present.
2. Missing a flaw when a flaw is present.
3. Indication of a flaw when a flaw is not present.
4. Verification that no flaws are present.

In the ideal sense events 2 and 3 are undesirable. These events are interrelated, thus, one must use conditional probabilities to analyze any given event. The influence of false calls (event 3) can be significant from the standpoint of economics. Figure 93, illustrates a situation of two liquid penetrant operators whose false call levels are at 6% and 36%, respectively. The top curve is the inherent and optimum reliability of the procedure and is based upon the ratio of the number of flaws detected to the number of flaws known to exist adjusted to the 95% confidence limit. The probability of detection of the procedure/operator is seen to degrade rapidly as the number of false calls increases. Again, an operator with a large number of false calls prompts one to question if he has indeed detected a bonified or real flaw, thus the reliability of the procedure is in doubt or less reliable.

The above analysesof surface flaw detection and characterization reliabilities were presented to indicate the scope of the work that is possible and necessary to totally define the ultrasonic reliability for subsurface flaws. The complexities of the ultrasonic method would make it a formidable task. As we have noted, the ultrasonic flaw characterization of subsurface flaws involves more than a size determination. Full

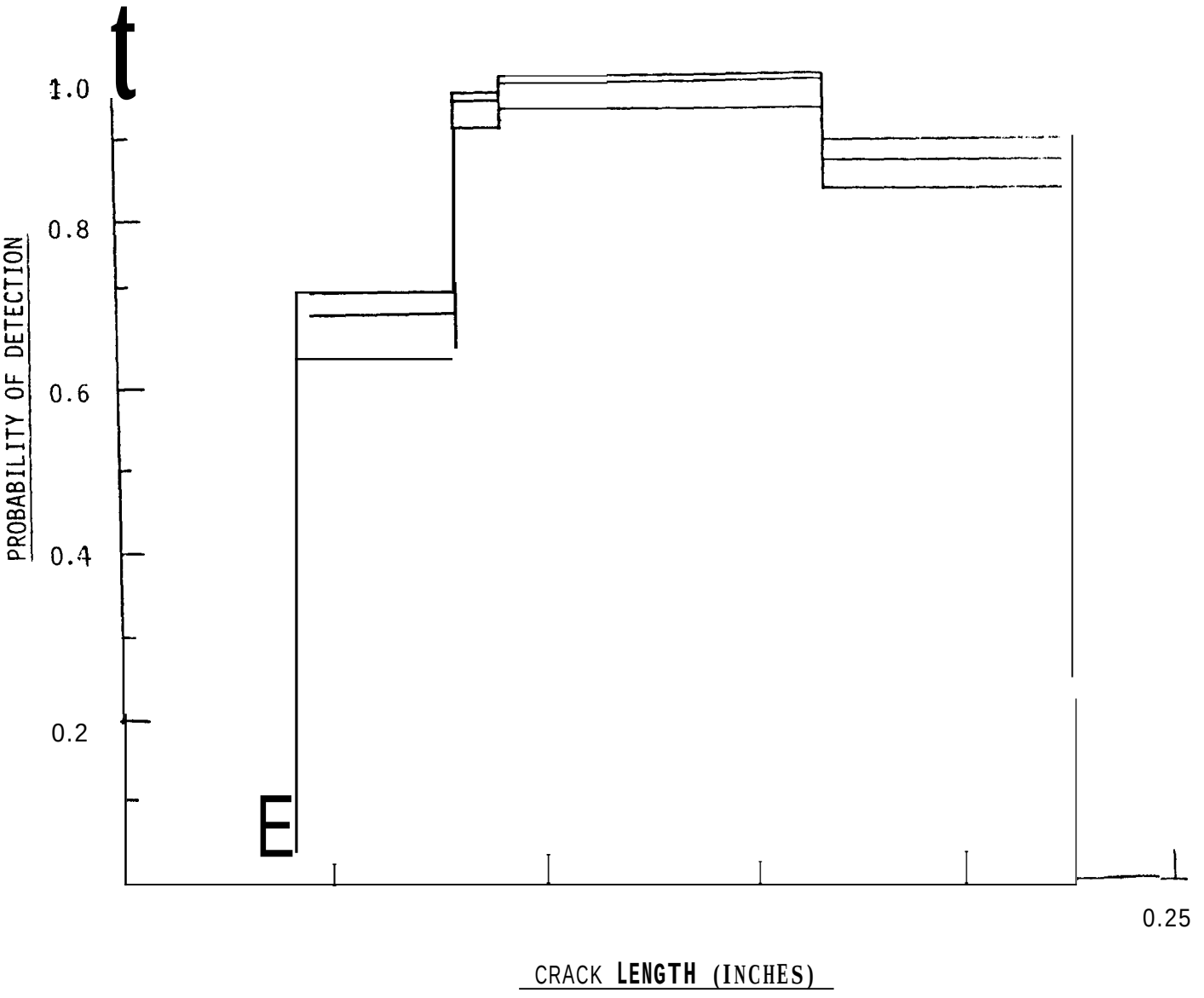

Figure **91 - Probability of detection for the magnetic particle** inspection method. **Material is steel. After** Packman **(1).**

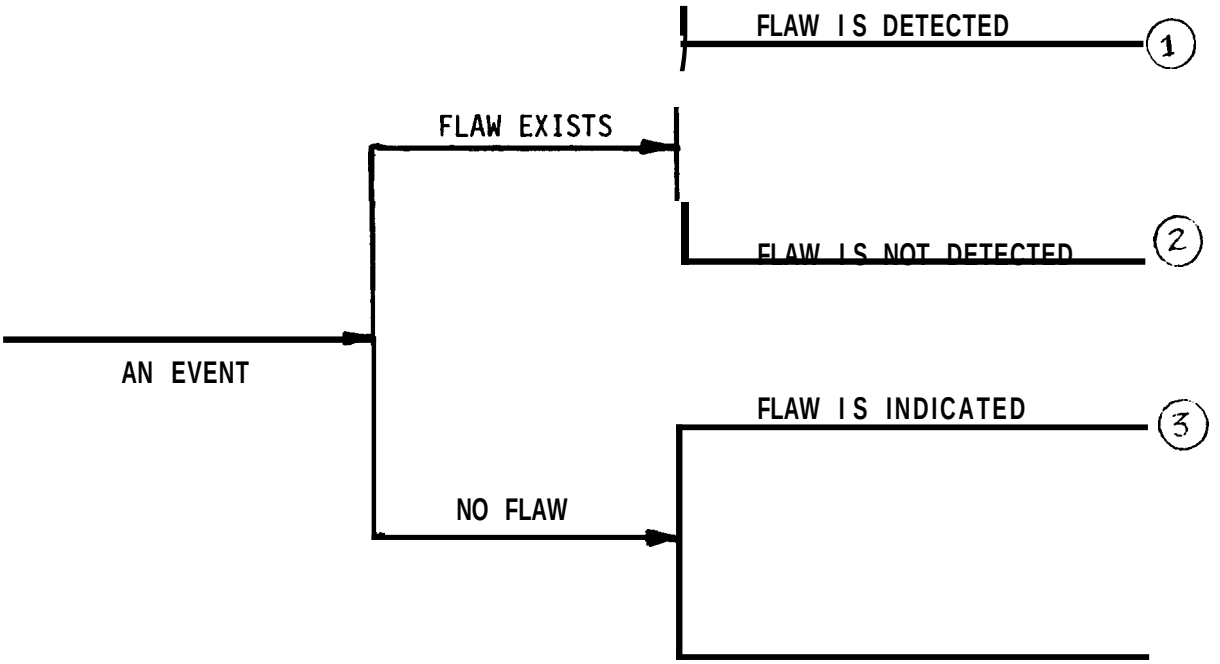

'Figure **92** - The multiple events of the flaw detection process. After Packman (1).

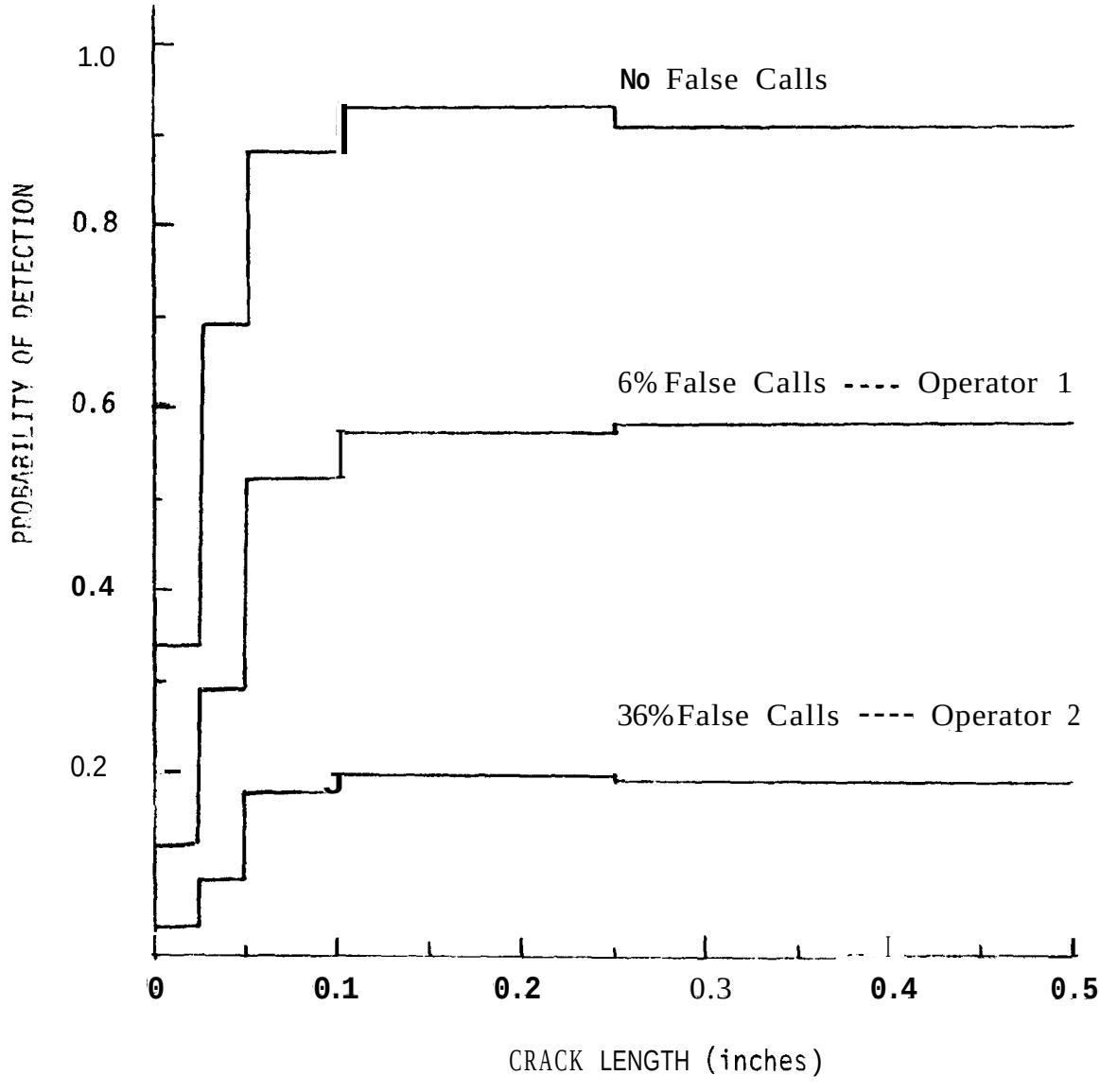

Figure 93 - Effect of false call count upon the probability of detection at 95% confidence level. The material is titanium; liquid penetrant method. After Packman (1).

characterization involves such flaw parameters as location, orientation, surface contour and roughness. The influence of the material comes into play by way of microstructure and its influence on ultrasonic propagation and the resulting radiation fields. The literature is essentially void of subsurface flaw characterization data suitable for probabilistic analysis.

One approach to the assessment of reliability for the ultrasonic detection of subsurface flaws is to generate predicted versus actual comparative data for the desired flaw characterization parameter to be studied -- e.g., size, orientation, etc. Such data would be highly dependent upon the circumstances of the particular interrogation scheme. The ability of the analysis of the data to note and separate each governing effect would not necessarily be possible. If the sampling number is sufficiently large, the data can place limits upon the reliability for the ultrasonic procedure to generate a given flaw characterization. Such reliability data can be incorporated into product design requirements.

Another approach, the one we shall consider in this report, is to subdivide the broad study of reliability into systematic and random contributions. The systematic contribution is void of such effects due to equipment, procedure, and the human influence of the operator. The latter are responsible for the random contributions of reliability. These random effects and the extent of their degradation of the overall flaw detection and characterization process may be studied individually.

Some random effect studies have been reported in the literature, however, they must be greatly expanded to allow analysis based upon probabilistic concepts. Hedden reported on the influence of the operator. (") Figure 94 presents the outcome of a round-robin involving five operator teams inspecting weld specimens containing ten flaws. The operators averaged 66% detection or in more alarming terms -- they missed 34% of the flaws. Also, an average of 2.4 false indications were recorded. The errors possible in flaw coordinate determinations has been a subject of interest. [24,25,26] The influence of uncertainties in velocity, entry angle, and attenuation upon flaw coordinate measurements is treated in terms of systematic and random error analysis. The results indicate an appreciable effect. The matter of highly attenuating material has led to suggestions that the ASME Boiler and Pressure Vessel Code be limited to essentially medium strength low allow steels and to eliminate austenitic and bi-metallic welds involving such materials as inconel. [55]

Team	Detected	Reported False Indicationd	Missed
A	5	0	5
B	9	2	1
C	5	6	5
D	7	3	3
E	7	1	3

Figure 94 - The results of a study considering ultrasonic operator error. After Hedden (55).

The systematic contribution of reliability may be viewed as the optimum inherent detecting ability. A possible method of studying this systematic contribution of the reliability is by mathematically modeling the processes involved. Each model should include as many influencing parameters as possible and should be verified by extensive controlled laboratory experimentation. The success of the model used throughout this report indicates its usefulness for the appraisal of the reliability of the angle beam interrogation method. The model is indicative of those physical elements responsible for the amplitude response from a flaw and includes the influence of the flaw size and misorientation with respect to the interrogating beam, transducer size and material attenuation. The literature also indicates the adaptability of the model to include flaw surface roughness[6]. As shown in Figures 76 through 78, the influence of attenuation involves geometric considerations of weld size and shape as well as flaw location, thus its effect cannot be generalized. Therefore, it appears fruitful to start with a model which initially only includes flaw size and misorientation and to add other material, flaw and calibration effects which require specific information on a given flaw/material/procedure combination. For this reason, the model as expressed by Equation 2 and the 2 1/4 MHz data displays of Figures 82 through 85 will be used.

There are some basic statements that must be made. The amplitude response from a 1/4 inch flat bottom hole oriented perpendicular to the interrogating beam and located at the same distance as the flaw of interest will be used as a standard. The latter eliminates function F_3 of Equation 2. An amplitude cutoff level of 20 db below the reference amplitude will be in effect. The detection process will be taken as a go or no-go event. There will be no differentiation in detection due to the amplitude involved -- detection is accomplished once the cutoff amplitude level is exceeded. In other words, all detection events have either a zero of 100% probability of detection (POD).

Consider the POD for the 1/4" diameter transducer (Figure 82). Using the detection criteria stated above, one can generate the dotted line POD displays of Figure 95. Figure 95 indicates that once a threshold or minimum flaw size diameter of 1/8" is exceeded the detection of all flaws whose misorientation angle is less than 14^{o} is a certainty - i.e., a POD of unity.

For flaws with misorientation angles of 14° and 15° the same statement can be made except for the fact that a larger threshold flaw size is required. For example, for 15° a threshold flaw size diameter of 9/8" is necessary. However, once a misorientation of 15° is exceeded, no flaw, regardless of size, will be detected - i.e., POD is zero for such flaws. The abrupt discontinuity of the POD at the detection threshold flaw size for each misorientation should be much less to indicate the fact that smaller amplitudes are less susceptible to detection. The solid lines are totally arbitrary and serve to illustrate this fact and are in line with Figures 90 and 91 for POD of the penetrant and magnetic particle flaw detection system. One can propose that the slopes involved should be governed by the slopes of the amplitude-size-orientation displays of the appropriate transducer -- i.e., in this case, Figure 82. In any event, Figure 95 does show that one can associate a POD with a given flaw at a specified misorientation with respect to the interrogating beam.

Figures 96 through 98 show the POD for the 1/2, 3/4 and 1 inch diameter transducers, respectively. In accordance with the amplitude-size-orientation displays of Figures 83-85, the POD can attain certainty and then be completely eliminated because of flaw misorientation. In Figure 96, for misorientation angles of 8° and 9° the POD drops abruptly to zero if the flaw size exceeds 9/8" and 3/8", respectively. As in the case of the 1/4" transducer of Figure 95, if the flaw misorientation exceeds a given value (9° in this case), detection of any flaw is impossible. It should be noted that the maximum misorientation angle where detection is possible to some extent decreases with transducer size; compare Figures 95 through 98. The slopes of the decreasing POD curves (dotted) are those arbitrarily used in Figure 95 and are justified by the fact that larger misoriented flaws are more difficult to detect. The latter is because of the limited width of the amplitude response envelope. As to be expected the narrow radiation fields of the larger flaws and transducers can greatly limit the POD. It is for the latter reason as well as attenuation effects that have led to the use of a longitudinal wave angle beam. In general, the shear wave attenuation can be an order of magnitude higher than its longitudinal counterpart. The decided advantage for using a longitudinal wave can be seen in Figure 99 which was generated from the amplitude-size-orientation data of Figure 100. It should be noted that the critical misorientation angles have doubled. Another approach to obtain wider radiation fields is to consider lower interrogation frequencies; see Figures 101 and 102. The detection advantage is obvious.

It has been shown that the probability of detection for a given size flaw is governed by the transducer size, misorientation angle and frequency. The notion that the POD can decrease as the flaw size increases is in direct contradiction to the reliabilities of the surface flaw detection where the POD is a monotonically increasing function of flaw size. It should be emphasized that Figures 95 through 102 are representative of the optimum probability of detection. There are still many sources of error to be considered such as a combination of flaw distance and attenuation, flaw and interrogation surface roughness and contour, and improper calibration procedures.

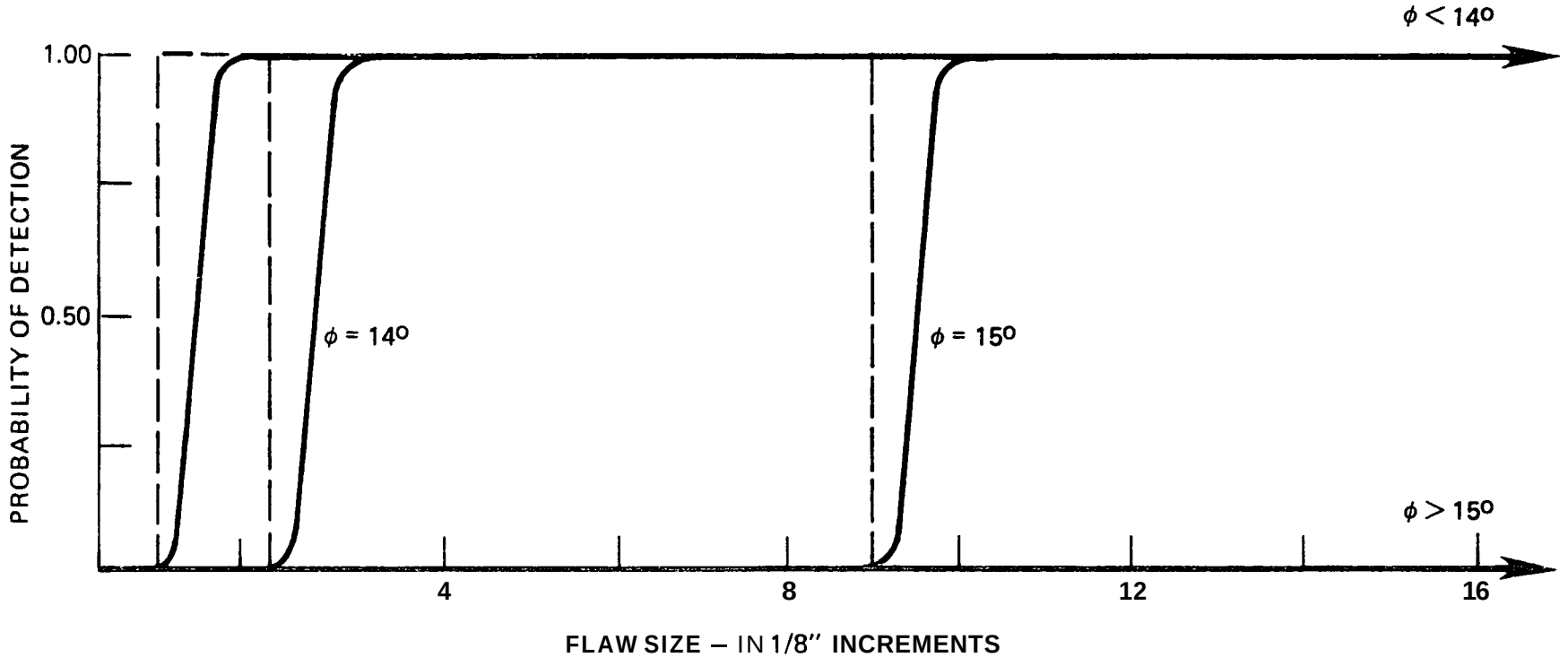

Figure 95 - The systematic contribution of the Probability of Detection for misoriented flaws for a 1/4" - 2.25 MHz angle shear wave transducer.

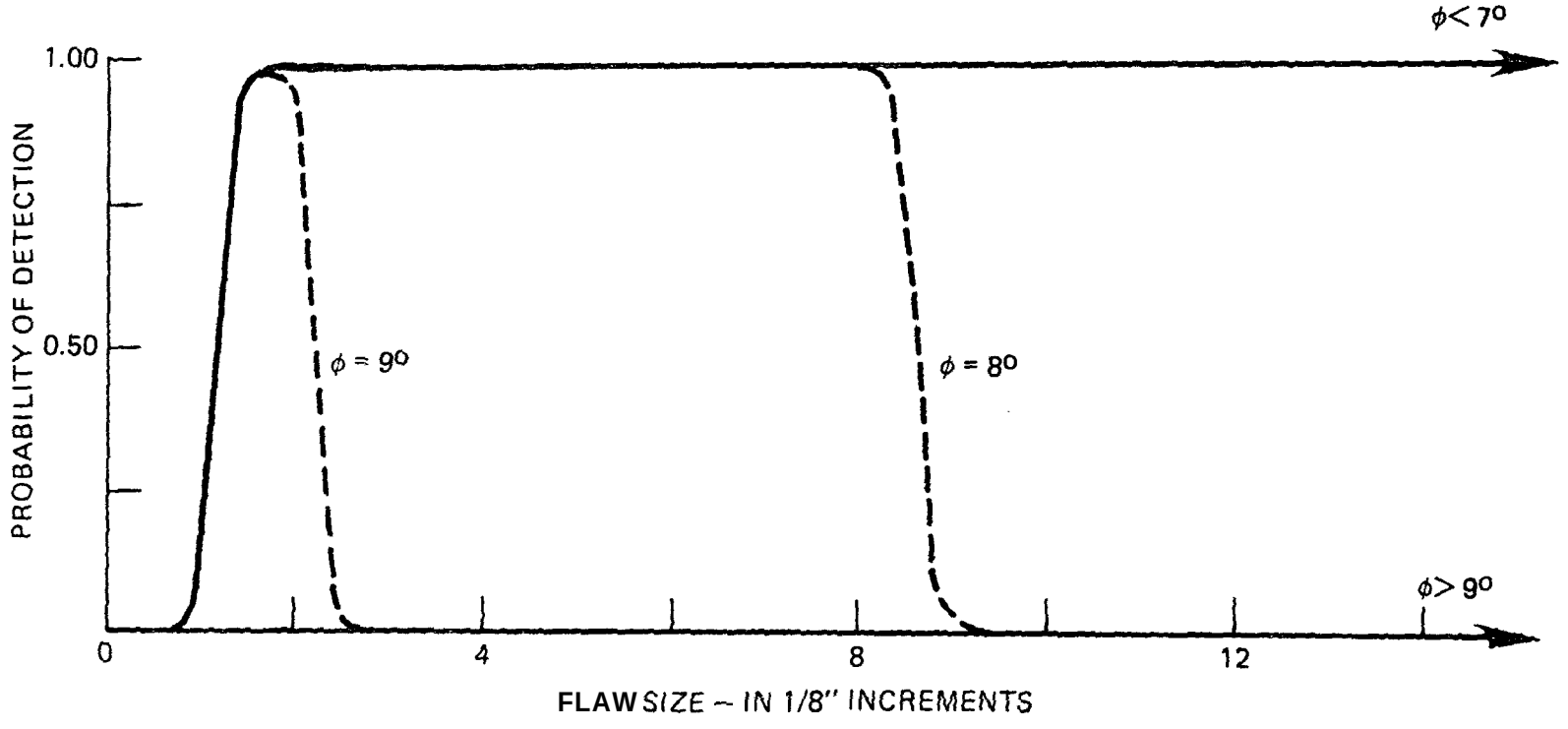

Figure 96 - The systematic **contribution** of the **Probability** of **Detection** for **misoriented** flaws for a 1/2" - 2.25 MHz angle shear wave *transducer.*

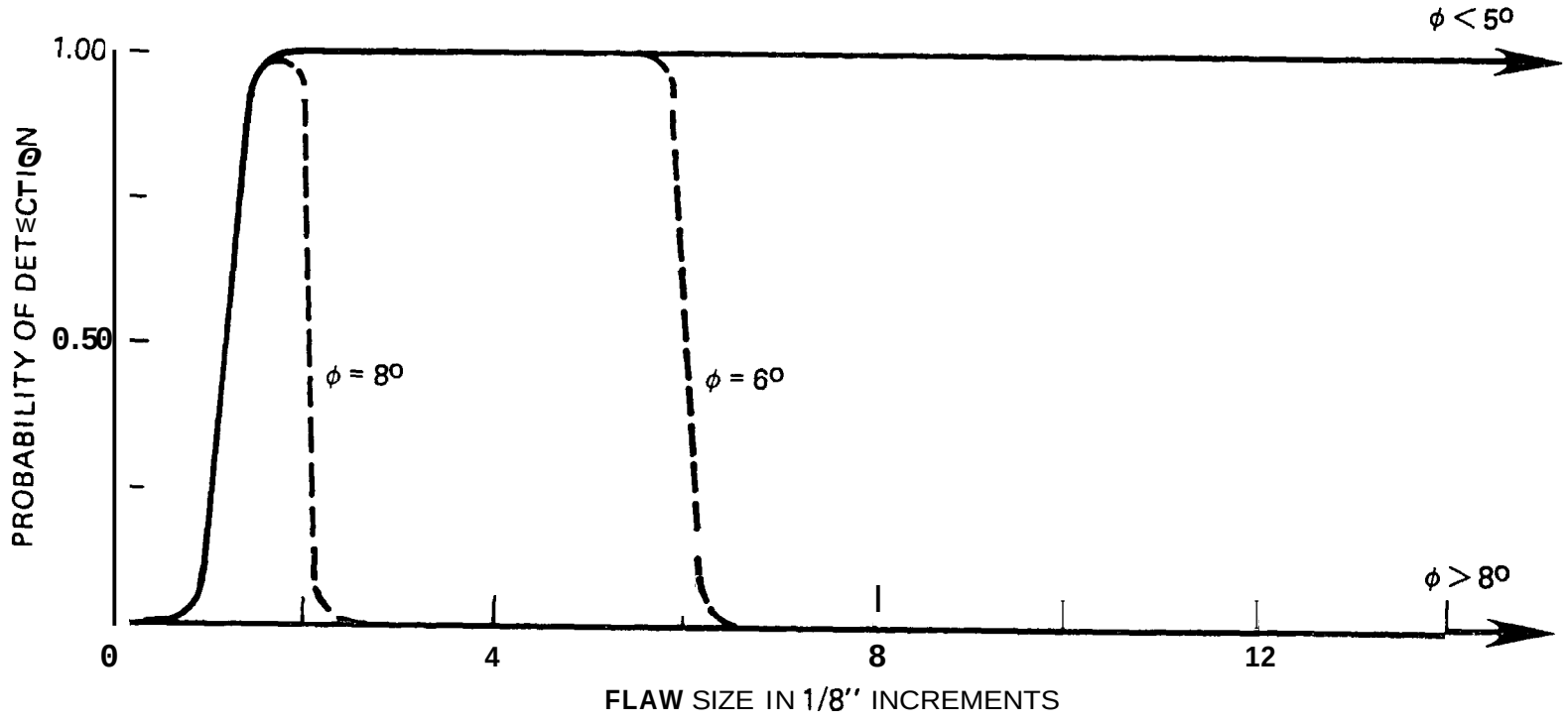

Figure 97 - The systematic contribution of the Probability of Detection for misoriented flaws for a 3/4" - 2.25 MHz angle shear wave transducer.

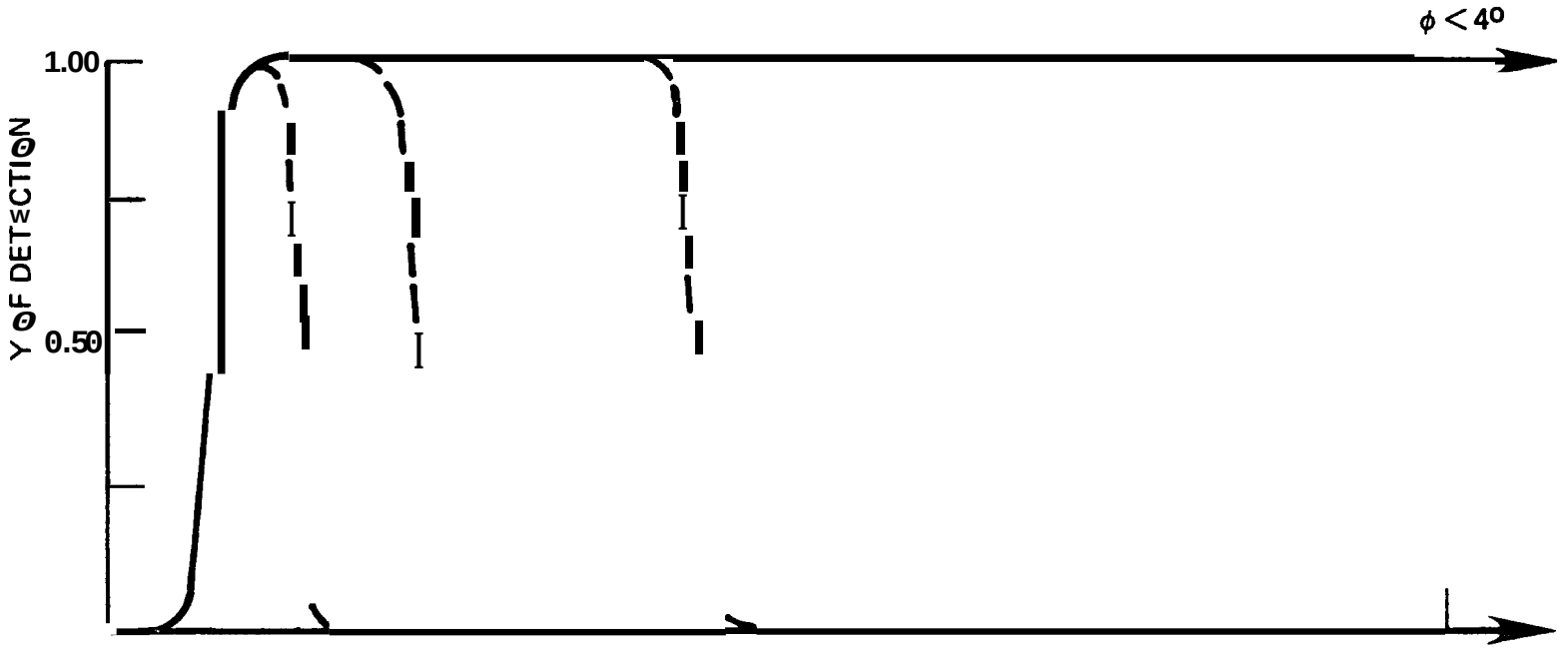

Figure 98 - The systematic contribution of the Probability of Detection for misoriented flaws for a 1" - 2.25 MHz angle shear wave transducer.

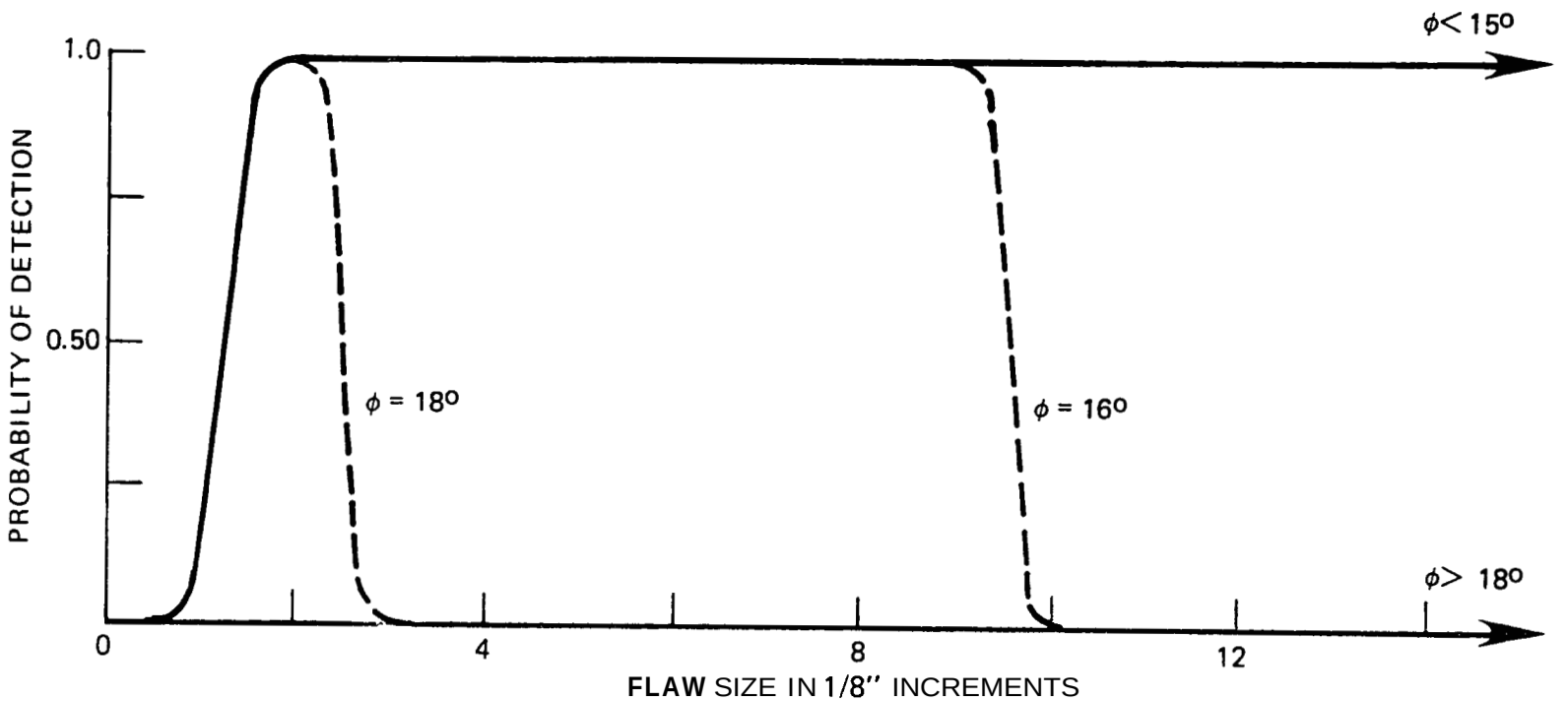

Figure 99 - The systematic contribution of the Probability of Detection for misoriented flaws for a 1/2" - 2.25 MHz angle longitudinal wave transducer.

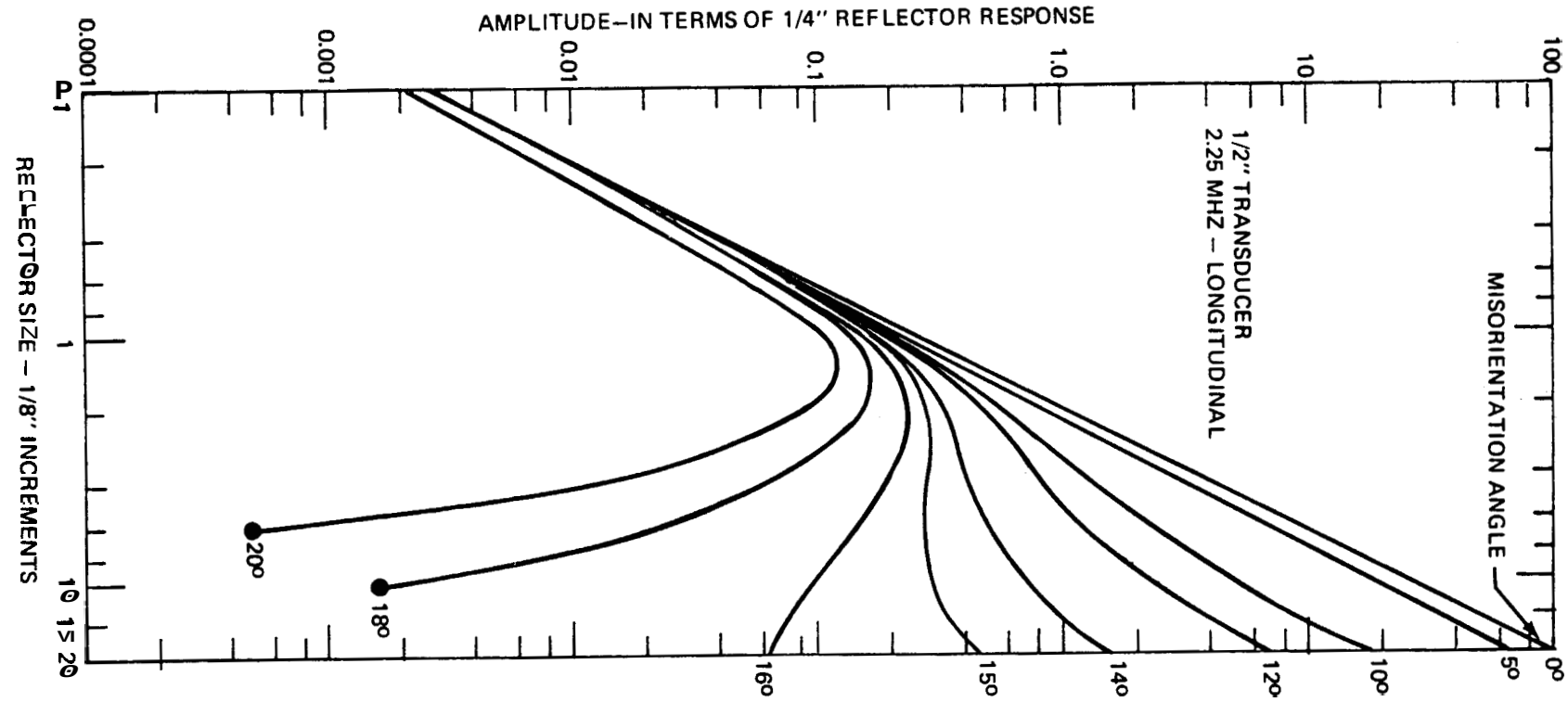

Figure 100 - Influence of flaw misorientation upon the angle longitudinal beam interrogation process for a 1/2" diameter transducer at 2.25 MHz.

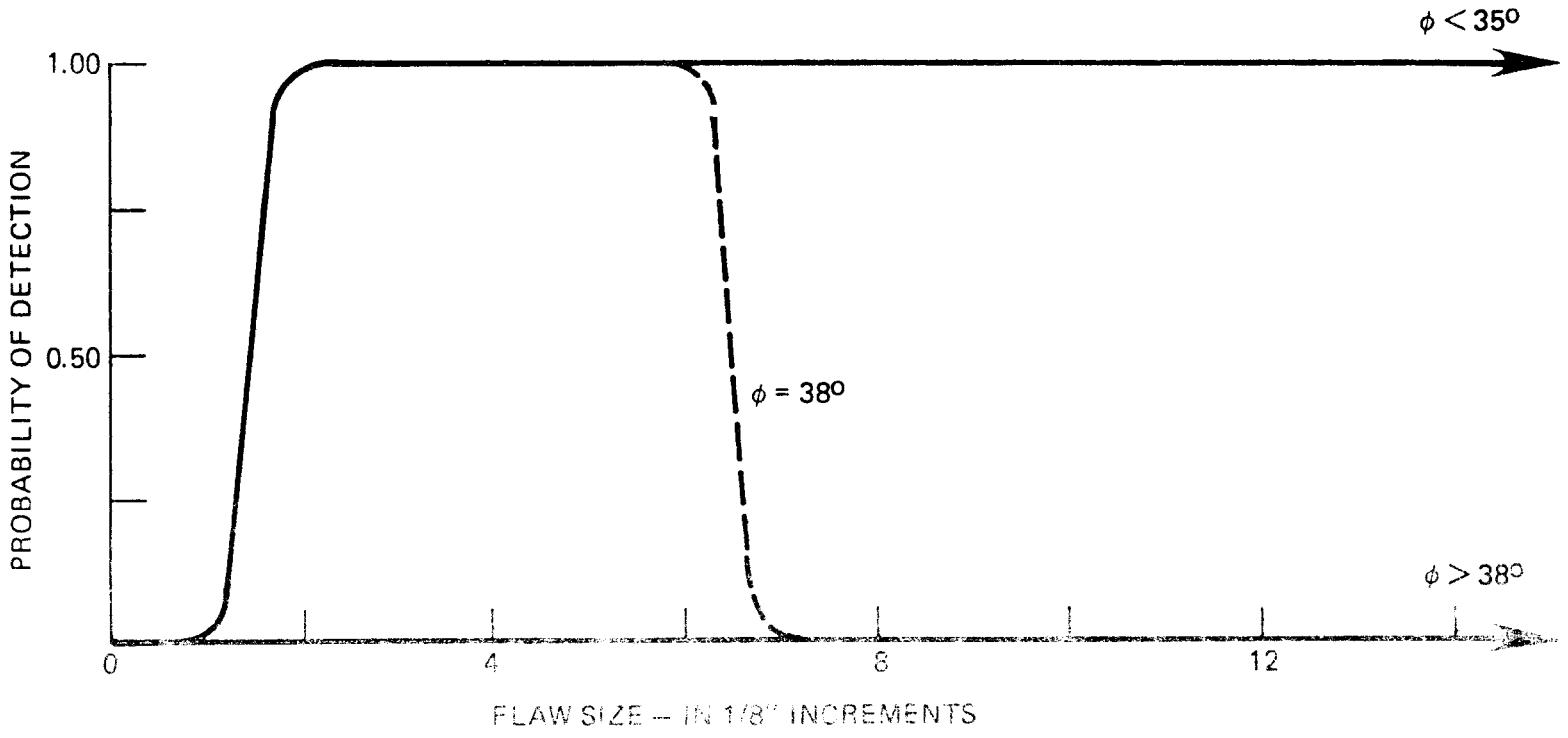

Figure 101 - The systematic contribution of the Probability of Detection for misoriented flaws for a 1/2" - 1.0 MHz angle longitudinal wave transducer.

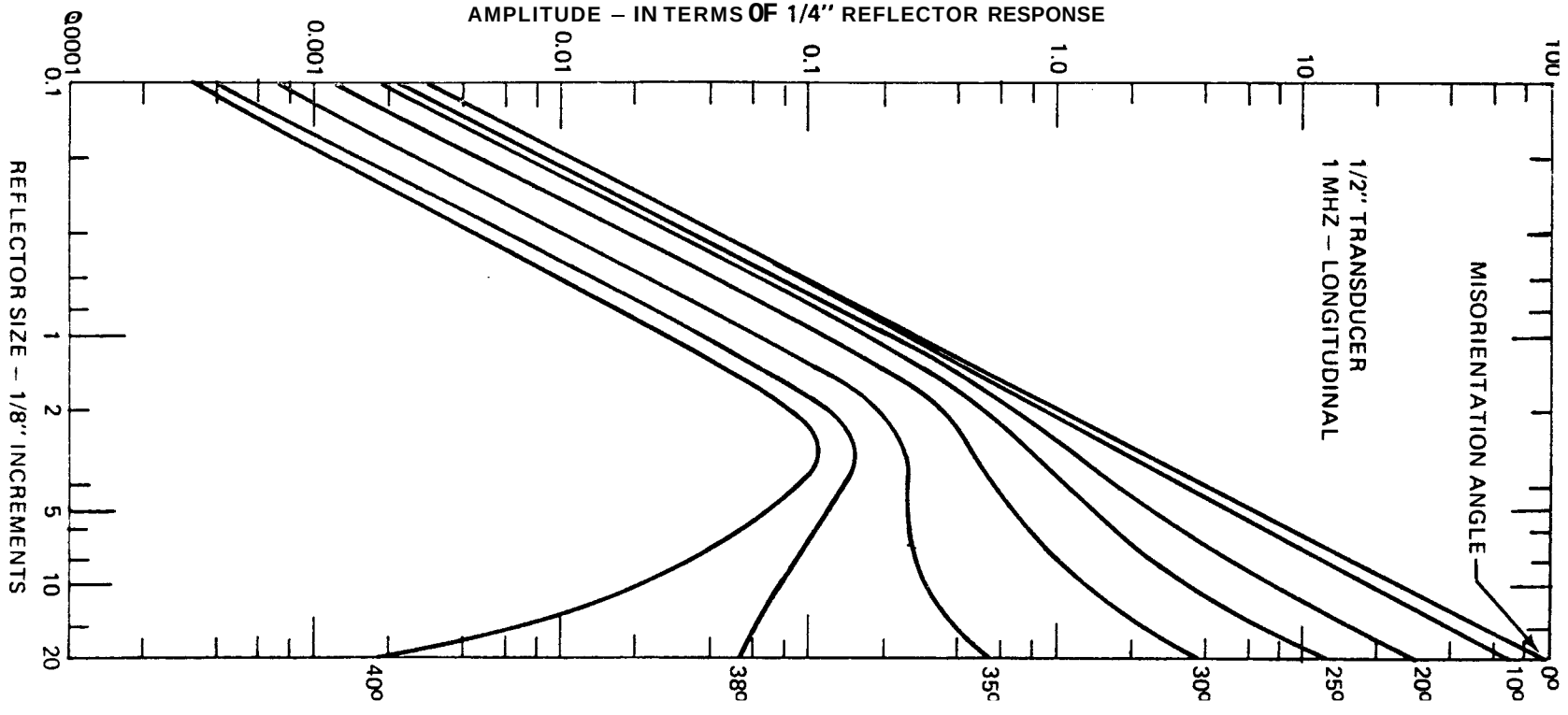

Figure 102 - Influence of flaw misorientation upon the angle longitudinal beam interrogation process for a 1/2" diameter transducer at 1.0 MHz.

2. New and Novel Flaw Characterization Techniques

a. Location of the Maximum Amplitude

As indicated in Figures 23 to 25, the location of the maximum amplitude observed during interrogation by longitudinal waves can be used to characterize the flaw in terms of size and orientation. Much the same results were found when using angle or shear waves on the blocks of Figure 66; see Figure 103. This technique has been demonstrated for characterizing simulated flaws and will be used in phase II of this program for studies involving natural flaws.

b. Spectrum Analysis

Gilmore and Czerw[48] first explored this technique in great detail however, the main impetus appeared to be to define the shape of the flaw rather than its size and orientation. The usefulness of the technique is obvious. In contrast to conventional flaw detection procedures the technique is amplitude-independent. The application of the technique is for flaw characterization and is not suitable for flaw detection purposes. The location of the flaw is a prerequisite.

Figure 104 may be used to indicate the technique. The flaw, having its normal at an angle η, is bathed by the ultrasound from the transmitter. The radiation emanating from the reflector or flaw is monitored by a receiving transducer shown indicated at the angle θ. The acoustic axis of the transducers and reflector are coplanar. The radiation reaching the receiver located at the given angle θ may be written as:

$$A(f) \sim D_T(f)\ D_F(f)\ D_R(f) \qquad (17)$$

where D_T, D_F and D_R are the directivity functions of the transmitter, flaw and receiving transducer, respectively. It is not necessary to fully quantize this equation; the parameters omitted are irrelative to this analysis. Directivity functions are usually given in terms of an amplitude-direction space for a given frequency. In this instance the directions are known such that the directivity functions are described in the amplitude-frequency space or by their frequency spectrums. The transmitter is placed directly above the

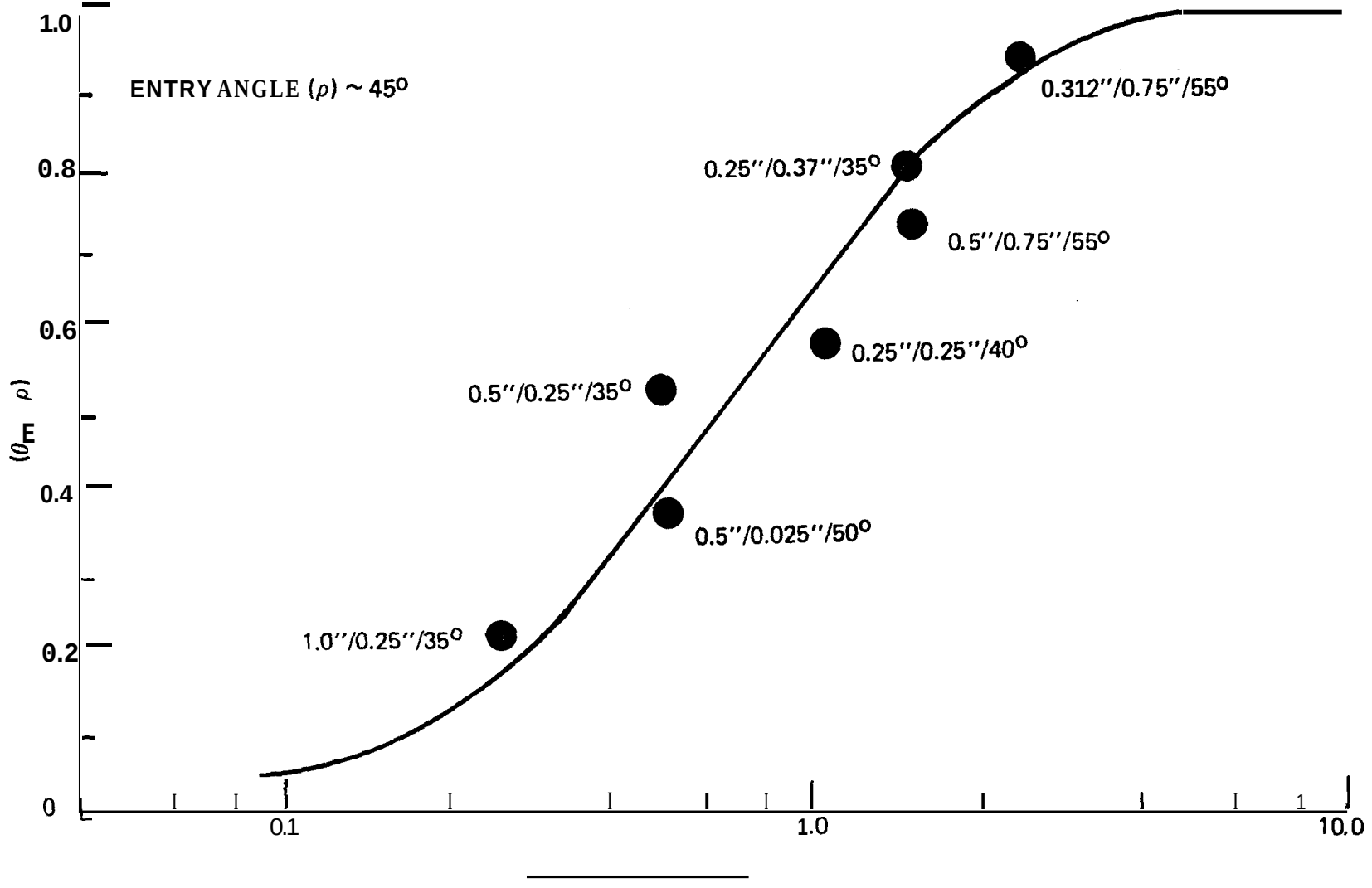

Figure 103 - The location of the maximum amplitude (θ_m) as a function of the ratio of the reflector to transducer *sites*. Each data point is given in terms of the transducer size/reflector size/reflector orientation.

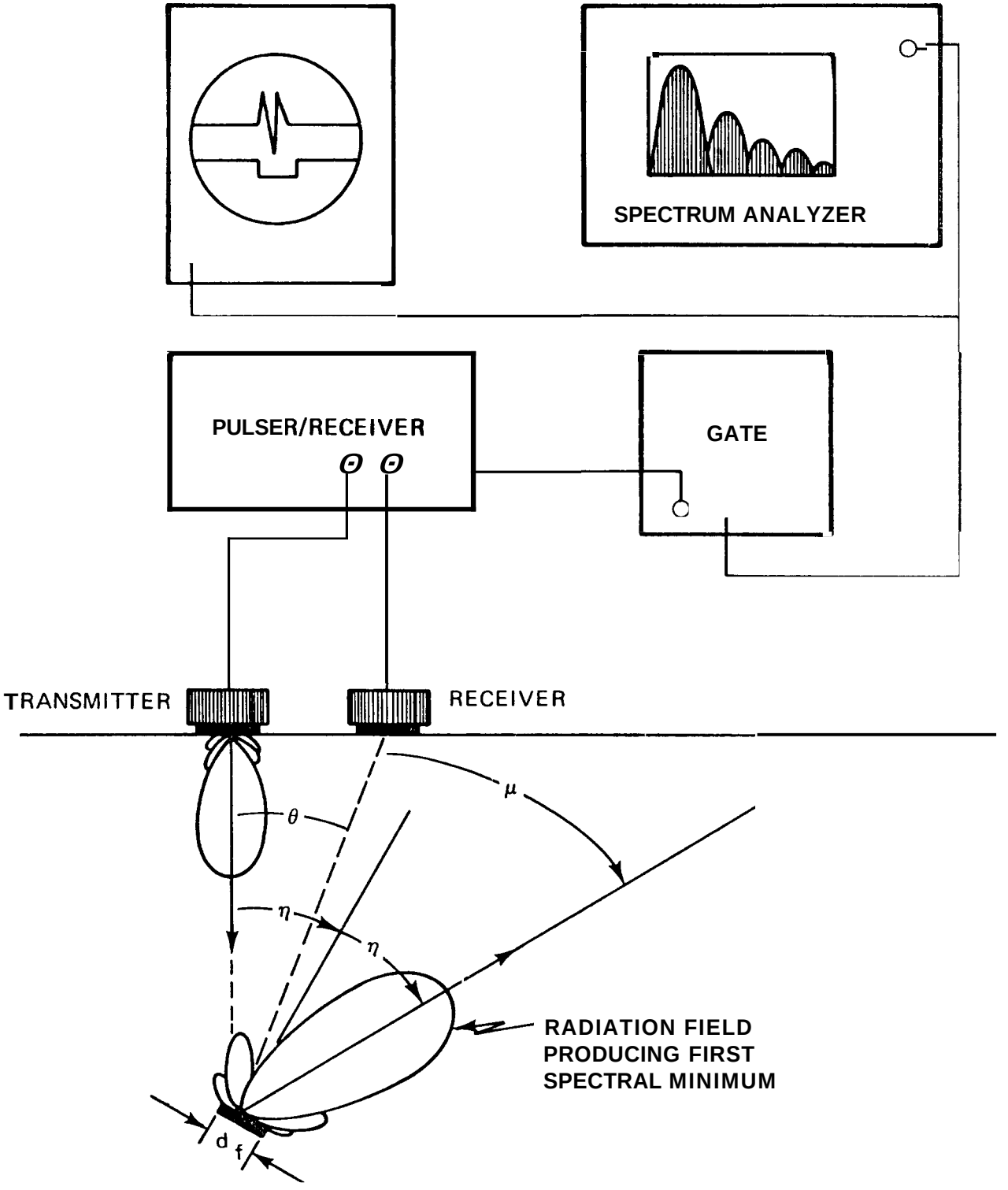

Figure 104 - Flaw characterization by the use of spectrum analysis.

flaw as acertained by minimum depth considerations while operating in the pulse echo mode. Since the centermost portion of the radiation from the transmitter is involved, its directivity function becomes unity. Therefore equation 17 becomes:

$$A(f) \sim D_F(f)\ D_R(f) \tag{18}$$

The crux of the technique is that for any given angle θ there are null or minimum points within the frequency spectrum from the flaw which are given by:

$$F_n = \frac{K_n c}{\pi d_f \mathrm{Sin}\mu} \tag{19}$$

where d_f is the diameter of the planar flaw and c is the velocity of the ultrasound. The angle μ is the misorientation angle between the receiver and the radiation from the flaw. The constants K_n are:

$$K_n = 3.83,\ 7.02,\ 10.15,\ 13.3\ \ldots \tag{20}$$

The existence of such frequency null points can be demonstrated by considering the experiment depicted in Figure 105. For this case

$$\begin{aligned} A(f) &\sim D_T(f) D_R(f) \\ &\sim D_T(f) \end{aligned} \tag{21}$$

Since the main beam of the receiver is always pointed towards the geometric center of the semicircular block, its directivity function is unity. Figure 106 shows the received pulse and spectrum when β is zero and 15 degrees. Minima rather than frequency null points are observed since the receiver integrates a range of β in the indicated angle β. Figure 107 compares the theoretical (equation 19) and the observed minima. It is significant to note that **a** response providing useful information is being obtained at angles approximately 60 degrees off axis. Beyond this point the frequency differences become very small. Contrast this to amplitude data where the response for the same transducer would bc limited to the main bcam or about $\pm$ 7 degrees.

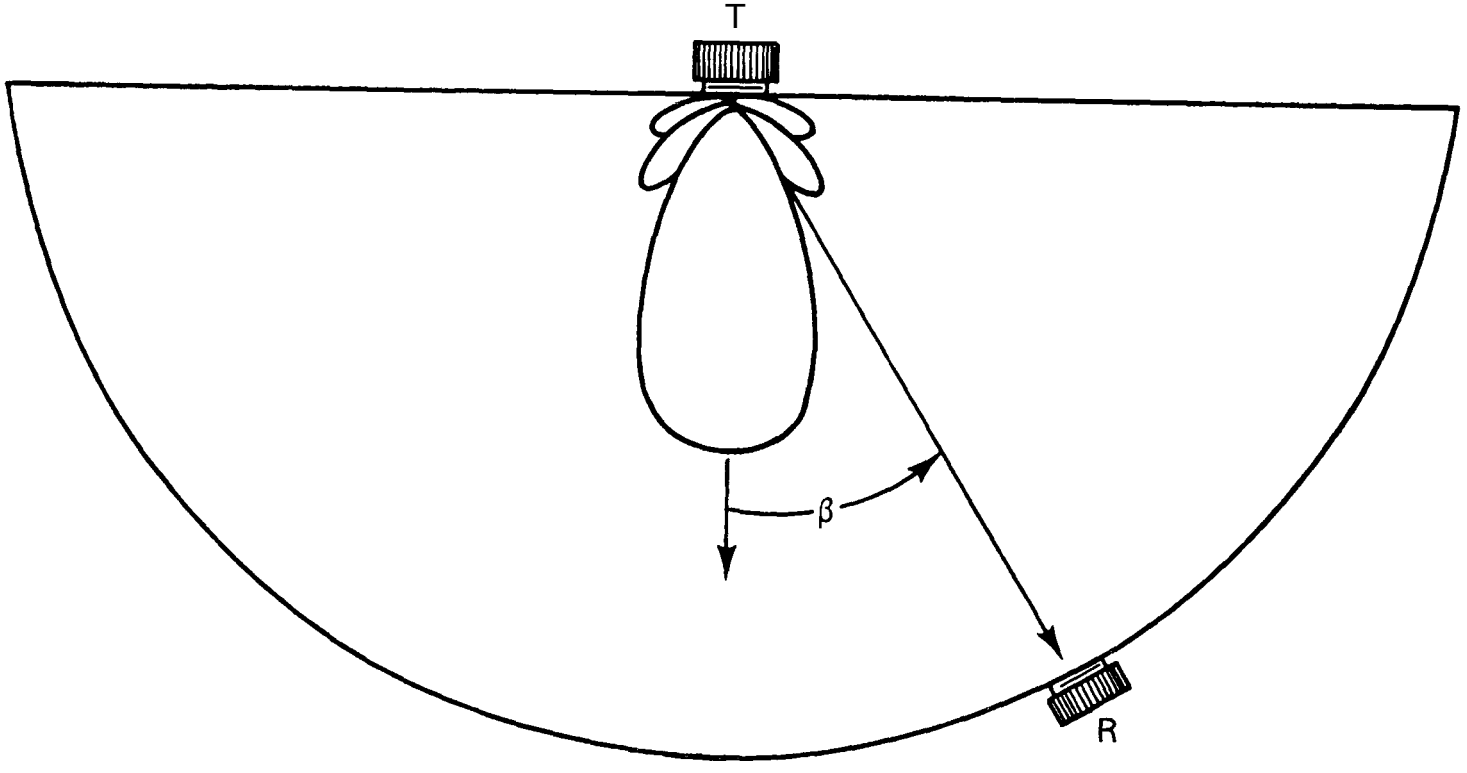

Figure 105 - An illustration of the radiation field that produces the first frequency minimum for the indicated rece-ver position.

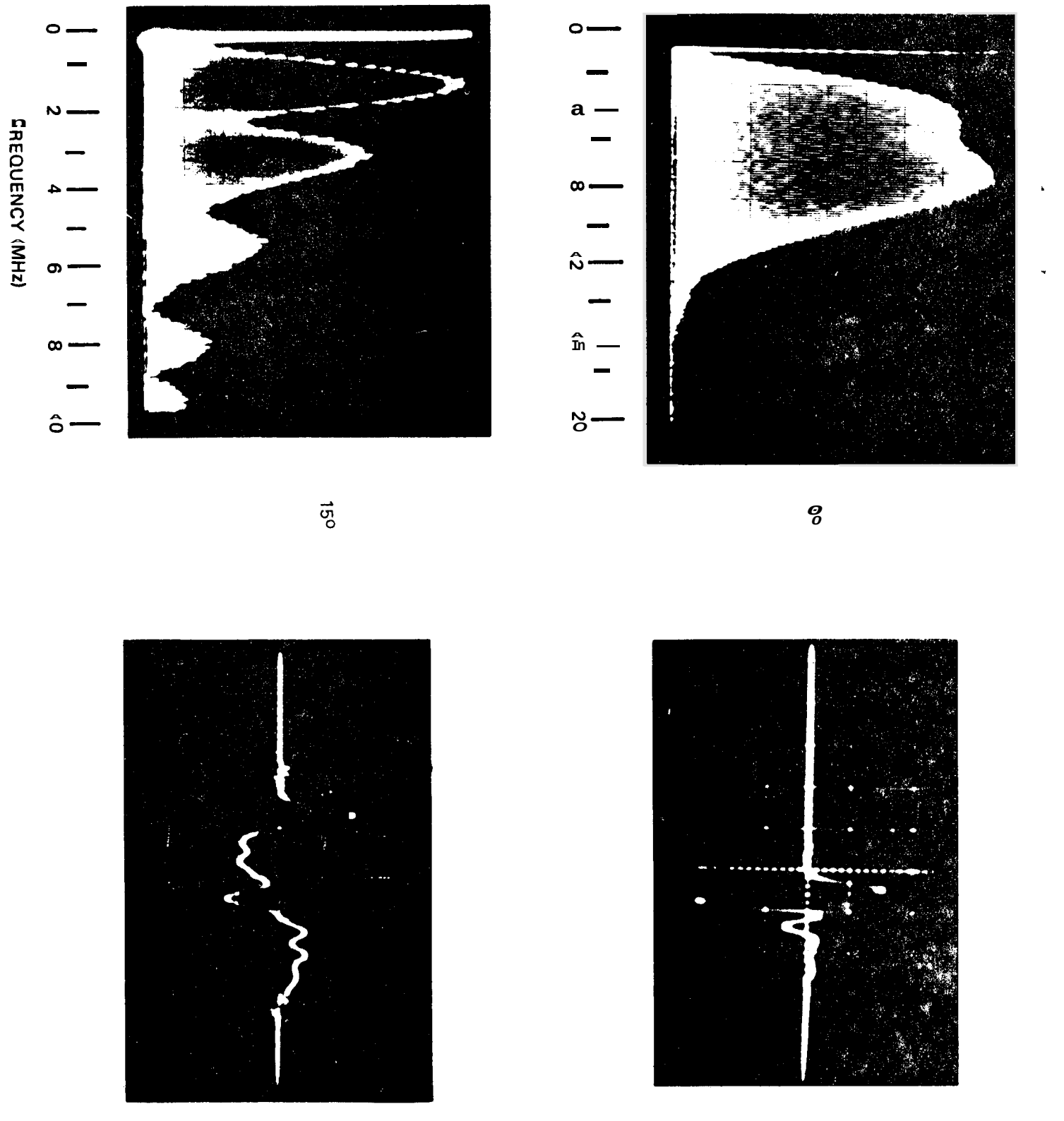

Figure 106 - Transmitted waveforms and spectra observed on specimen shown in Figure 105. On axis (0) and 15° off acoustic axis are shown.

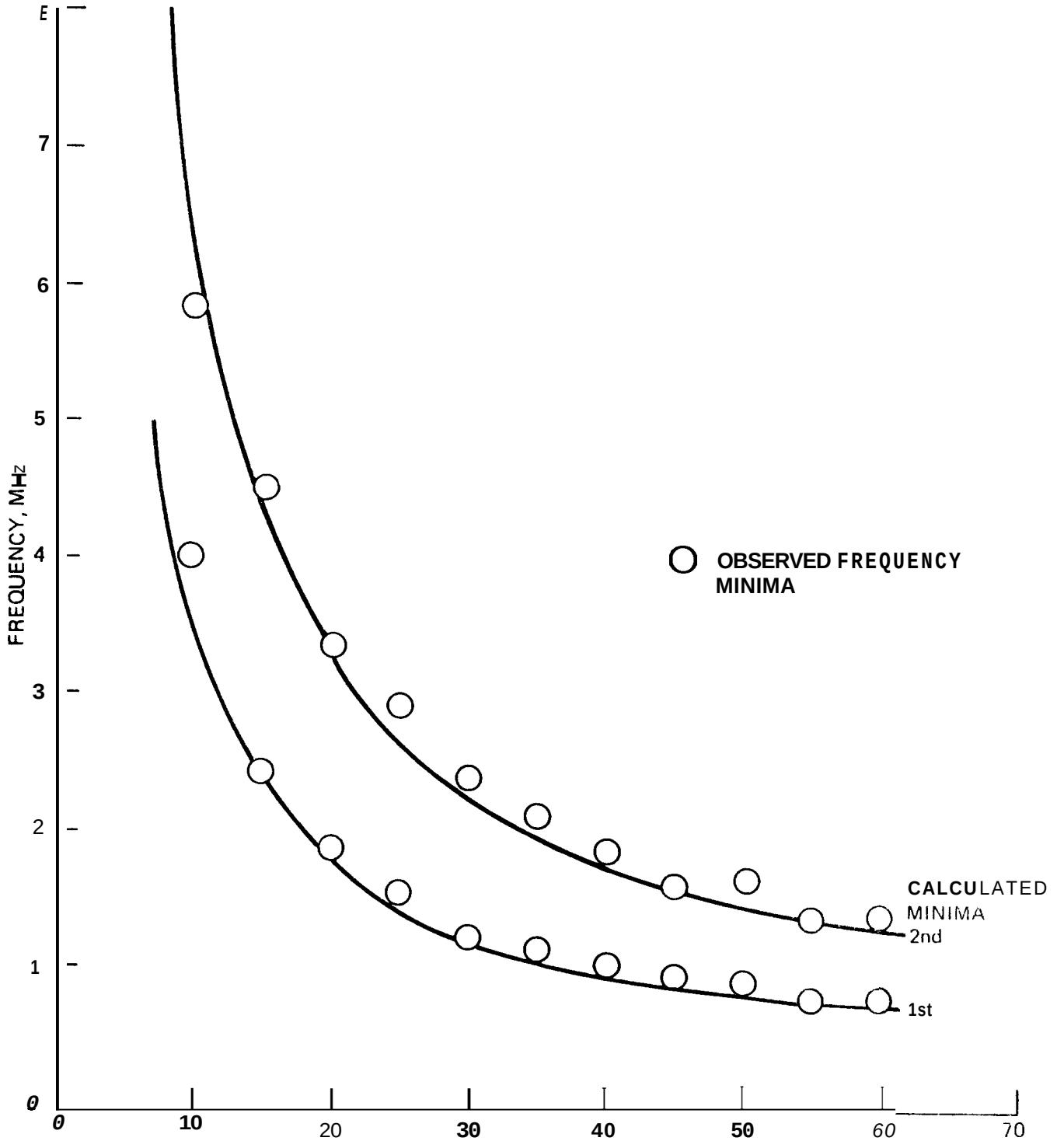

Figure 107 - Frequency minima as a function of the **off-axis** angle for a 1/2" - 2.25 MHz longitudinal transducer.

The analytical parameters of this technique are illustrated in Figure 108. It should be noted that there are two distinct zones where the receiver transducer may be placed. The dividing line is generated by the direction of the maximum power of the radiation from the flaw. The frequency minima for each zone are also indicated. A minimum of two receiver position observations are needed to produce a flaw size and orientation determination. Considering two such observations in Zone I one can write:

$$F_1 \, Sin(\theta_1 - 2\mu) = F_2 \, Sin(\theta_2 - 2\eta) \qquad (22)$$

where F_1 and F_2 are the first minima for receiver positions $\theta 1$ and θ_2, respectively. In most cases the first minima are used since they are the best defined. By the use of trignometric identities the orientation can be expressed as:

$$Tan\ 2\mu = \frac{F_1 Sin\theta_1 - F_2 Sin\theta_2}{F_1 Cos\theta_1 - F_2 Cos\theta_2} \qquad (23)$$

and the size of the flaw is:

$$d_f = \frac{3.83C}{\pi F_1 Sin\mu} \qquad (24)$$

The same formulation results when the receiver observation points are located in zone 11. However, when an observation point is taken in each zone, Equation 23 becomes:

$$Tan\ 2\mu = \frac{F_1 Sin\theta_1 + F_2 Sine_2}{F_1 Cos\theta_1 + F_2 Cos\theta_2} \qquad (25)$$

Not all receiver positions yield usable data because of frequency minima due to the receiver. The receiver minima hinder recognition of reflector minima of similar frequency. The n^{th} frequency minimum (F_{Rn}) for the reflecto of diameter d_f may be expressed as:

$$F_{Rn} = \frac{K_n \, c}{\pi d_f Sin\eta} \qquad (26)$$

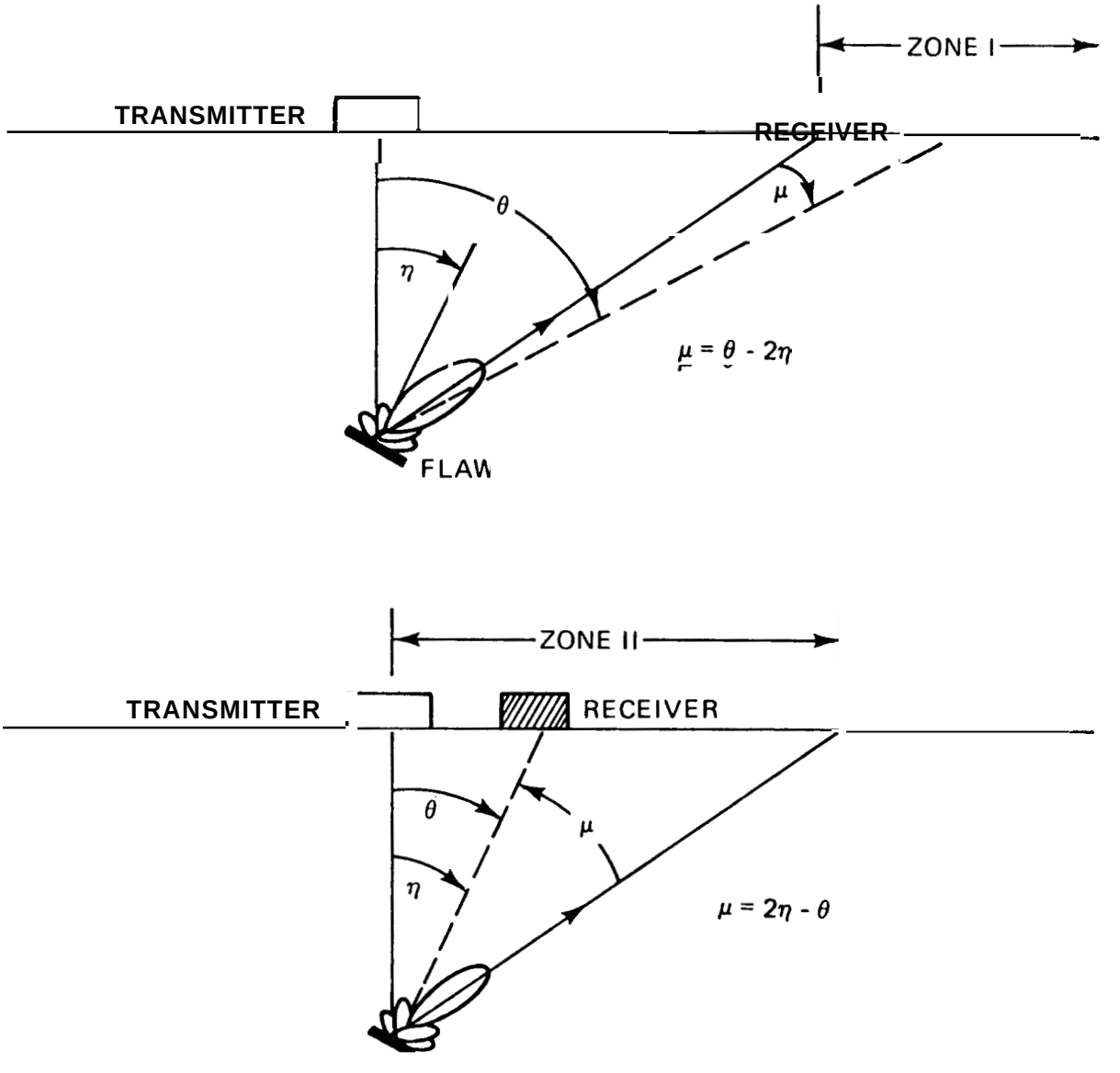

Figure 108 - Geometric particulars for the spectrum analysis technique.

where the constants are given as per Equations 19 and 20. It should be noted that the frequency minima given by Equation 26 is dependent on the direction of the flaw normal (η). The first minima for a typical reflector are shown in Figure 109. It is significant to note the loci of the minima are quite extensive in frequency.

Experimental verification was sought for this flaw characterization technique for both longitudinal and shear or angle beams; blocks shown in Figures 10 and 66 were used. Broadband transducers (150%) were ordered for this purpose. A typical transducer frequency spectrum is shown in Figure 106a. Figure 110 shows the reflector and receiver minima for a 3/4" flaw oriented at ten degrees (Figure 10) for a 1/4" diameter receiver. Observations were made at four different positions. The spectra and a typical wave form are shown in Figure 111. The zero degree observation was made by a single transducer operating in the pulse echo mode. The useable minima for each observation are indicated in Figure 110 and illustrate the close comparison of theoretical and experimental results. Using the various minima of Figure 111, the flaw size and orientation as calculated using Equations 23 and 24 are tabulated in Figure 112. The results attest to the accuracy of the technique. Figure 113 displays a summary of the results of the characterization of the 3/4" diameter flat bottom hole at other angles. The results are very good in comparison with such measurements by other ultrasonic techniques.

With the aid of the blocks shown in Figure 66 the technique was evaluated for angle shear waves. The attenuation difference between longitudinal and shear waves becomes very apparent and can be a limiting factor. The normalized frequency spectra for longitudinal and shear waves are shown in Figure 114. It can be seen that the higher frequencies of the shear wave spectrum have been eliminated. Figure 115 displays the geometric parameters for the case of angle beam characterization. The transmitter is now placed such that the main beam is directed toward the flaw. At the receiver position shown, the receiver would note the indicated flaw frequency minimum. As per Equation 18 the frequency content response is independent of the transmitter. If there are no receiver minima involved, the observed minima are generated by the flaw. For this case the misorientation angle at the receiver (μ) is given by θ-ρ where p is the entry angle. Figure 116 shows

the first four calculated angle shear wave minima at 2 1/4 MHz for both the reflector and receiver for a 3/8" flaw oriented at $35^{o}(\eta)$. Figure 117 shows two observations that were made; these observations are also located in the displays of Figure 116. It can be seen that the high attenuation limits the number of useable minima. It is obvious that the second minimum of each observation is poorly defined. Using the first minimum in each case results in a flaw characterization of 0.47" in diameter and an orientation of 37^{o}. These are in line with the results obtained for flaw characterization by longitudinal waves for this technique.

During the second phase of this program the use of this spectrum analysis flaw characterization technique will be expanded to include characterization by longitudinal angle beams. It is anticipated that more frequency minima will be noted for each observation, thus allowing for the generation of more flaw determinations per observation.

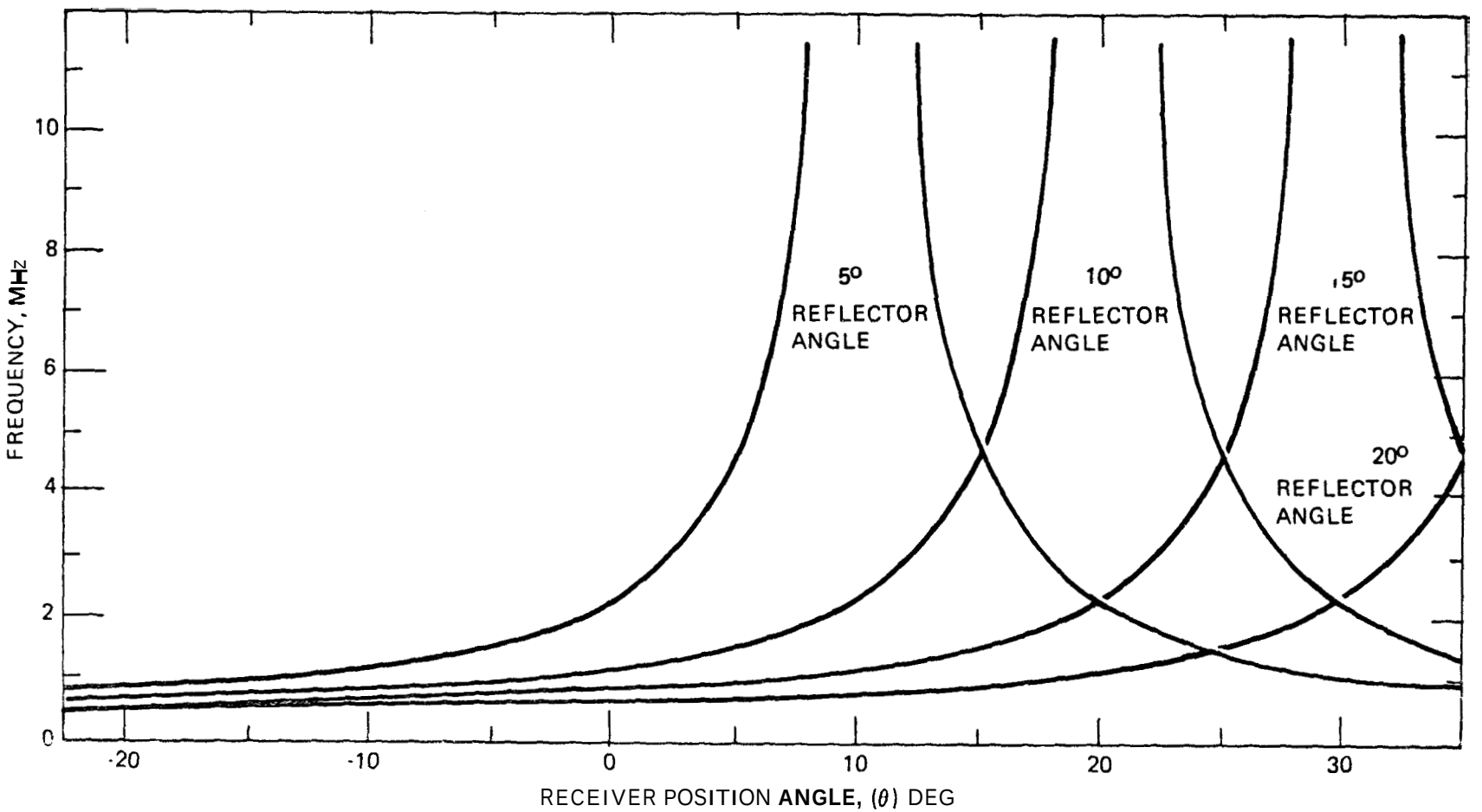

Figure 109 - Calculated frequency minima as a function of receiver positioning for a 3/4" *reflector* at various orientations. First minima are indicated.

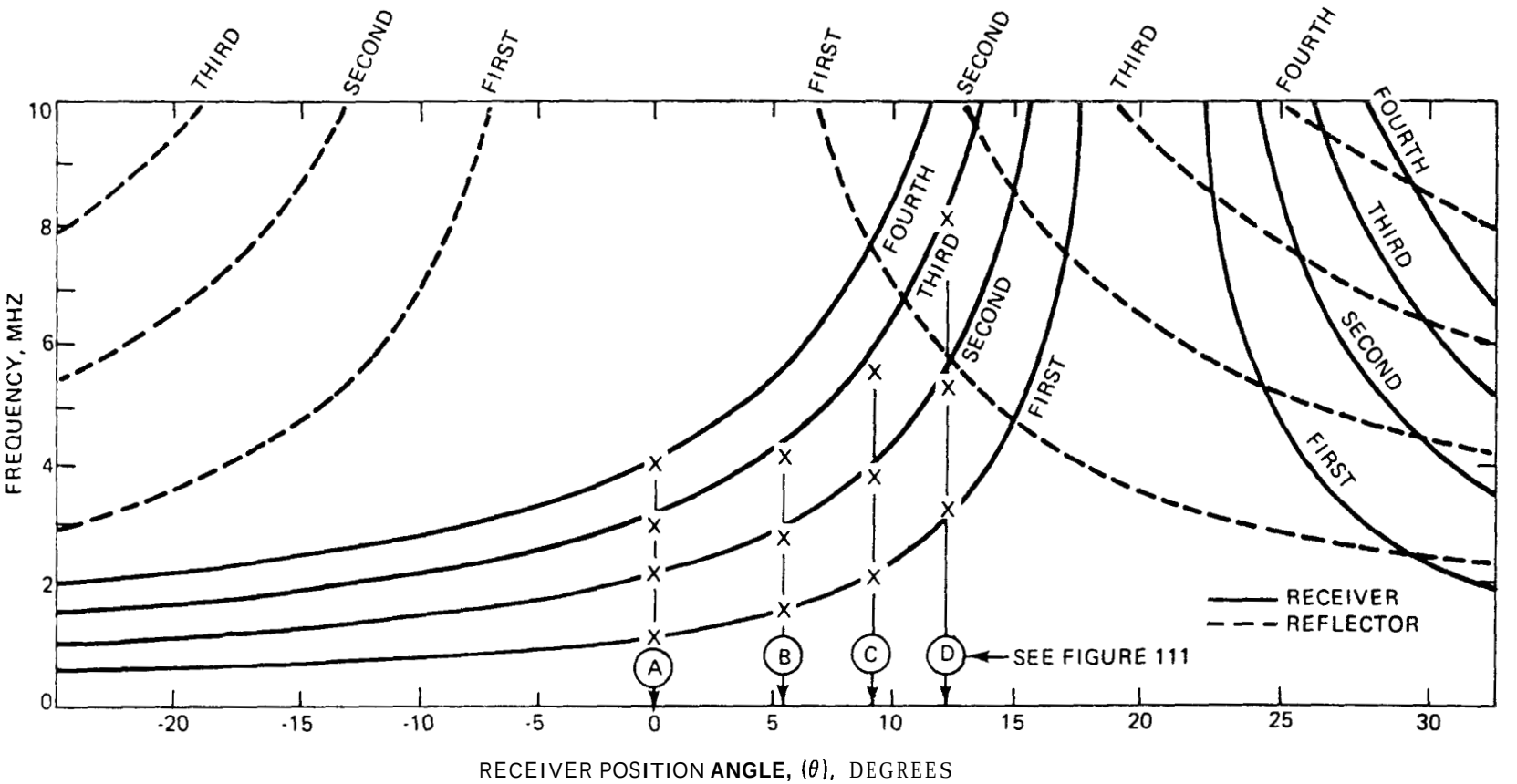

Figure 110 - Frequency minima for a 3/4" diameter reflector oriented at 10^{O} as detected by a 1/4" diameter receiver. Also shown are the observed minima shown in Figure 111; see cross point data.

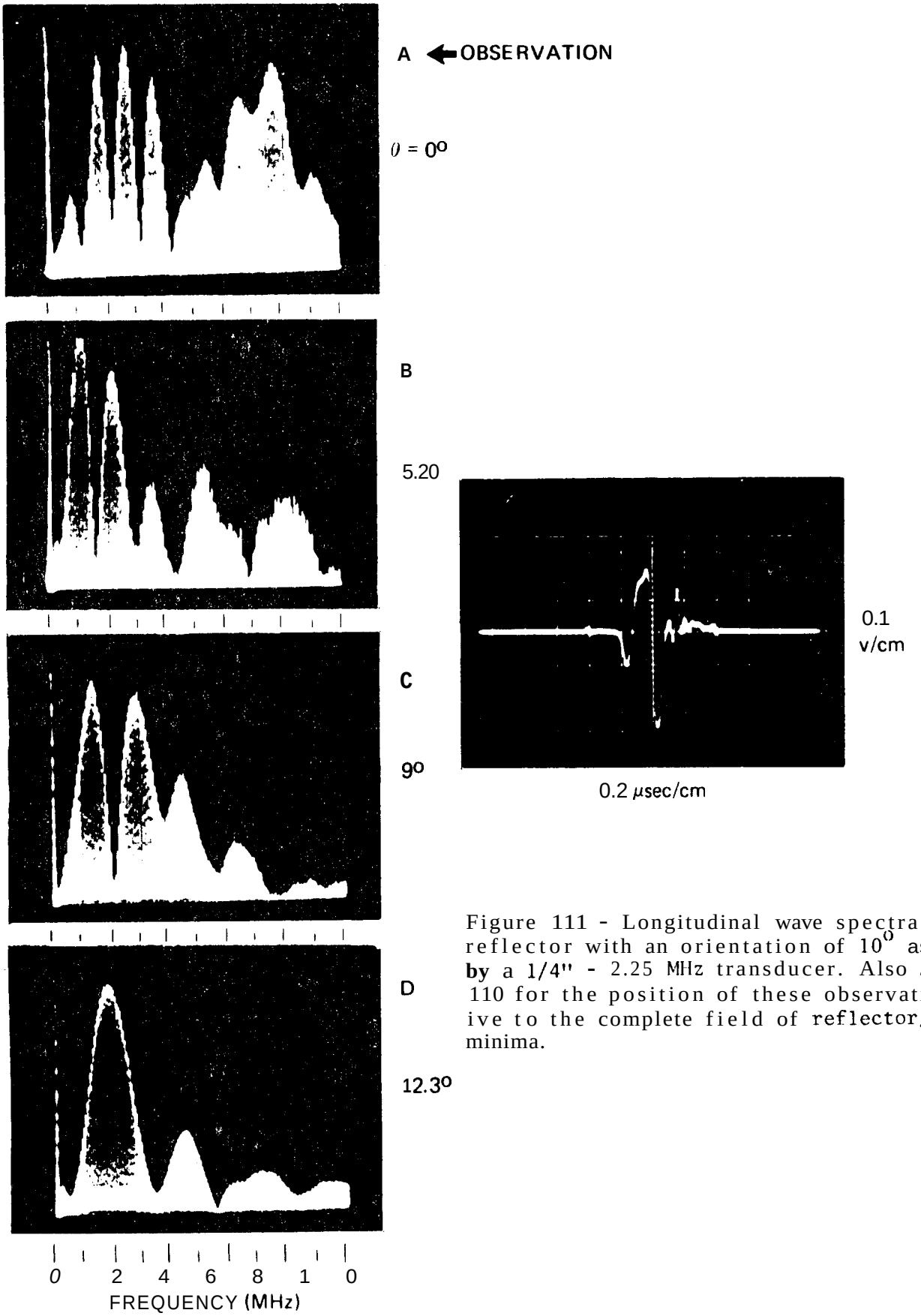

Figure 111 - Longitudinal wave spectra of a 3/4" reflector with an orientation of 10^{0} as detected by a 1/4" - 2.25 MHz transducer. Also *see* Figure 110 for the position of these observations relative to the complete field of reflector/receiver minima.

RECEIVER POSITION ANGLE(θ), DEG			0				5.14				9.00				12.3	
FREQUENCY MINIMUM NUMBER			1st	2nd	3rd	4th	1st	2nd	3rd	4th	1st	2nd	3rd	4th	1st	2nd
OBSERVED VALUE, MHz			1.2	2.2	3.2	4.3	1.6	2.9	4.3		2.1	3.8		7.5	3.3	
PREDICTED FLAW CHARACTERISTICS CALCULATED WITH OBSERVATION:																
ANGLE θ	FREQUENCY MINIMUM	PREDICTED SIZE IN ANGLE, DEG														
5.14	1st		0.74 10	0.74 10	0.76 9.9	0.69 11					0.64 11	0.67 11		0.75 9.9	0.80 9.5	
	2nd	SIZE ANGLE	0.72 10	0.72 10	0.74 10	0.67 11					0.67 11	0.70 11		0.78 9.7	0.81 9.4	
	3rd	SIZE ANGLE	0.74 10	0.74 10	0.76 9.9	0.69 11					0.64 11	0.67 11		0.75 9.9	0.80 9.5	
9.0	1st	SIZE ANGLE	0.70 10	0.70 11	0.71 11	0.67 11	0.64 11	0.67 11	0.64 11						0.99 8.8	
	2nd	SIZE ANGLE	0.71 10	0.71 10	0.72 10	0.68 11	0.67 11	0.70 11	0.67 11						0.94 8.9	
	4th	SIZE ANGLE	0.75 10	0.74 10	0.75 10	0.72 10	0.75 9.9	0.78 9.7	0.75 9.9						0.86 9.2	
12.3	1st	SIZE ANGLE	0.78 9.6	0.78 9.6	0.78 9.6	0.75 9.7	0.80 9.5	0.81 9.4	0.80 9.5		0.99 8.8	0.94 8.9		0.86 9.2		

INTERFERENCE

INTERFERENCE

INTERFERENCE

Figure 112 - Flaw characterization of a 3/4" reflector oriented at 10°. All possible pair combinations of the various observed minima were used. The minima used are shown **as observation C in Figures 110 and 111.**

FLAW ORIENTATION ANGLE (α), DEGREES	5		10		15		20	
RECEIVER POSITION ANGLE (θ), DEGREES	5.15	-5.15	5.14	12.3	7.7	15.1		24.2
OBSERVED FIRST FREQUENCY MINIMA, MHz	5.4	1.7	1.6	3.3	1.0	1.7		1.5
PREDICTED FIRST FREQUENCY MINIMA, MHz	4.80	1.56	1.58	3.02	1.07	1.58		1.49
PREDICTED FLAW SIZE DIAMETER (INCHES)	0.69		0.80		0.96		0.70	
PREDICTED FLAW ANGLE DEGREES	5.0		9.4		13		21	

Figure 113 - Flaw characterization of a 3/4" reflector at various orientations. First minima were used.

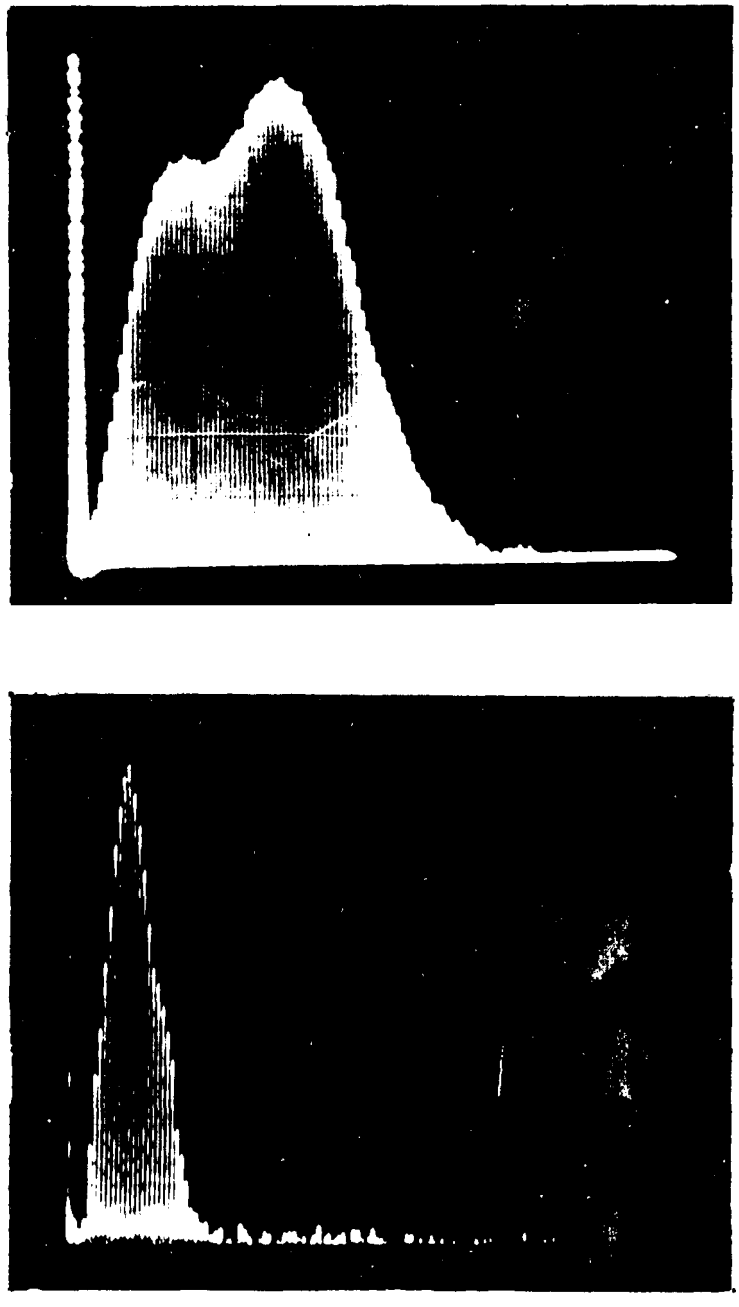

Figure 114 - The top spectrum is that due to a longitudinal wnvc while the bottom spectrum is that produced by a shear wave in the same medium (aluminum). A comparison of the two indicates the extent of the influence of attenuation. The transducer may be characterized as a 1/4" diameter and was operating at 2.25 MHz. The same path length is involved for both cases.

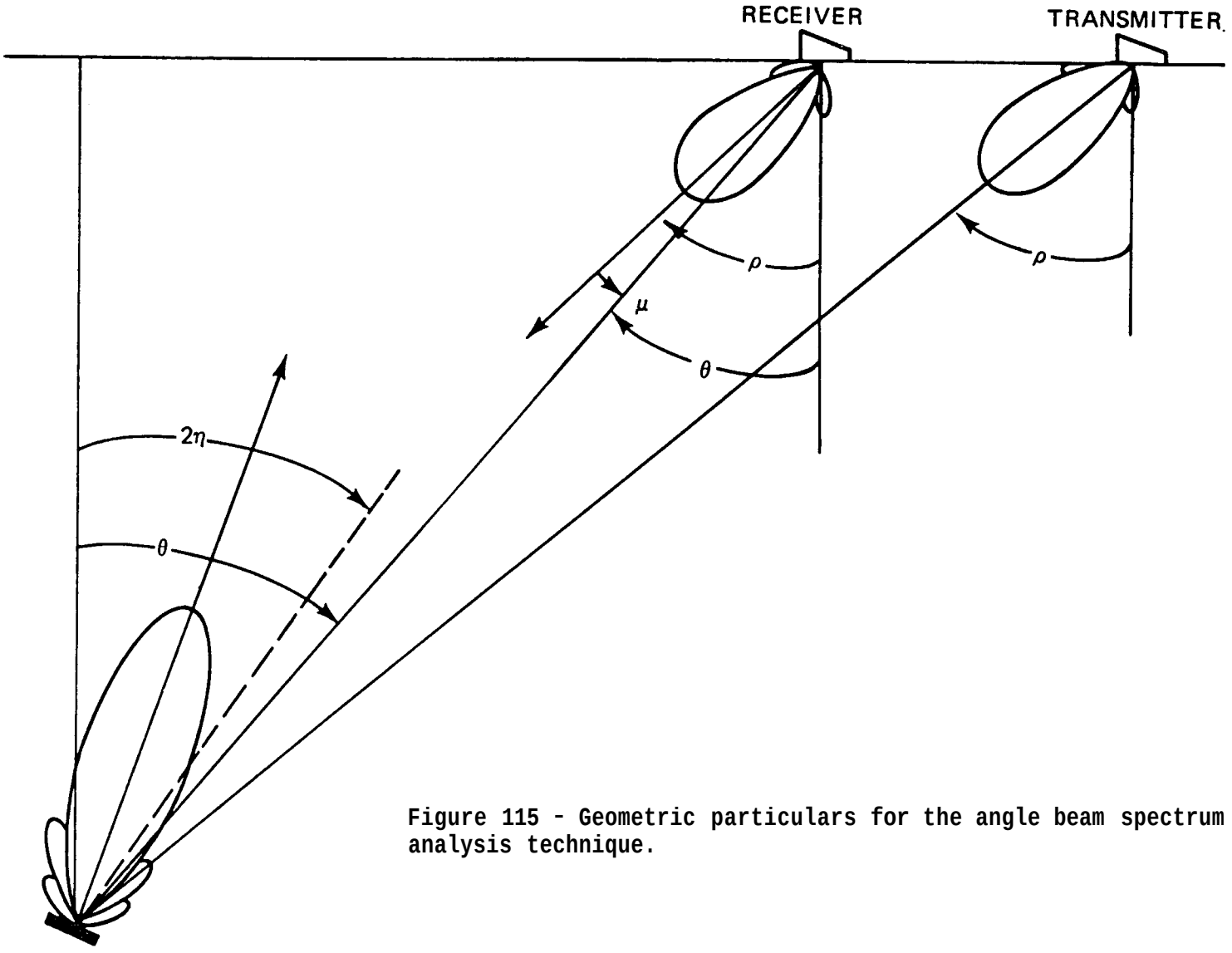

Figure 115 - Geometric particulars for the angle beam spectrum analysis technique.

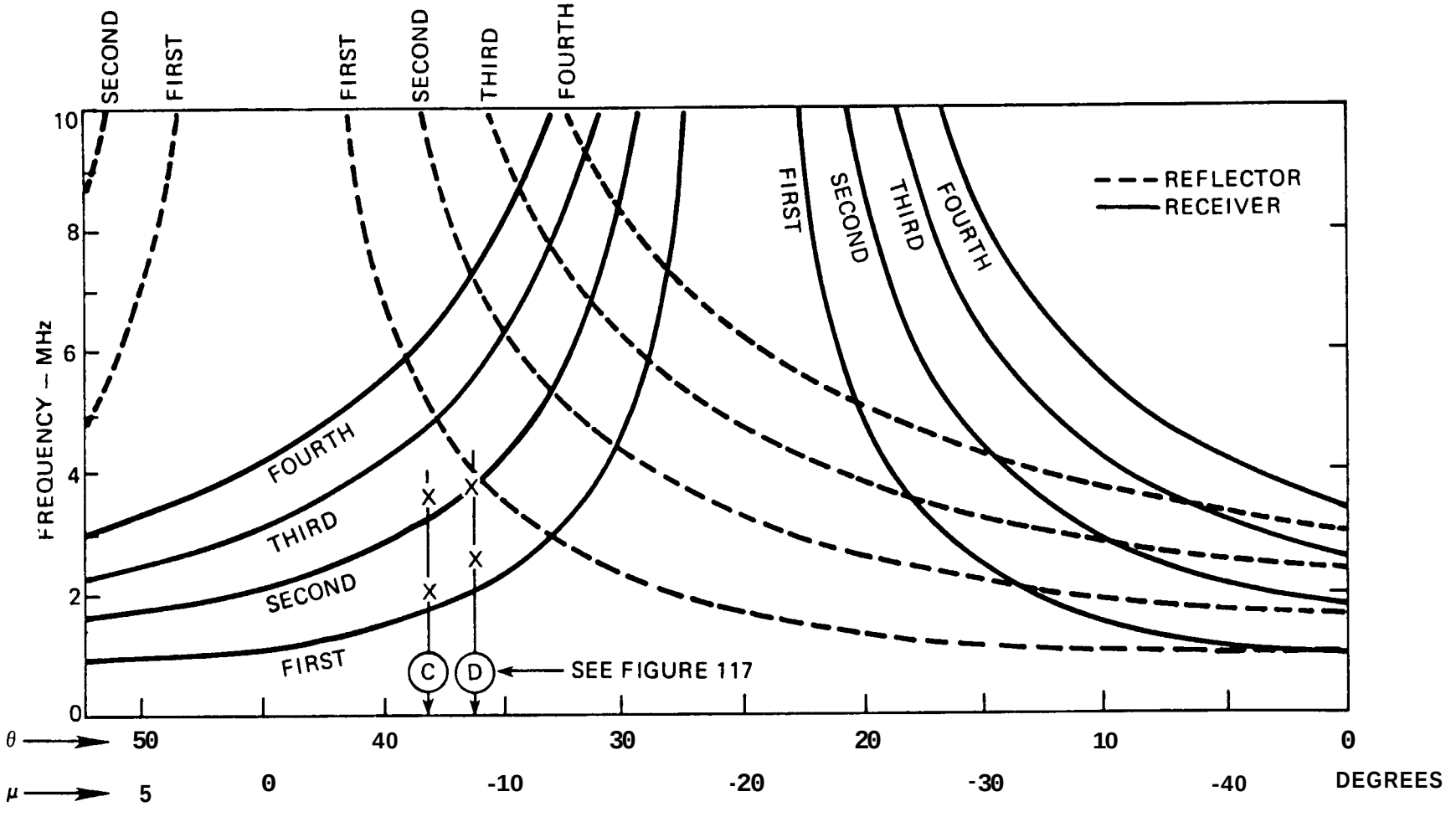

Figure 116 - Frequency minima for a 3/8" diameter reflector oriented at 10^{o} as detected by a 1/4" diameter angle shear wave transducer. Also shown are the observed minima of Figure 117; see cross point data.

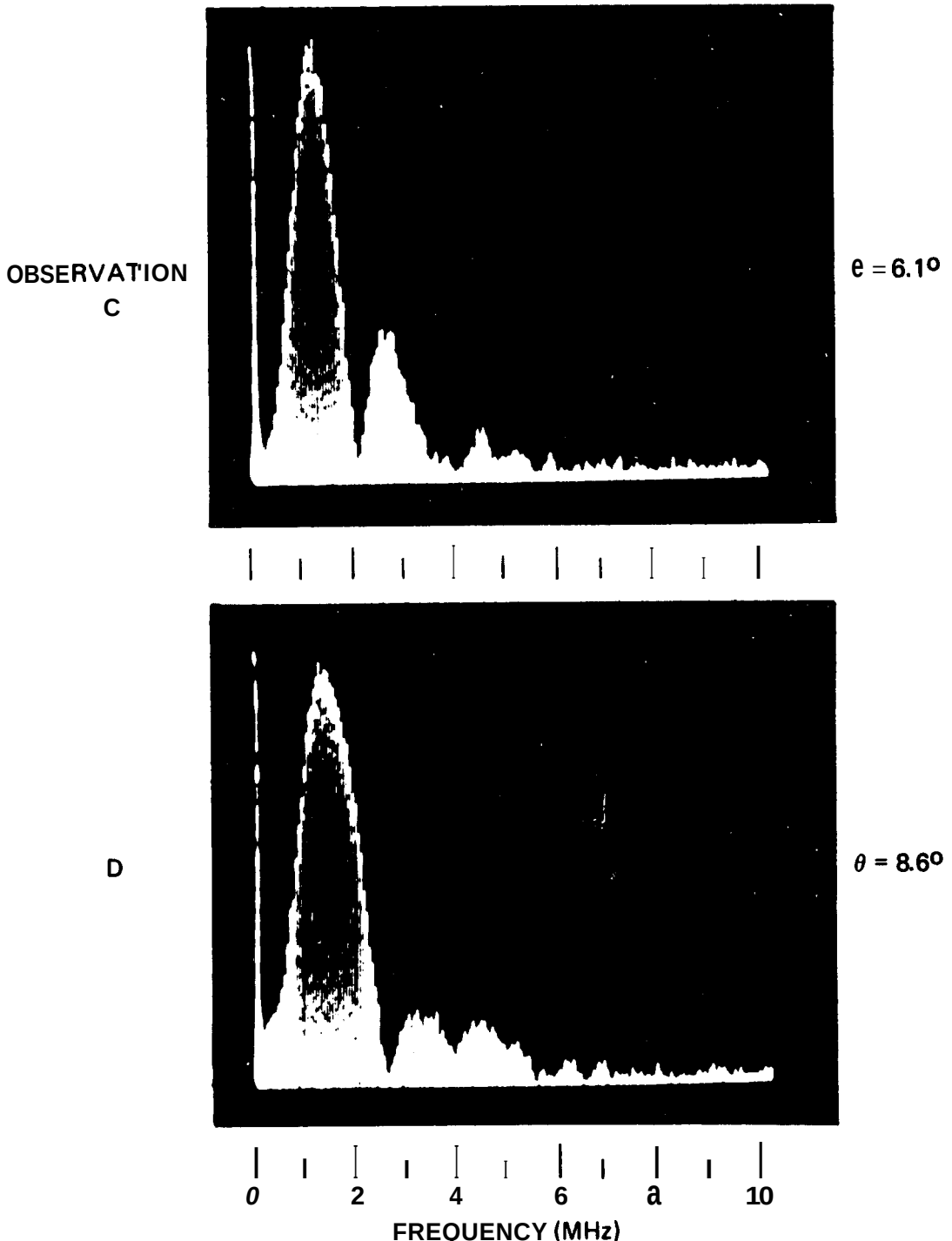

Figure 117 - Spectra obtained with a angle shear wave transducer (1/4" - 2.25 MHz: entry angle of 45°). The reflector size is 3/8" in diameter and was oriented at 10 degrees. Also see Figure 11c for the position of these observations relative to the complete field of reflector/receiver minima.

VIII. FUTURE WORK

The next phase of this program will consider experimentation that will be concerned with the detection and characterization of natural flaws in bimetallic weldments. An attempt will be made to secure a representative cross section of currently used weldment/base material combinations. Using the techniques enumerated in this report, the flaws will be characterized as per their size, orientation, location and shape. The flaws will then be extracted in a manner to present an assessment of the latter mentioned flaw characteristics. A compendium of comparisons of predicted and actual flaw characteristics will be generated. Analysis will be made to note the extent of the influence of each flaw parameter upon each flaw characterization. It is envisioned that such an analysis will provide a realistic evaluation of the ability of ultrasound for the detection and characterization of totally embedded flaws. Also such work can provide insight to the direction for further development efforts.

The flaw detection model as presented in this report will be further expanded to include more material, flaw, and equipment parameters. Of particular interest will be the inclusion of multiple frequency pulse packets to replace the presently used single frequency continuous wave radiation.

IX. CONCLUSIONS AND RECOMMENDATIONS

The below indicated remarks are limited to the detection and characterization of planar, totally embedded flaws by the ultrasonic method.

1. It is apparent that the available flaw detection processes are limited and all are related to some form of what one may generally describe as the pulse-echo technique of ultrasonics. There are some variations within this technique as generated by the use of multiple transducers, however, all have a common detection process. Detection involves striking the flaw with some ultrasound and followed by the necessity of getting some ultrasound from the flaw back to the interrogating transducer. The flaw in this case acts as a secondary source of radiation. The detection process can be modeled in terms of the spatial interplay of the radiation fields from the transducer(s) and the flaw. It would appear that every effort is made to properly bathe the flaw with ultrasound by way of directed beams and focusing devices. The need to consider the return of the ultrasound from the flaw back to the interrogating transducer is recognized but not given adequate attention. It is assumed that the surface roughness of natural flaws will scatter or otherwise increase the angular distribution of the radiation from the flaw to enhance the detection event. Experimental data disproves this contention.

2. A great deal of effort is relegated to the development of transducer and instrumentation technology. The physics of the ultrasonic detection process itself receives a disproportionate amount of attention.

3. Virtually all existing flaw characterization processes are amplitude-dependent and are based upon the direct relationship between the maximum amplitude response and flaw area. The latter is only valid under very restricted conditions or when amplitude loss or degradation parameters are not present.

4. Degradation in the amplitude response due to flaw, material and instrumentation characteristics as well as operator induced errors can be appreciable and often result in rendering a flaw undetectable.

5. The misorientation of the flaw with respect to the beam of the interrogating transducer appears to be one of the major causes of amplitude degradation. Such degradation is sufficient to obviate the accepted association of large flaws with large amplitude response. A small favorably oriented flaw can produce a greater amplitude response than a large misoriented flaw. For a nominal size transducer the maximum misorientation is 5-10° at an operating frequency of 2.25 MHz. Beyond this angle detection is not possible regardless of the flaw size. The affect of flaw misorientation can be reduced appreciably if highly divergent transducer radiation fields can be developed. To this end, beam steering by one and two dimensional arrays and convex curved surface transducers represent possible means.

6. It would be highly advantageous to separate the flaw detection and characterization processes. Such action would facilitate the optimization of each of these distinct processes.

7. It is imperative that amplitude-independent flaw characterization techniques are developed.

8. It is alarming to note that the utilization of the computer in ultra sonics appears to be minimal and limited to rapid data recording. No significant attempts have been made to use logic schemes to analyze the data in a meaningful manner.

9. The use of an amplitude-distance standard (DAC) as generated by the response of a side drilled hole at various distances has two serious deficiencies when used for the inspection of weldments. First, the DAC curve is usually generated in the base material, hence any attempt to use it for the bimetallic structure of a weld is not valid. Since the attenuation within the weldment is much higher than the base material, the added attenuation within the

weldment produces greater decreases in the amplitude response than those predicted by the DAC curve. Second, the shape of the flaw is responsible for the distance dependency of its amplitude response. For example, planar flaws have a $1/S^3$ distance dependency while the side drill hole has a $1/S^{3/2}$ dependency. Therefore, a planar flaw cannot be monitored by a side drilled hole generated DAC curve. Both of the above mentioned effects can lead to optimistic flaw size evaluations. Techniques for eliminating these difficulties should be implemented.